NTNU

Norwegian University of
Science and Technology

Power Supply for Down-hole Applications Based on Flow

Syed Ali Irtaza Kazmi

Master of Science in Electric Power Engineering
Submission date: June 2017
Supervisor: Lars Einar Norum, IEL

Norwegian University of Science and Technology
Department of Electric Power Engineering

Abstract

The main focus of this thesis is to develop a power supply for feeding power to the down-hole electronic devices such as, instrumentation and communication units. The traditional way of supplying power using long cables from the topside seems to be an expensive approach. So, the present work aims to validate an alternative technique of feeding power to these devices. Numerous types of energy sources are accessible in the process of oil and gas production. The source of kinetic energy from a flowing fluid or gas is one of the useful source of energy which contributes in the generation of electrical power for the down-hole devices.

This study mainly focuses on the modelling of a switched mode power supply for down-hole devices using MATLAB/Simulink. The design of the system model is based on the method of using a permanent magnet synchronous generator coupled to a specific type of turbine, which converts the kinetic energy of the flowing fluid into mechanical energy on the shaft. The PMSG converts the mechanical energy of the shaft into uncontrolled electrical power. The output power from the generator is rectified using a three-phase diode rectifier. Moreover, the rectified power is stabilized and supplied to the dc loads using a large filter capacitor and several types of dc-dc converters. The stability of the system for supplying stable power to the dc load is thoroughly investigated in this research work. Consequently, feedback control loops for the dc-dc converters are examined to make a stable power supply using a storage unit and a dump-load. Therefore, the principle objective of the feedback control loops is to regulate the dc link voltage across the filter capacitor. Controlling the power from the source side is not applicable in this method, therefore a pitch angle control is eliminated and not implemented in this thesis.

The feedback control loops have been simulated for different cases to investigate the behavior of the system for varying nature of input flow rates and variable load demands. Therefore, various simulation results have been presented to analyze the performance of the system regarding the dc link voltage across the filter capacitor. The system has been examined for three different methods, the first and the second method are inspected by having a storage unit and a dump-load. The third method is considered to analyze the stability of the system without having any storage unit, because rechargeable are batteries not available for very high temperatures.

Finally, the feed-back control loops of the system model have been modified by using embedded coder target library which can be implemented on a Texas Instrument microcontroller. The process of code generation and system with a digital controller is studied and simulated using MATLAB/Simulink in the last section of the thesis report.

Acknowledgement

I would like to express my deep gratitude to my supervisor Prof. Lars Norum of the department of Electric Power Engineering at NTNU for his excellence in supervision, guidance and providing me the opportunity to be involved in such an exciting project.

I would like to acknowledge the department of Electric Power Engineering at NTNU for providing me full support throughout the final year of study. I am also thankful to the senior Engineer Kurt Salmi for granting me the required accessories to complete my research work at NTNU.

I gratefully acknowledge the help of PhD candidate Anirudh Budnar Acharya at NTNU for his valuable support regarding the code generation process in MATLAB/Simulink.

I am also thankful to my friends at NTNU and in Pakistan: Yunus, Reza, Shaine, Muzammil, Zamin, Mulugeta and Zaw for their valuable advices and fruitful discussions.

Finally, I would like to express my affectionate appreciation to my parents, brothers and sister for their continuous support, care and love throughout my educational career.

Trondheim, 18th June 2017

Syed Ali Irtaza Kazmi

Table of Contents

Abbreviations

AC/DC	Alternating Current/Direct Current
PMSG	Permanent Magnet Synchronous Generator
PID	Proportional Integral Differential
SOC	State of Charge
SMES	Super Conducting Magnetic Energy Storage
TI	Texas Instruments
DSP	Digital Signal Processor
CPU	Central Processing Unit
ADC	Analog to Digital Converter
PWM	Pulse Width Modulator
ePWM	Enhanced Pulse Width Modulator
eCAP	Enhanced Capture
HRCAP	High Resolution Capture
eQEP	Enhanced Quadrature Encoder
RTDX	Real Time Data Exchange
GPIO	General Purpose Input/output Pins
MSB/LSB	Most Significant Bit/Least Significant Bit
MIL	Model in Loop
HIL	Hardware in Loop
PIL	Processor in Loop
SIL	Software in Loop

Chapter 1 Introduction

1.1. Background and Motivation

The global demand of energy is growing continuously in most of the developing countries with the increase in population and the standard of living. The world can use all the produced energy from the oil, gas and renewable sources and it has been predicted that the main source of energy for the next few decades will be from oil and gas production. So, the industry must keep on increasing the supply of hydrocarbon fuels to meet the worlds energy demand [1].

Many industries are using advanced electronic devices for increasing the production of oil and gas fields, which can be achieved by monitoring and controlling the changing parameters (temperature, pressure, flow rates) of the oil and gas wells. The field operators usually control the flow rates of oil, water and gas and monitors the temperature and pressure of the well. The electronic devices used by the field operators includes instrumentations, actuators, sensors and several other control devices which are becoming more and more sophisticated for handling the smart wells system. These types of systems always require electric power to operate and control various parameters of the oil and gas wells. Therefore, the demand of electric power in down-hole applications is increasing with the advancement of the smart wells system. Supplying electric power to the down-hole devices is the main topic of discussion in this report. A typical way of feeding power to these devices are usually done from the topside by using batteries or surface power supplies connected through long cables. The cost of this method increases with an increase in depth, so an alternative approach is required for providing power to these control devices [2]. Therefore, a power supply unit is modelled in this research work to fed power in a controlled manner by protecting the electronic devices from any kind of failures. The Power supply unit is usually designed by using Specialized power electronics devices to control the flow of power for different conditions.

This research work thoroughly investigates the alternative method of building the power generating unit for the down-hole control devices. Moreover, the stability of the proposed method and its limitations have been discussed in this thesis work. The idea of this method is to use a specific type of generator coupled to a turbine to generate power for the down-hole devices using the available source of energy deep down inside the well. The generated power from the turbine and the generator is controlled and converted into ac/dc forms using power converters. The down-hole electronic devices are usually located at level where the temperature

and the pressure is very high and it increases with an increase in depth. So, the power generating unit must be designed using high temperature electronics. The power generating unit consists of power electronics converters which are made from wide band gap devices, such as silicon carbide and gallium nitride, in addition with high temperature inductors and capacitors for operating in these harsh environments. The effect of having harsh environment on the proposed technique and the modelling of the converters using wide band gap devices is not discussed and is outside the scope of this thesis work.

1.2. Planning and Scope

The system is designed in such a way that a permanent magnet synchronous generator (PMSG) connected to a specific type of flow turbine, is utilized for making a power generating unit. The turbine coupled to a PMSG is the backbone of this exciting approach for feeding power to the down-hole devices. The turbine captures the available kinetic energy of the flow inside the well and changes it into mechanical energy for rotating the shaft of the PMSG, which delivers electrical energy on its output terminals. The output power of the PMSG is rectified using a three-phase diode rectifier which is converted into desired level using specific types of dc-dc converters. The advantage of using a PMSG is that there is no requirement of a dc excitation system. Furthermore, the generator can also be operated without having a gear box which decreases the complexity of the overall system.

The power generating unit must be capable of delivering constant dc voltages to the down-hole devices, which can be achieved by controlling various types of dc-dc converters. So, it is necessary that the power generating unit is a switched-mode power supply to fulfill the requirement of having a controlled constant dc voltage across the loads (down-hole electronic devices). A switched-mode power supply having high switching frequencies stores energy in the inductor and keeps the desired constant voltage across the filter capacitor. The power generating system is designed for supplying the dc loads only, because the down-hole devices requires dc power for their operation. The voltage regulations of the switched-mode power supplies are carried out using a single loop feedback or a double loop feedback control of the dc-dc converters. The feedback loops are designed to vary the duty cycle of the converter switches in such a way that the output voltage across the dc loads regulates to a desired reference value. The feedback loops are constructed using proportional-integrator (PI) controllers to vary the duty cycle of the switches according to various situation.

The Control algorithms for the dc-dc converters are modelled which controls the flow of power across the system to generate stable power supply for the dc loads. The complications for the stable operation of the system is the variable nature of flow rate and the varying load demands. Therefore, several types of control algorithms have been studied and verified in this report to come up with a best solution. The dc-dc converters are used for the storage units and dump-loads to control the flow of power in the system. The hardware implementation of the control algorithms for the dc-dc converters have also been investigated in this report. A suitable type of microcontroller is chosen for the implementation of the control algorithms from the Texas Instruments microcontroller families, which is thoroughly investigated in this report. The complete hardware implementation of the system model is outside the scope of this project and it can be assumed that the turbine is chosen and installed in such a way that it doesn't block the flow of fluid or gas inside the well.

1.3. Organization of the Thesis

The thesis is organized into seven chapters, and the overview of the work is described as follows:

In chapter 2, an overview regarding the available energy source such as kinetic, vibrational, chemical and thermal energy in down-hole application is presented. The chapter also emphasis on the utilization of kinetic source of energy using turbines. In addition, the modelling and usage of several energy storage units has been discussed in this chapter which includes a battery storage unit, a super capacitor and several other types of energy storage units. The chapter also introduces and discuss the importance of a dump-load for various type of conditions.

In chapter 3, a simple block diagram is presented, which is used to illustrate the basic structure of the system. The basic structure of the system includes a turbine, PMSG, rectifier, filter capacitor, dc-dc converters and dc loads. In addition, the chapter also reports the modelling of the system components and the relationship between the mechanical and electromagnetic torque. furthermore, the chapter introduces a three-phase diode rectifier, a dc-dc bi-directional buck-boost converter and a buck converter used for the controlling of the dc link voltage across the loads.

In chapter 4, several topologies of the system have been investigated using various types of storage units and dump-loads. A literature review related to standalone power generating systems and dc grid is presented. The system can be modelled using a battery bank or a hybrid storage unit having a dump-load.

In chapter 5, the power management scheme for a battery storage system and dump-load is presented. Three methods have been discussed for making the control algorithm of the system using dedicated dc-dc converters. The control loops for the dedicated dc-dc converters are constructed and several simulations have been performed to examine the stability of the system. The first method is based on a system having a bi-directional buck-boost converter for the battery storage unit and a switch connected dump-load. In the second method, the dump-load switch is replaced by a dc-dc buck converter. The last method is presented to study the nature of the system without having a storage unit, where the system only relies on a dump-load.

In chapter 6, implementation of the control algorithm using Texas Instruments microcontroller has been investigated. The chapter starts with an overview of data type representation and a brief discussion about the fixed-point representation has been carried out. The control loops for the battery bank and the dump-load is implemented using embedded coder target libraries and finally the chapter gives an overview about the process in loop simulation and code generation steps.

Chapter 2 Energy Sources and Storage Units

2.1. Down-hole Energy Sources

The process of oil and gas extraction has been classified into several processes. The major processes include the exploration, well development, production and finally the site abandonment. The entire process can provide several types of energy source, which can be in the form of thermal or mechanical energy. The available source of energy can be transformed into electrical energy for providing power to various electronics and electrical circuits. Several types of patent devices have been used to convert the available source of energy inside the well into electrical forms. According to patent [3-5], a source of kinetic energy can be transformed into electrical energy and according to patent [6-9], the vibrational energy can provide electrical power in the well. In patent [10], [11] and [12], thermal, electrostatic and chemical energies are transformed into electrical power to supply the load demands. A comparison between various type of power sources for the down-hole application has been shown in Table 2.1.

Table 2.1 Comparison Between Various Power Sources [13]

Energy Source	*Maximum power Estimated per single unit [W]*	*Transforming Means*	*Generated Power Achieved [W]*
Kinetic	800	Turbine	15
Vibration	1200	Electromagnetic coil	30
Chemical	2000	Fuel cell	1000
Electrostatic	10	Capacitor	No data
Thermal	0.01	Thermocouple	No data

The production of mud fluid provides the main source of kinetic energy which can deliver power up to hundreds of watts [13]. The kinetic energy of the mud fluid can be converted into electrical energy by using a turbine as discussed in patents [3, 4]. The vibrational energy in the well is another useful source of downhole energy which is either caused due to the flow of fluid or due to the drilling process. According to patents [6, 7], the fluid is passed through a down-hole power generator which utilizes the vibrations caused by fluid flow to produce electrical

power. The vibrations can also be used in several other ways to generate electrical power. The vibrations are either transferred to a magnetic element which is positioned relative to an electromagnetic coil or it can be transferred to a piezoelectric material. The vibrations can generate an electromagnetic force on the coil due to the mechanical movement of the magnetic element while in the other method theses vibrations can apply stress on the piezoelectric material. In patent [8], the vibrational energy from a drilling process is converted into electrical power using the discussed procedures. The high operating temperatures in the down-hole environment can also be utilized as an efficient energy source. The temperature gradient can vary for different places and it is recorded around 25 to 30°C/km on average. A thermoelectric device can be used to convert the down-hole temperature gradient into electric power. The temperature gradient of the well is being applied across the thermoelectric device which comprises of two thermocouples. The thermocouples are exposed to higher and lower temperatures which generates voltage difference across the output electrical terminals [10].

According to patent [11], the electrostatic energy produced by the fluid flow can also be used as a source of energy that can be transformed into electrical power. An electrostatic potential between the flow-stream and a tubular section is created by the flow of non-conductive hydrocarbon based fluids having relative permittivity around 2 to 40. A ground electrode is connected on the flow-stream and another electrode is connected with the tubular section to produce electrical energy from the created electrostatic potential. The electrostatic potential can be in the range of 0.5mV to 50kV.

Another available source of energy can be termed as chemical energy source discussed in patent [12]. This chemical method of supplying electrical energy is obtained using a fuel cell which involves a chemical reaction between hydrogen and oxygen. The chemical reaction generates electrical energy up to 2 kilowatt-hours and its advantage is that it can produce electrical power at high temperature range.

2.2. Fluid Flow Power Production

The power production method for the down-hole devices presented in this work is being carried out by using a turbine and a permanent magnet synchronous generator (PMSG). The method used for producing electrical power for down-hole applications can be achieved by consuming the kinetic energy generated from the flow of a fluid or gas inside the well. The kinetic energy of the flowing fluid can be extracted by using a turbine. The turbine converts the obtained kinetic energy into mechanical energy on its output shaft. The choice of the turbines can be

made by considering the direction of the fluid flow inside the well. A permanent magnet synchronous generator is then utilized to convert the mechanical energy from the turbine into electrical energy, as the PMSG is coupled on the output shaft of the turbine. The electrical energy is stabilized and changed from ac to dc or dc to ac forms using power electronics devices. The stabilized electrical power is then supplied the down-hole electrical loads connected across the filter capacitor.

The volume of a flowing fluid is measured in terms of flow rates which is represented using the letter 'Q' and it can be estimated in cubic meters per second. More energy is available for the turbine when the volume of the flowing fluid is higher. However, all the available flow cannot be used for power generation as the turbine should not block the flow of oil or gas inside the well for down-hole applications.

2.3. Battery Energy Storage

A rechargeable energy storage unit is beneficial for the performance and stability of the proposed method presented in this thesis work such as, a battery unit. The batteries are divided into two group named as primary (non-recharge) and secondary (rechargeable) batteries. A best choice for a battery storage unit has to be made from the secondary group, which consists of several types of batteries. Figure 2.1 shows the list of non-rechargeable and rechargeable batteries, where the Primary batteries are usually used in medical and military applications.

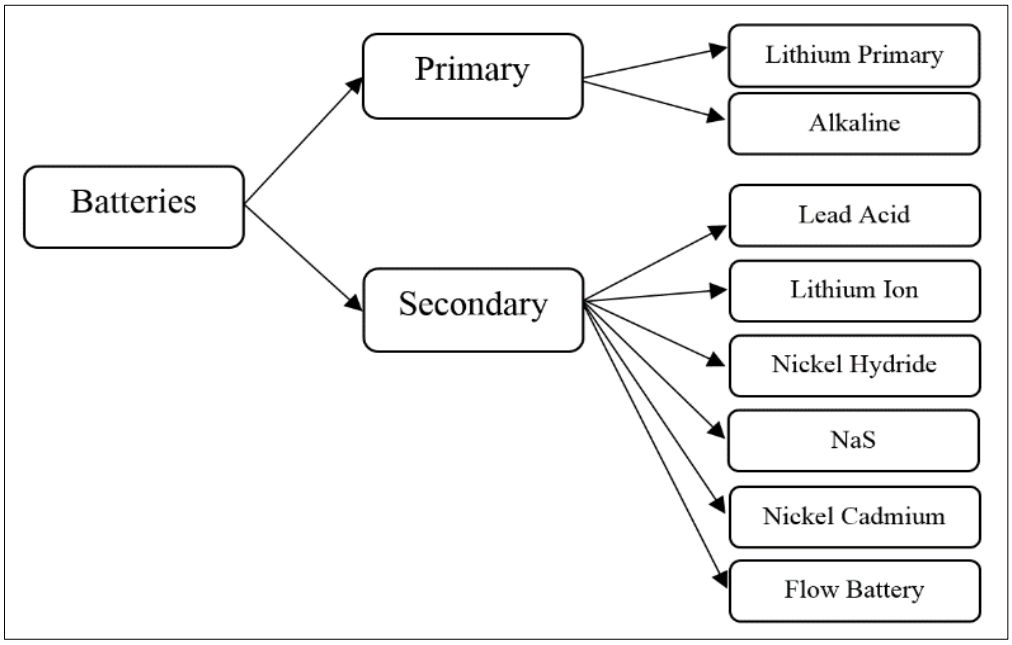

Figure 2.1 Types of Batteries

Lead acid battery are mostly used for renewables while nickel-hydride and lithium ion batteries are mainly used in mobile phones and laptop computers. These are the most expensive type of batteries because of their high-energy densities. Nickel-cadmium batteries are also used to some extent in renewables but they cause environmental hazards from cadmium disposal, while there are very few application for the use of nickel-iron batteries. NaS batteries are also being utilized for renewables because of their high efficiency and higher power density. Flow batteries are another type which stores liquid electrolytes externally in separate tanks [14], [15].

A lead acid battery is considered as an energy storage unit in this report which is the most common device for storing and delivering electric power. These batteries are cheap and can be used for variety of application, allowing better performance and lifetime. A lead acid battery is capable of storing and delivering voltage around 5V to 24V dc [16]. Different phenomena can occur while using a lead acid battery such as charging, discharging and overcharging. The battery parameters such as, the battery voltage, battery current, capacity, resistivity and temperature can change during the charging, discharging and overcharging phenomena. This makes the battery unit more complicated and to make a prediction about its state of charge becomes more challenging. There are various models for lead acid battery found in the literature such as the shepherd model, Monegon model and CIEMAT model. These models need the information about the appropriate parameters of the battery storage unit, so the parameters need to be fit for each battery design [15]. The lead acid battery stores the energy by converting the chemical energy into electrical energy during charging and discharging. The positive electrode is the lead oxide while the negative electrode is made of lead which are dipped into sulfuric acid. The electrodes are converted into lead sulfate when the battery is discharging.

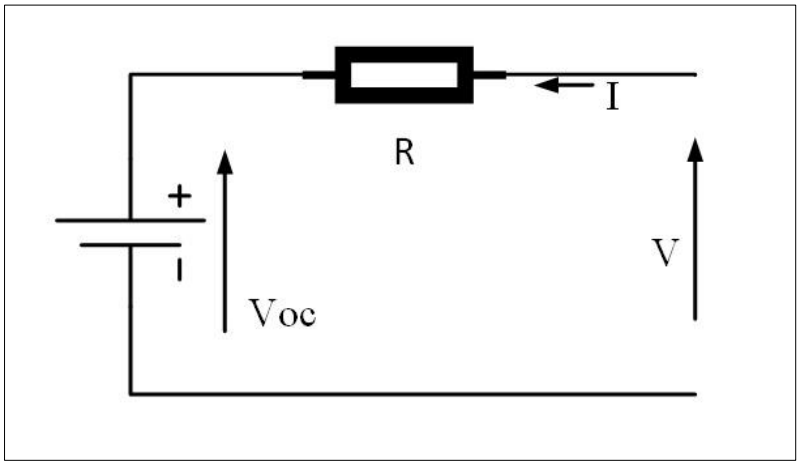

Figure 2.2 Simple Model of the Battery

The CIEMAT model is considered in this report which is the most correct and detailed model of the battery unit. A general relationship between the voltage and current for charging and discharging is shown in equation 2.1 and displayed in Figure 2.2.

$$V = V_{oc} \pm I R \tag{2.1}$$

Where I show the current, which is positive in case of charging and negative for discharging case. V_{oc} represents the open circuit voltage and R is the internal resistance which depends on the capacity, the current and the temperature. The CIEMAT model is now analyzed under the variation of current, voltage, state of charge and temperature to describe the behavior of the battery storage unit as a function of charge and discharge [15], [17]. The discharging process is represented using the equation 2.2.

$$V = \left[2.085 - 0.12\left(1 - SOC\right)\right] - \frac{1}{C_{10}}\left(\frac{4}{1+I^{1.3}} + \frac{0.27}{SOC^{1.5}} + 0.02\right) \times \left(1 - 0.007\ \Delta T\right) \tag{2.2}$$

C_{10} represents the capacity at constant current during ten hours ($C_{10}=10I_{10}$), ΔT is the temperature variation which is shown in equation 2.3.

$$\Delta T = T - 25 \tag{2.3}$$

SOC represents the state of charge which is the percentage of capacity available in the battery unit and it can be represented using equation 2.4, while equation 2.5 shows the relationship for the available amount of charge.

$$SOC = 1 - \frac{Q}{C} \tag{2.4}$$

$$Q = I t \tag{2.5}$$

The total amount of charge available for the discharging process can be limited by the current rate and the temperature, so equation 2.6 shows that if the battery discharges with higher current, then the actual battery capacity will decrease. I_{10} represents the discharge current corresponding to C_{10}.

$$\frac{C}{C_{10}} = \frac{1.67}{1 + 0.67\left(I / I_{10}\right)^{0.9}}\left(1 + 0.005\,\Delta T\right) \tag{2.6}$$

In a similar way, the charging process can be represented using equation 2.7.

$$V = \left[2 - 0.16SOC\right] + \frac{1}{C_{10}}\left(\frac{6}{1+I^{0.86}} + \frac{0.48}{(1-SOC)^{1.2}} + 0.036\right) \times \left(1 - 0.025\ \Delta T\right) \qquad (2.7)$$

The state of charge in this case can be represented using equation 2.8, where η_C shows the efficiency conversion and can be written as shown in equation 2.9.

$$SOC = SOC_0 + \frac{\eta_C Q}{C} \qquad (2.8)$$

$$\eta_C = 1 - \exp\left[\frac{20.73}{I/I_{10} + 0.55}\left(SOC - 1\right)\right] \qquad (2.9)$$

Finally, the over voltage equation for the model can be shown using equation 2.10.

$$V = V_g + \left(V_{ec} - V_g\right)\left[1 - \exp\left(\frac{0.95C - Ah_{restored}}{I\tau}\right)\right] \qquad (2.10)$$

Where V_g is the gassing voltage represented in equation 2.11 and V_{ec} is the final charge voltage represented in equation 2.12.

$$V_g = \left[2.24 + 1.97\ln\left(1 + \frac{I}{C_{10}}\right)\right]\left(1 - 0.002\,\Delta T\right) \qquad (2.11)$$

$$V_{ec} = \left[2.45 + 2.011\ln\left(1 + \frac{I}{C_{10}}\right)\right]\left(1 - 0.002\,\Delta T\right) \qquad (2.12)$$

$Ah_{restored}$ is the ampere-hours stored in the battery unit with respect to the capacity (C) for the charging current (I) during this hour. Lastly, the time constant (τ) can be shown using equation 2.13.

$$\tau = \frac{17.3}{1 + 852(I/C_{10})^{1.67}} \qquad (2.13)$$

A generic battery model from Simulink library has been chosen for the simulation stages as represented in Figure 2.3. The figure also shows a bus selector which can be used to pick out the output parameters of the battery storage unit.

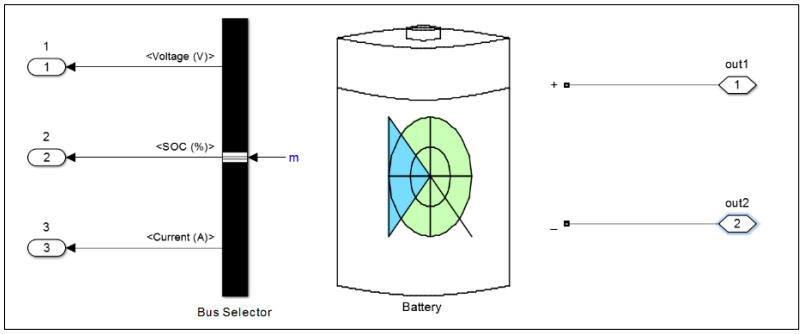

Figure 2.3 Simulink Model of the Battery Unit

The battery model has several options which are adjusted to set a specific type of battery unit, that can be used in the simulation processes. The generic battery model consists of several tabs such as the parameters tab and the discharge tab. In the parameters tab, a desired type of battery can be chosen from the four common types. The nominal voltage, initial state of charge, rated capacity and the battery response time can also be changed using the parameters tab. In the discharge tab the maximum capacity, nominal discharge current, fully charged voltage, capacity at nominal voltage, internal resistance and exponential zone can be altered. Moreover, the battery characteristics can also be plotted by adjusting the discharge currents. The battery characteristics for the default values of the generic battery model is displayed in Figure 2.4 [18].

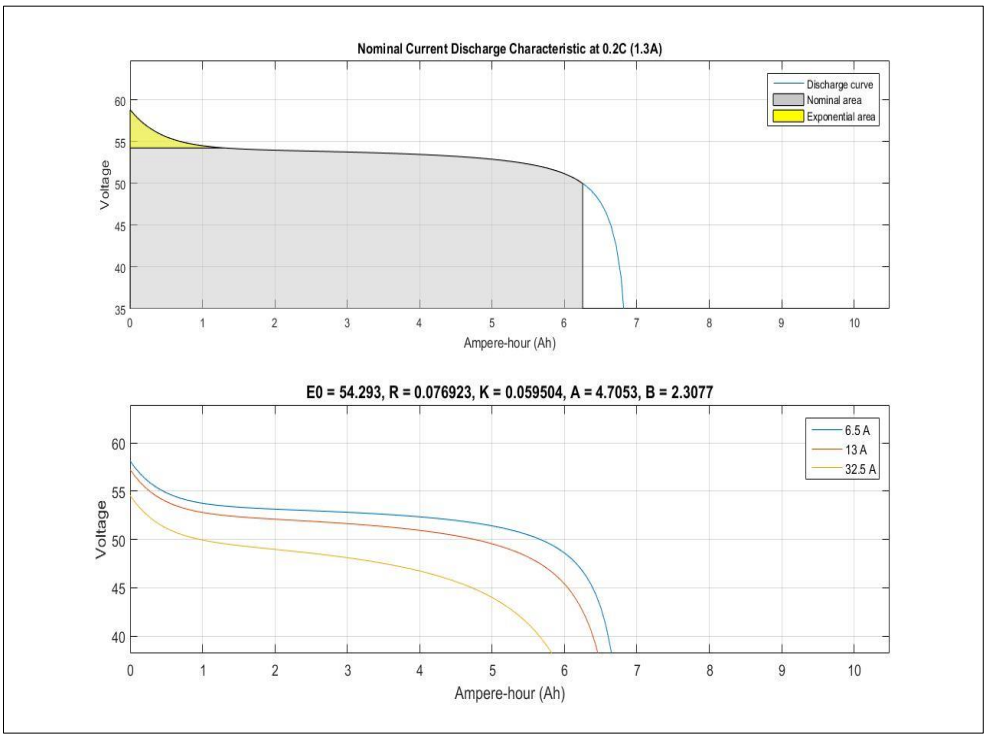

Figure 2.4 Battery Bank's Characteristics

2.4. Super Capacitor

Capacitors is a type of electrical component which stores energy by using the electric field created by charge movements. Capacitors can charge and discharge in a fast manner and will not degrade because of overcharging and over discharging due to the absence of any chemical substance. Super capacitors are special types of capacitors which can be used as another type of energy storage devices. Recently the super capacitors have gained much interest due to their high-power densities and lower energy densities. Super capacitors of capacitance up to 1000-5000F from various companies such as Maxwell, EPCOS, Ness, Chemi-Con, Power systems and Nippon are available in the market today [19]. The usage of super capacitors is becoming wide due to their capability of pumping high currents at lower voltages and providing the possibility of storing 100 times more power than the battery banks. Super capacitors are being utilized in different applications such as solar generation, wind generations and hybrid vehicles [20]. The modelling of the super capacitors can be carried out by considering a classical model which comprises of a double layer capacitance with an equivalent parallel and equivalent series resistance as shown in the Figure 2.5.

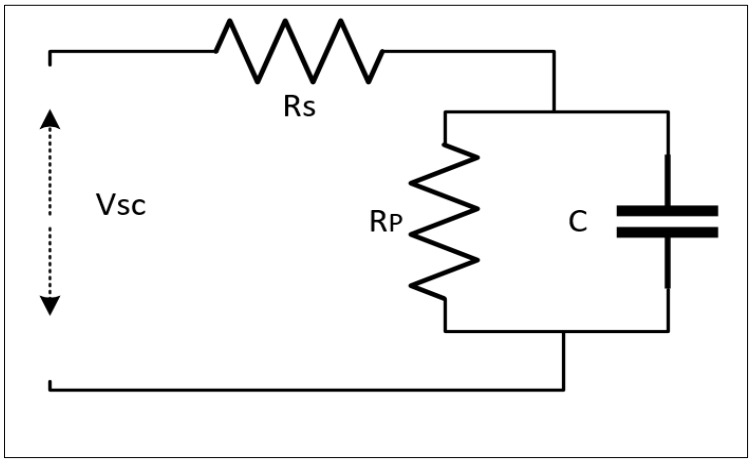

Figure 2.5 Classical Model of the Super Capacitor

The sum of energy drawn from a super capacitor can be directly linked with the voltages as given in equation 2.14. So, when the super capacitor absorbs energy it will start increasing the voltage level and the voltage level falls when the super capacitor delivers some amount of power.

$$E_{SC} = \frac{1}{2} C (V_{initial}^2 - V_{final}^2) \tag{2.14}$$

By considering the equation, C shows the capacitance of the super capacitor, $V_{initial}$ and V_{final} represents the initial and final voltages and E_{sc} is the energy stored or delivered by the super capacitor. The amount of energy demanded by the load can be fulfilled by integrating several units of super capacitors in series or in parallel. The voltage across the terminals are determined by the total number of capacitors connected in series combination with each other, while the total capacitance and total resistance of all the connected units can be determined using equation 2.15 and equation 2.16 [21].

$$R_t = n_s \frac{R_s}{n_p} \tag{2.15}$$

$$C_t = n_p \frac{C}{n_s} \tag{2.16}$$

Where R_p and R_s are the equivalent series and parallel resistances, while C_t and R_t represents the total resistance and capacitance of the super capacitor. n_p is the total number of strings in parallel and n_s is the total capacitors connected in series. Figure 2.6 represents the total number of series connected units and total number of strings formed.

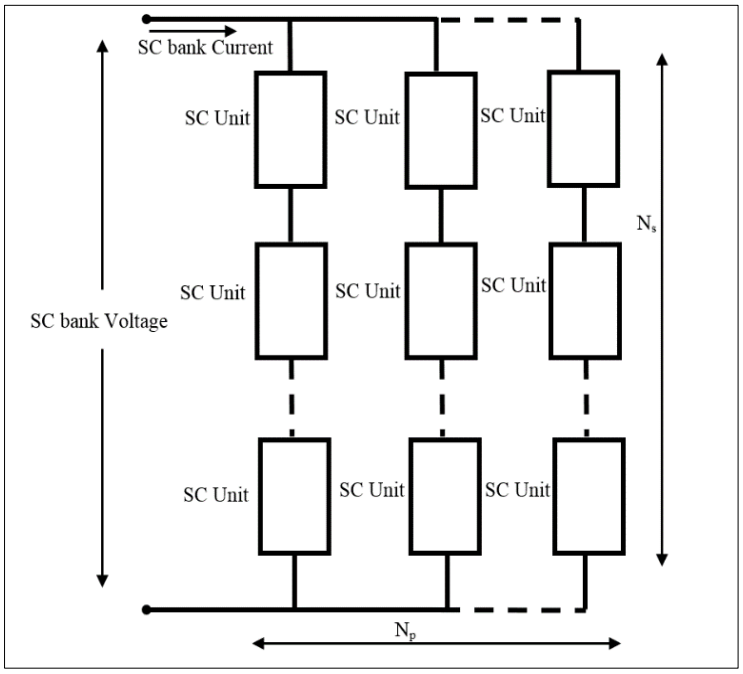

Figure 2.6 Series and Parallel Connected Super capacitors

2.5. Other Types of storage units

Fuel cell and Superconducting Magnetic Energy Storage (SMES) are several other types of energy supplying device. These devices can be used in various applications but the usage of these devices in down-hole application may face lots of challenges. A fuel cell is a device which converts chemical energy from a fuel into electrical energy through chemical reactions of hydrogen and oxygen. Over the past few years, various types of fuel cells are utilized in various applications such as electric vehicles and residential power systems due to their small size and light weights [22].

The main components of a fuel cell plant include a fuel stack, a fuel processing unit and a power conditioning unit. The processing unit produces hydrogen fuel by using hydrocarbons. The fuel cells deliver an output dc power which is passed through a power conditioning unit to make the dc power useful for the various types of dc and ac loads. The working temperature of the fuel cell plants are very low, which is beneficial for utilizing them in residential and vehicular application [23]. The usage of fuel cells can be limited in down-hole application with the increase in depth, where the temperature and pressure keeps on increasing with the increase in depth. Different types of fuel cell modeling methods have been done in the literature which has been discussed in [23], [24], [21].

SMES system is a latest technology which stores the energy in the form of magnetic field, when a dc current is passed through a superconducting coil. The superconducting coil is cooled cryogenically which allow their application in dc microgrids. The power density of the SMES is 10 times higher than the lead acid batteries [25, 26]. Using SMES in down-hole application needs a thorough investigation of the storage system regarding the temperature and pressures issues, which can make the system very complicated.

2.6. Dump-loads

Dump-loads are types of loads which are used to dissipate excess amount of energy coming from the source. The dump-loads are usually heating elements which are resistive in nature and they are connected to dissipate the surplus amount of electric power to prevent other units from damaging and failures. These loads can be utilized in an intelligent way to prevent energy storage units from overcharging such as the batteries. The dump-load is activated to absorb the excess power, when the storage unit is fully charged which allows the storage unit to work within its operating limits. The dump-load can be a water heater or an air heater or any other

type of load which is resistive in nature whereas, an inductive load is avoided to be used as a dump-load [27].

The importance of using a dump-load is immense in the proposed model which has been investigated in this research work. The dump-load has been connected by using various methods to study and analyze the response of the system. In the literature, the dump-loads have been utilized for various type of renewable system configurations. These loads has been used for the protection of battery banks and for making intelligent energy & power management strategies in various standalone power generations systems as discussed in [28], [29], [30], [31]. In this report the dump-load is considered to be connected in parallel across the filter capacitor and ideally the dump-load must be capable of absorbing the maximum amount of power generated from the source side using PMSG by keeping a constant dc link voltage. A correct approximation for the dump-load resistor is important to be made in order to dump all the excess amount of power from the source to the dump-load. The value of a dump-load connected in parallel to a dc load for keeping a constant dc link voltage across the filter capacitor can be approximated using equation 2.17. The equation has been derived for no load condition, where all the generated power from the source can be dissipated in the dump-load [30].

$$R_{dump} = \frac{V_{dclink}^2}{P_{source-max}} \tag{2.17}$$

Chapter 3 System Components and Structure

In this chapter the basic structure of the system is presented. The main objective of the system is to supply power to the down-hole dc loads by keeping constant dc voltages. As discussed in the previous sections, the system uses the kinetic energy from the flow to generate electrical energy by using a turbine coupled to a generator connected to a rectifier. The electrical power from the rectifier comes out in an uncontrolled manner which can vary depending on the fluctuating nature of flow and load demand. In this way, the dc voltage across the filter capacitor also varies. Therefore, the system uses dedicated dc-dc converters to make a controllable electrical power supply for the down-hole devices. These dc-dc converters are used to control the power flow in the system between all the connected components by keeping a constant voltage across the load. The power flow of the system is controlled by making intelligent control loops for the dc-dc converters which reacts to any kind of change in the system. The working of each system component is briefly described in this chapter and Figure 3.1 depicts the block diagram of the proposed system using all the components. The block diagram shows a turbine connected to a low power three phase permanent magnet synchronous generator, which is further connected to an uncontrolled diode rectifier. The dc-dc converters are connected across a large filter capacitor to transfer the power from the source side to the loads.

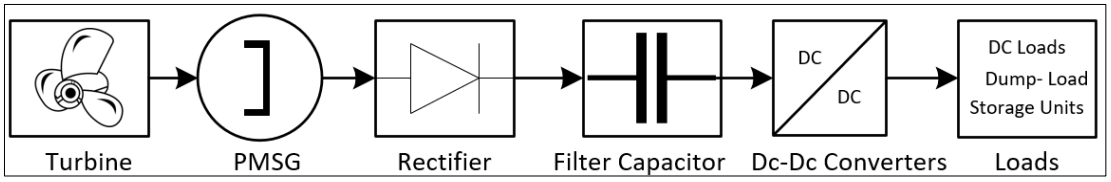

Figure 3.1 Block Diagram of the System

3.1. Turbine

Turbine is a rotating mechanical device which is used to extract energy from a flowing fluid, wind or gas. The energy is extracted in the form of kinetic energy and converts it into mechanical energy which is further used for generating electrical power. There are various types of turbines such as wind turbines, water turbines and steam turbines. A hydraulic type of turbine is the subject of interest in this project, which is a normally a water turbine. It is a type of turbine which can convert both the kinetic and potential energy of a fluid into mechanical energy and its main function is to drive an electrical generator. Hydraulic turbines are generally classified

as impulse turbines (Pelton and Turgo turbines) and reaction turbines (Francis, Kaplan and Propeller turbines). A suitable type of turbine can be selected depending on the nature of the flow. The mounting of these turbines in the downhole application is a challenging task to be done. The turbine coupled with a generator must be placed in such a way that it should not interrupt the flow of a fluid or gas inside the well. As the diameter of the well is not very large, so an intelligent approach is required for the placement of the turbine. A method which can be suggested, is to place the turbine generator in an additional tube of small length which is integrated in parallel to the well. In this way, the parallel path will not interrupt the flow but it will only capture some part of the flowing fluid. The various types of hydraulic turbine are displayed in Figure 3.2.

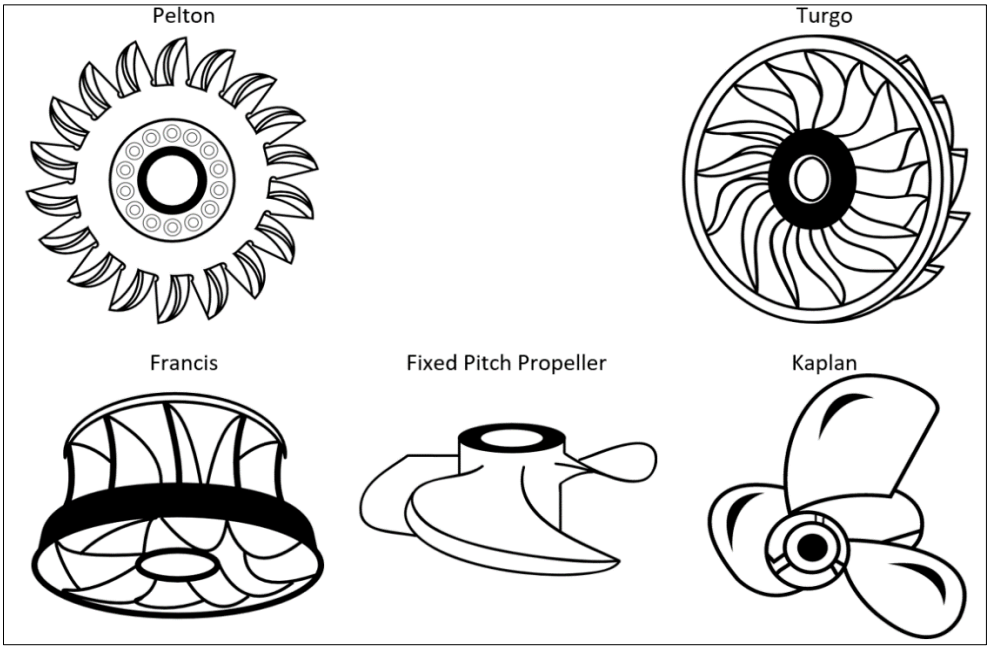

Figure 3.2 Types of Turbine

The amount of kinetic energy from the fluid flow depends on the flow rate and the size of the turbine, so the power extracted from the flow depends on various factors such as, the density, the flow rate and the head. In steady state condition the hydraulic power available from a turbine can be expressed as shown in equation 3.1.

$$P_{Flow} = \rho g Q H \tag{3.1}$$

Where g is the acceleration due to gravity (m/s^2), ρ is the density of the fluid (kg/m^3), Q is the fluid flow rate (m^3/s) and H is the head (m). The power from the fluid flow cannot be transferred

into mechanical power with hundred percent efficiency. So, the available mechanical power at the output of the turbine depends on its efficiency. The power coefficient C_p is termed as the efficiency of the turbine which is the ratio between the output mechanical power and the hydraulic power as shown is equation 3.2 [32, 33].

$$P_T = C_p \times P_{Flow} \tag{3.2}$$

The power coefficient of the turbine is usually a nonlinear term which depends on the tip speed ratio and the flow rate of the fluid and it is different for various types of turbines.

3.2. Permanent magnet synchronous generator

Permanent magnet synchronous generator is a type of ac synchronous machine, which utilize permanent magnets instead of excitation windings. Figure 3.3 shows a permanent magnet synchronous machine having permanent magnets on the rotor and three phase sinusoidally distributed windings in the stator.

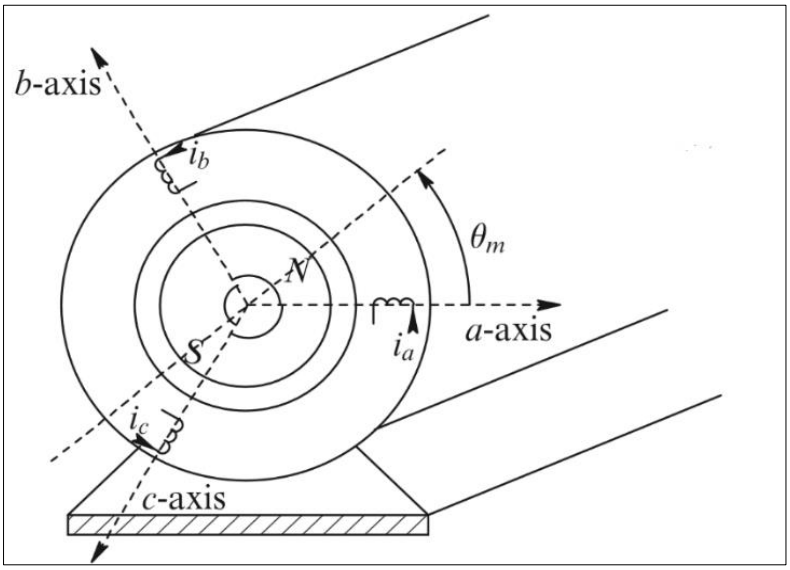

Figure 3.3 Permanent Magnet Machine [34]

The permanent magnet synchronous machines (PMSM) are classified into two types, depending on the mounting of the magnets on the rotor. The first type is made with surface-mounted permanent magnets, which makes the rotor non-silent because the reluctance is constant. In the second type the rotor is made salient by using interior permanent magnets which results in an unequal reluctance in the machine [34]. Figure 3.4 shows the position of the permanent magnets for the surface-mounted and interior permanent magnet machines.

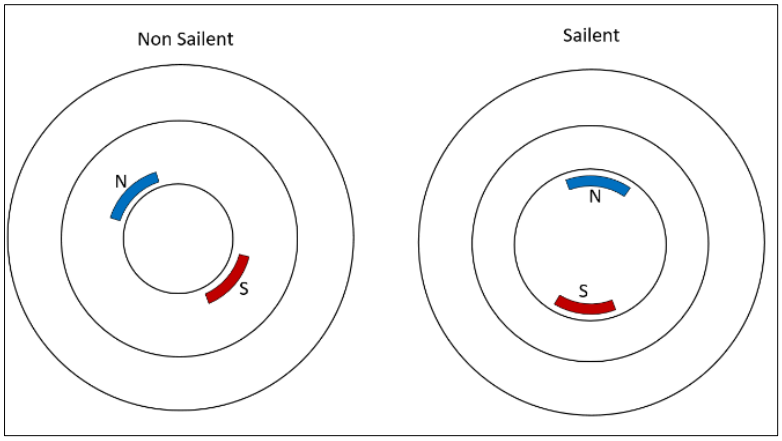

Figure 3.4 Salient and Non-Salient PMSM

The advantage of replacing the rotor windings with permanent magnets is that it reduces the copper losses which occurs due to the rotor windings. This will increase the efficiency of the machine and it will also allow easy methods for cooling the machine [35]. A physical model of the permanent magnet machine has a three phase stator windings and a field winding in the d axis of the rotor which is fed from a fictitious current source I_F. The physical model of the machine is represented by using equation 3.3 and equation 3.4, while the flux linkages are shown in equation 3.5 and equation 3.6.

$$U^s_{s\alpha} = R_s I^s_{s\alpha} + d\frac{\varphi^s_{s\alpha}}{dt} \tag{3.3}$$

$$U^s_{s\beta} = R_s I^s_{s\beta} + d\frac{\varphi^s_{s\beta}}{dt} \tag{3.4}$$

$$\varphi^s_{s\alpha} = L_{s\alpha s\alpha}(\theta) I^s_{s\alpha} + L_{s\alpha s\beta}(\theta) I^s_{s\beta} + \varphi_{\alpha f}(\theta) \tag{3.5}$$

$$\varphi^s_{s\alpha} = L_{s\beta s\alpha}(\theta) I^s_{s\alpha} + L_{s\beta s\beta}(\theta) I^s_{s\beta} + \varphi_{\beta f}(\theta) \tag{3.6}$$

To make an equivalent model of the permanent magnet synchronous generator the three phase ac quantities are transformed into alpha-beta axis, which is then further transformed into d-q axis. The reason of modelling the permanent magnet synchronous generator using the d-q axis is because the machine can be modelled using dc quantities instead of the ac quantities. The transformed model of the machine is presented using equation 3.7 and equation 3.8.

$$U_{sd} = R_s I_{sd} + (L_d)\,d\frac{\varphi_{sd}}{dt} - \omega L_q I_{sq} \tag{3.7}$$

$$U_{sq} = R_s I_{sq} + (L_q)\,d\frac{\varphi_{sq}}{dt} + \omega\left((L_d I_{sd}) + \varphi_m\right) \tag{3.8}$$

The voltage balance equations can also be shown by using Figure 3.5.

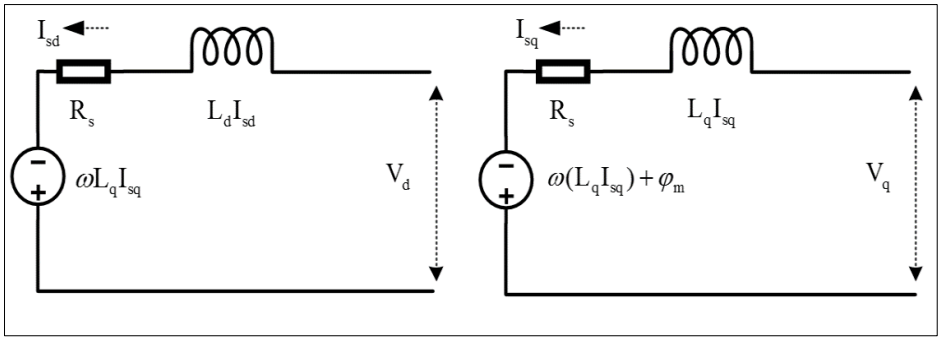

Figure 3.5 Equivalent Circuit of Voltage Balance Equations

The relationship between the mechanical torque of the turbine and the electromagnetic torque of the generator is important to discuss which describes the transfer of the mechanical power from the turbine to the PMSG. Equation 3.9 shows the relationship of the mechanical system acting on the combined inertia J of the turbine and the generator. The mechanical system either accelerates or decelerates with a speed ω_r depending on the generated torques. M_L and M_e represents the mechanical torque of the turbine and the electromagnetic torque of the generator respectively.

$$J\frac{d\omega_r}{dt} = M_L - M_e \tag{3.9}$$

A permanent magnet synchronous machine block can be used from the Simscape library of Simulink, which is modelled using the d-q voltage equations of the machine as discussed above. The block takes input in the form of mechanical torque, which is provided by the turbine and the output of the block consist of a vector containing of several measurement signals. The measurement signals depend on the selected model of the machine. A bus selector is generally used from the Simscape library to obtain a desired measurement signal from the block. The input torque of the machine specifies whether the machine is being utilized in a motor mode or in a generator mode. A negative torque shows that the machine is being operated in a generator

mode. Furthermore, three input/output terminals are also available, which can be connected to a rectifier or an inverter depending on the various types of applications. The block has been presented in Figure 3.6 including a bus selector block for getting the measurement signals.

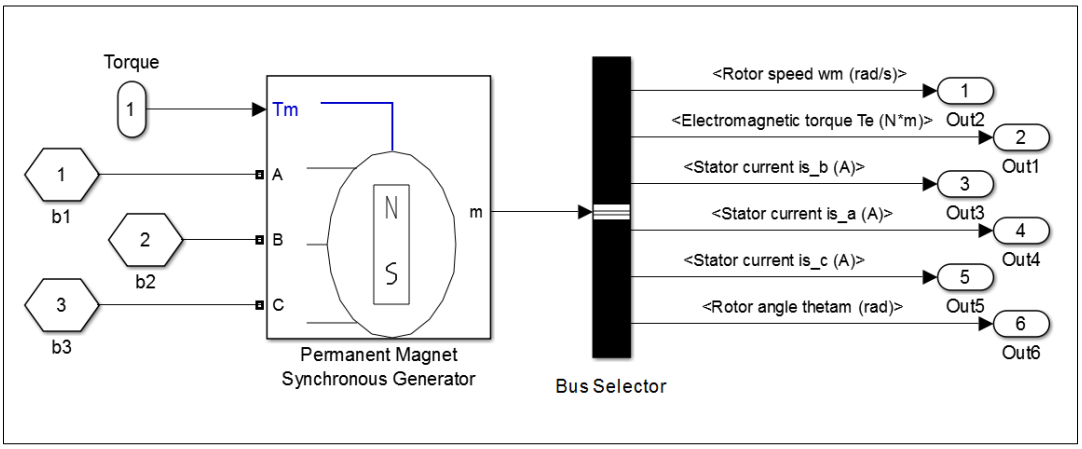

Figure 3.6 PMSG Block including a Bus Selector

3.3. Power Electronics Converters

The power converter used for the stable operation of the system consists of an uncontrolled diode rectifier as shown in Figure 3.7, a filter capacitor and dedicated dc-dc converters for the storage units and the dump-loads. The dc-dc converters used for the storage units and the dump-loads depends on the control strategy of the system. For the system discussed in this report, a buck-boost converter is used for the storage units, while for the dump-loads a MOSFET switch or a dc-dc buck converter is being utilized.

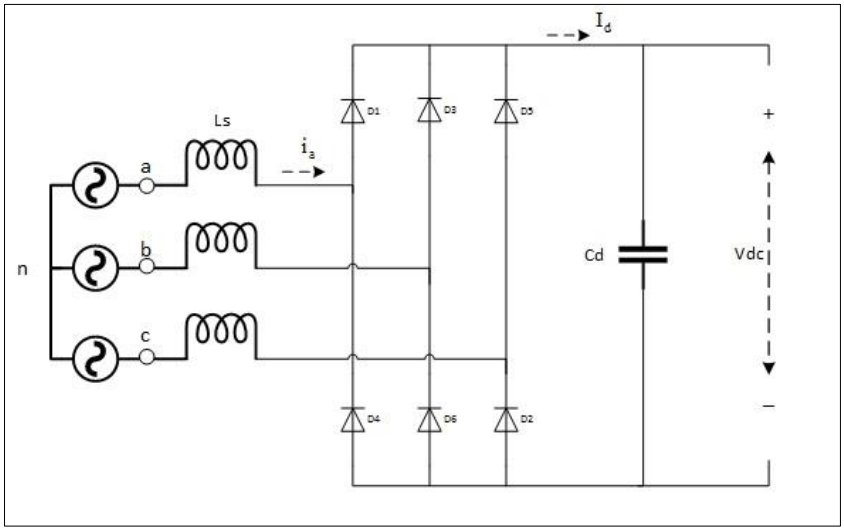

Figure 3.7 Three Phase Diode Rectifier

The buck-boost converter is used in a bi-directional way, to operate the storage unit in both charging and discharging mode. The flow of current can be either from the storage unit or towards the storage unit, which means that the current will be either positive or negative. Figure 3.8 shows the working of a bi-directional buck-boost converter. The buck-boost converter works either in a boost mode or in a buck mode for the bi-directional flow of power. The converter operates as a dc-dc boost converter when the power flows from the storage unit towards the dc link capacitor. In the similar manner, when the power flows from the dc link towards the storage unit then it operates as a dc-dc buck converter. The flow of power from the either side can be seen in Figure 3.8.

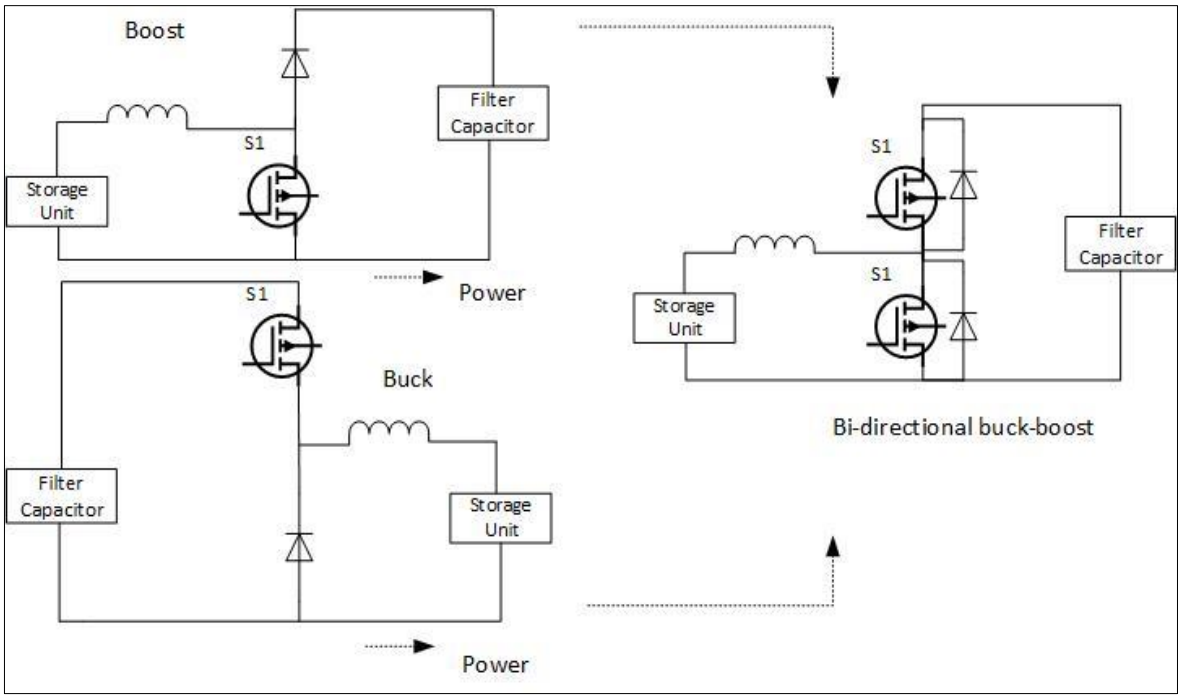

Figure 3.8 A Bi-Directional Buck-Boost Converter

In case of a dump-load the power flows in one direction only. So, the current only flows from the source side to the dump-load side in case of having a dump-load connected to a switch or a dump-load connected via buck converter. A buck converter used for the dump-load has been displayed in Figure 3.9. A large filter capacitor is usually connected in between the rectifier and the dc-dc converters. The potential across this capacitor is termed as dc link in this report, where the dc load, the dump-load converter and the storage unit converter are connected in parallel to each other. The value of the filter capacitor is kept very large to ripple out the dc voltages coming from the rectifier. The bi-directional buck-boost converter for the battery storage unit

and the dc-dc buck converter for the dump-load has been utilized in the system to make an intelligent power management system discussed in the later sections of the report.

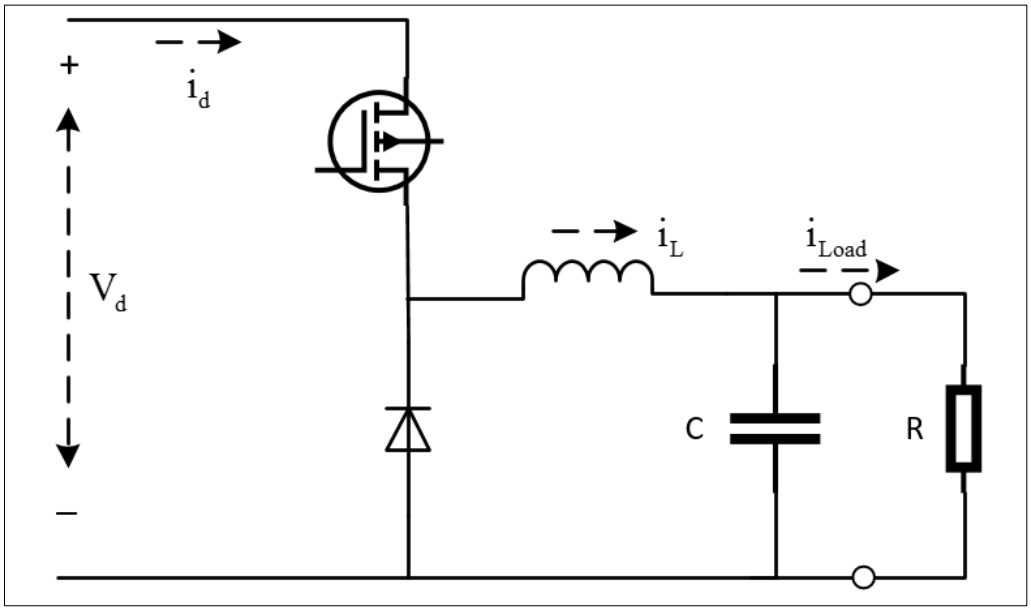

Figure 3.9 Dc-Dc Buck Converter

Chapter 4 Storage Units and Dump-Load based Literature Review

There are several solutions of making an intelligent energy management system using a turbine, a PMSG generator, a dc load, a dump-load and a storage unit. The input power coming from the turbine is uncontrollable for the down-hole application, which means that controlling the pitch angle of the turbine is not applicable in this project. The main aim of designing the system is to keep a constant voltage across the dc load. To fulfill the objective of keeping a constant dc link voltage, initially the system can be considered similar to standalone power generating system. To find the best possible solution for the down-hole power generating system, various types of energy management configurations have been studied which are related to standalone wind power systems and dc grids. The storage units are used in almost all the power system configurations found in the literature. In the case of generating power for deep down-hole applications, the harsh environment of the down-hole can eliminate the possibility of using any kind of storage unit.

4.1. Battery Unit and a Dump-load

The first energy management configuration uses a battery storage unit and a dump-load to keep a constant voltage across the load. This is the most common type of method for making an energy management strategy which has been accomplished for different types of system applications. This management strategy is mostly used in the wind power generation systems for supplying power to the ac/dc loads. The power generation system can either be in standalone mode or in a grid connected mode. In this type of power generation systems, the generated power from the turbine is supplied to the ac loads by keeping constant voltages at the input side of the inverter. In other words, it can be summarized that a power balance has to be maintained between the generated power from the source and the consumed power of the load. Therefore, the battery storage unit and the dump-load plays a vital role for maintaining the power balance [36], [28], [29], [31], [37], [38]. The authors have used different types of control algorithms for the battery bank and the dump-load for maintaining a constant dc link voltage.

In this type of system configuration, the battery storage unit and the dump-load are connected in parallel to the dc load for keeping a constant voltage across it. The power generated from the source is always variable and continuous. It can either reach to a very high value or it can fall to a very low value. In either case the battery bank has to deliver or absorb some amount of

power by charging or discharging itself to keep a constant load power. The battery bank storage unit have some defined operating limits, which has to be maintained during the charging and discharging processes to allow longer life times and to prevent it from failures. The operating limits of the battery bank can be monitored by keeping the status of its state of charge (SOC) or the current flowing through it. The maximum and minimum limits of these parameters define the allowable range of operation for the battery bank. When the battery bank reaches its maximum allowable limit then the dump-load must be activated, in order to consume the excess amount of power coming from the source side. The complete structure of system in this type of configuration can be displayed in Figure 4.1, which shows a PMSG coupled to a turbine with a rectifier, dedicated dc-dc converters for the battery bank and the dump-load and several types of dc loads connected to the dc link.

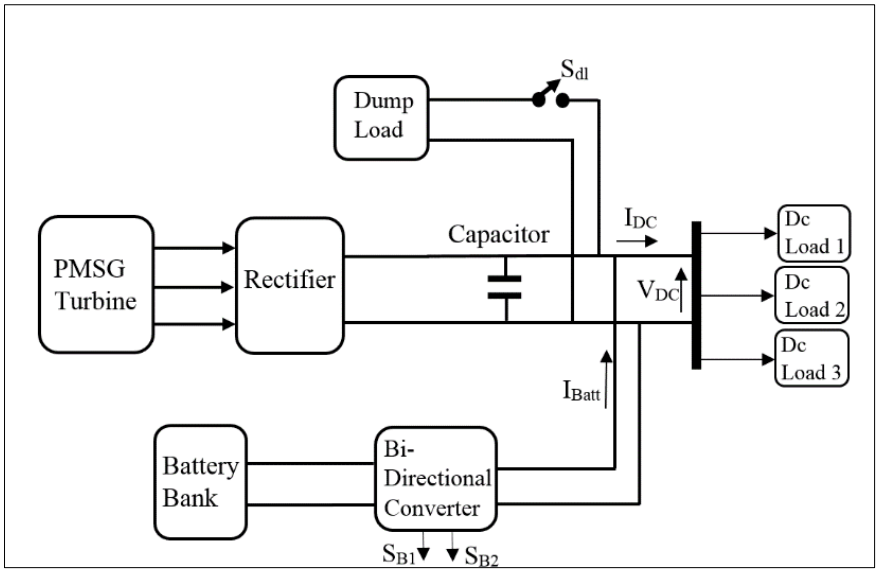

Figure 4.1 System with a Battery Bank and a Dump-Load

From the figure, it can be seen that PMSG turbine is the main source of power which is connected to an uncontrolled rectifier to convert the ac power into dc power. A bi-directional buck-boost converter is used for the battery bank, while the dump-load is connected in series to a switch. By controlling the bi-directional buck-boost converter and dump-load switch, the dc voltage across the filter capacitor is kept constant. The power balance between the source and the load is the key for making this energy management strategy. Two cases must be considered for balancing the power of the whole system. The first case happens when the generated power from the source is either equal or greater than the required power of the load ($P_{turbine} \geq P_{load}$). In this case the battery bank has to absorb the excess power ($P_{turbine} - P_{load}$) which is not required

by the load. The battery bank will consume all the excess power by charging to a certain maximum limit. As mentioned earlier the control algorithm uses the battery parameters to keep the status of the maximum and minimum operating limits of the battery bank. The power balance equation for the first case can be written by using equation 4.1. In equation 4.2, all the power terms have been directly replaced with the currents because the voltage is constant and the current flows and varies from the source side to the load, which also changes the power.

$$P_{turbine} = P_{batt} + P_{load} + P_{dumpload} \tag{4.1}$$

$$I_{turbine} = I_{batt} + I_{load} + I_{dumpload} \tag{4.2}$$

The second case happens, when the generation of power from the source side is less than the demanded power of the load ($P_{turbine} < P_{load}$). Here the deficit power must be supplied by the storage unit which means that the battery bank tends to reverse its flow and start discharging to meet the load demand [39], [38]. Various types of control algorithm can be found in the literature which uses the battery parameters to design the control loops for the bi-directional buck-boost converter and the dump-load controller.

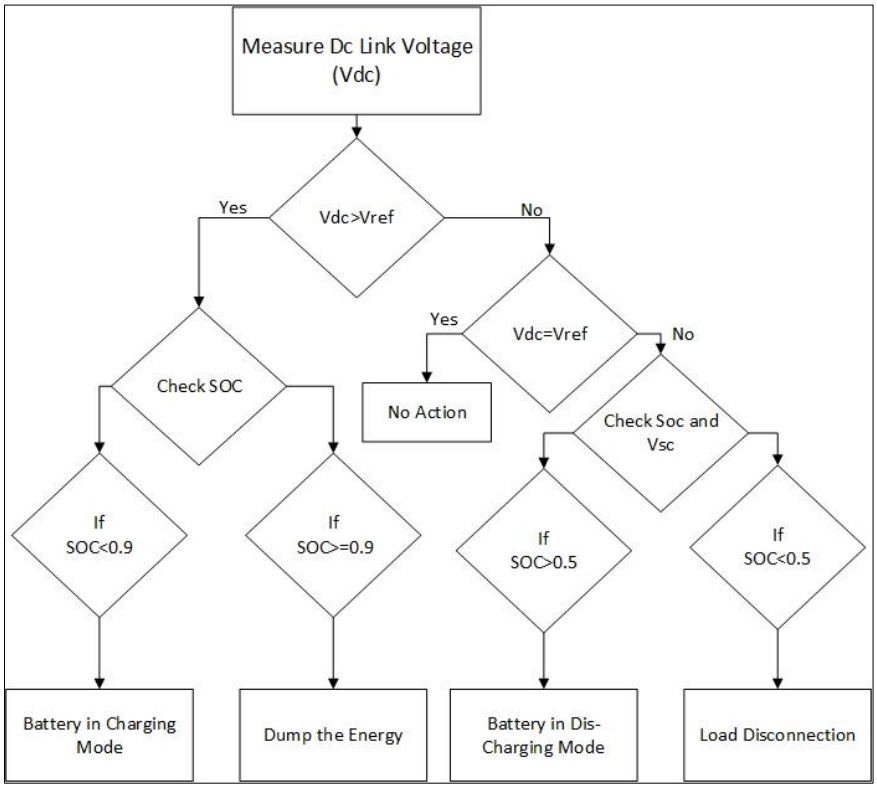

Figure 4.2 Control Algorithm using SOC of the Battery Bank

The most common way for controlling the battery banks converter is to keep the status of the state of charge of the battery storage unit. In this control method, the operating limits of the battery bank is based on its state of charge (SOC) which must be kept in a certain allowable range (50-90%). The SOC of the battery bank must be kept within this range to avoid it from over charging and over discharging. Preventing the battery bank from over charging and discharging will allow the battery bank to have longer life times. So, when the SOC of the battery bank reaches its maximum limit, then the dump-load controller is activated for dumping the excess power in the form of heat. If the SOC of the battery bank falls to the minimum limit, then load shedding has to be performed or the dc loads must be completely disconnected from the system to avoid further failures [29], [40]. The proposed control strategy is indicated in Figure 4.2.

4.2. Battery Unit and a Super Capacitor

In this energy management scheme a hybrid energy storage unit has be utilized by combining a battery bank and a super capacitor. The battery bank and the super capacitor are connected in parallel to each other across the filter capacitor by using dedicated dc-dc converters as shown in Figure 4.3.

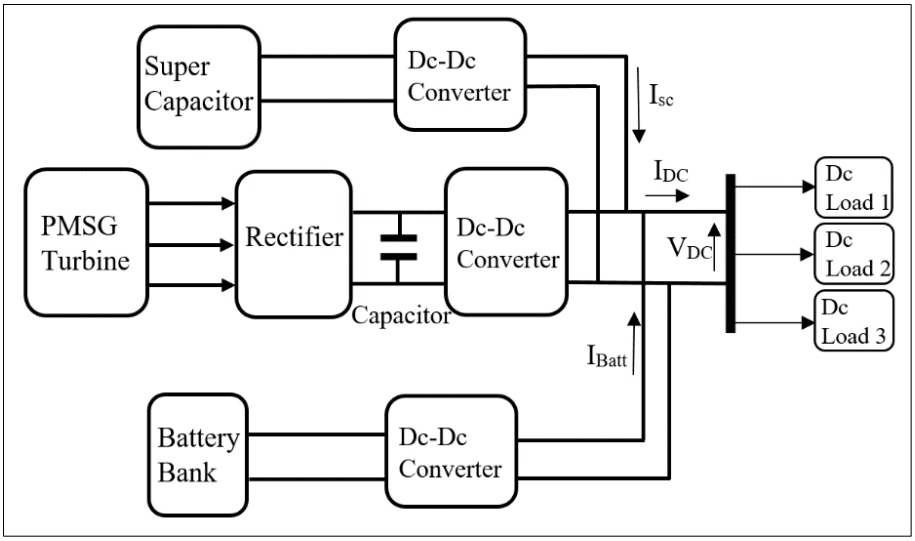

Figure 4.3 System with Hybrid Storage Unit

The battery bank has the characteristic of having high energy density and low power density, while the super capacitor has a higher power density and low energy density. This difference between the battery bank and super capacitor allows the system to have a smart energy management strategy. In this management scheme the battery bank will be protected from high

current dynamics without over charging and over discharging the super capacitor. Consequently, the life span of both the storage units are increased [19]. The management strategy between the super capacitor and the battery bank has been designed by using various methods found in the literature. In [41], the author has used the hybrid storage unit including a dump-load to make an intelligent energy management system. The algorithm is implemented for maintaining the power balance and improving the performance of battery by increasing its life time. So, the control algorithm keeps the power balance between the sources, the storage units and the loads. When the power difference is greater than zero, the hybrid energy storage absorbs the excess power while it delivers the deficit power to the load when the power difference is less than zero. The control scheme also represents the possibility of the activation of the dump-load, when the battery bank reaches its maximum SOC and the super capacitor reaches its maximum operating voltage. Similarly, if the source power gets lower than the demanded power, the hybrid storage will start discharging. The author has also discussed the possibility of a pitch angle control, which is not applicable in this research work. The key of the control method is to operate the energy storages in such a way that the super capacitor saves the battery bank to operate in high depth of discharge regions. A control algorithm which can be implemented for a hybrid storage unit and a dump-load is shown in Figure 4.4.

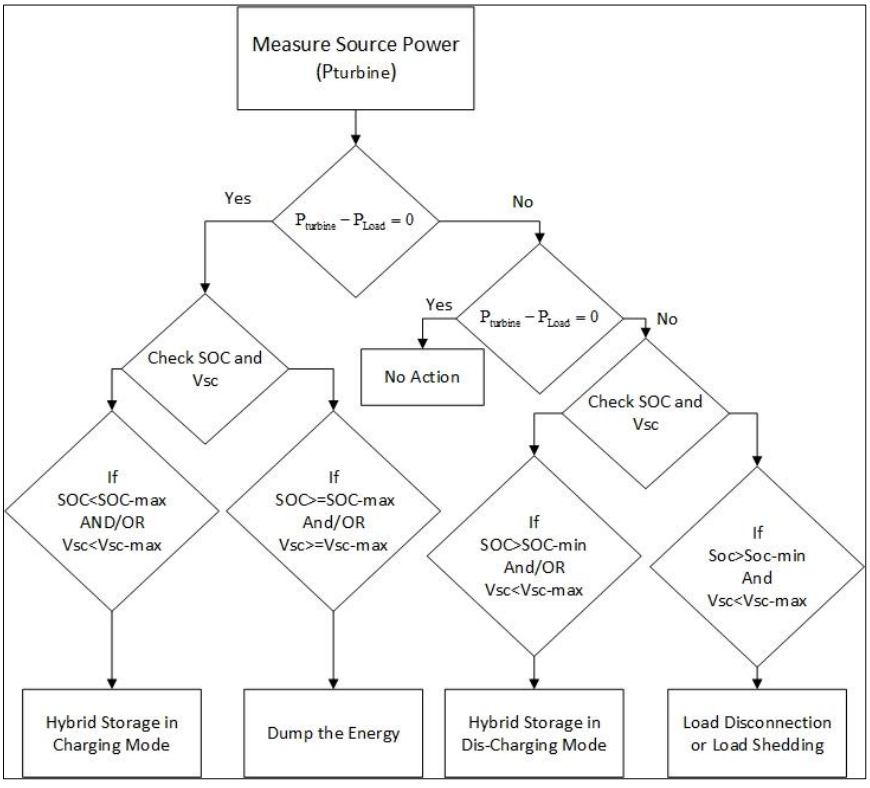

Figure 4.4 Control Algorithm using Hybrid Storage Unit and a Dump-Load

In [42], another type of control scheme has been proposed where the energy of the system is maintained constant to regulate the dc voltages across the load. The energy across the dc link always varies according to the power supplied or consumed by the subsystems. This control scheme uses the super capacitor to regulate the dc voltage when a rapid change occurs in the load as the super capacitor is the fastest energy storage element. Whereas, the battery bank is used to regulate the energy stored in the super capacitor. The energy stored in the super capacitor can be shown using equation 4.3.

$$Y_{dc} = \frac{1}{2} C_{dc} V_{dc}^2 \tag{4.3}$$

According to the power balance equation the sum of all power across the dc bus must be zero, so by taking the derivate of the energy the power absorbed and supplied by all the subsystems can be shown using equation 4.4.

$$Y_{sc}^{\bullet} = P_{sc-ref} + P_{turbine} + P_{battery} - P_{load} \tag{4.4}$$

The reference power for the super capacitor to compensate the rapid change can be expressed as shown in equation 4.5.

$$P_{sc-ref} = P_{sc} - P_{turbine} - P_{battery} + P_{load} \tag{4.5}$$

And finally, the reference current of the super capacitor can be measured by dividing the power with voltage measured across the super capacitor. The battery bank is responsible to regulate the energy of the super capacitor which can be represented using equation 4.6. The energy management algorithm can be constructed similar to the method discussed above and the control loops in this type of control algorithm can be implemented using all the discussed equations.

$$Y_{sc} = \frac{1}{2} C_{sc} V_{sc}^2 \tag{4.6}$$

4.3. Other Possible Types of Energy Management Systems

There are various other methods for making energy management strategies which is more challenging to use and implement in the down-hole applications. A brief discussion about these methods have been presented. These methods include the utilization of fuel cells and superconducting magnetic energy storage using solenoid coil with battery banks. In [43], it has

been discussed how to use a fuel cell plant along with a battery storage unit to supply stable power to the loads. In this method, the excess energy from the source is stored in the form of hydrogen using water electrolysis in the electrolyzer. The produced hydrogen is stored under medium pressure inside the cylinders. In case of having less generation, the fuel cell will use the stored hydrogen to supply the deficit power to the load and the water produced by the fuel cell will be sent back into a water tank for using in electrolyzer. The battery storage unit in this method is used to overcome short-term power fluctuations. The battery bank act much faster than the electrolyzer and the fuel cell, so the battery bank will react to any power difference as long as it operates within its specified limits. By monitoring the SOC of the battery bank, the fuel cell and the electrolyzer can be activated in case the battery bank reaches its maximum or minimum SOC.

A new approach for regulating the power fluctuations and maintaining voltage stability has been discussed in [44]. In this paper a superconducting magnetic energy storage (SMES) is used to make an energy management system between the source and the load.

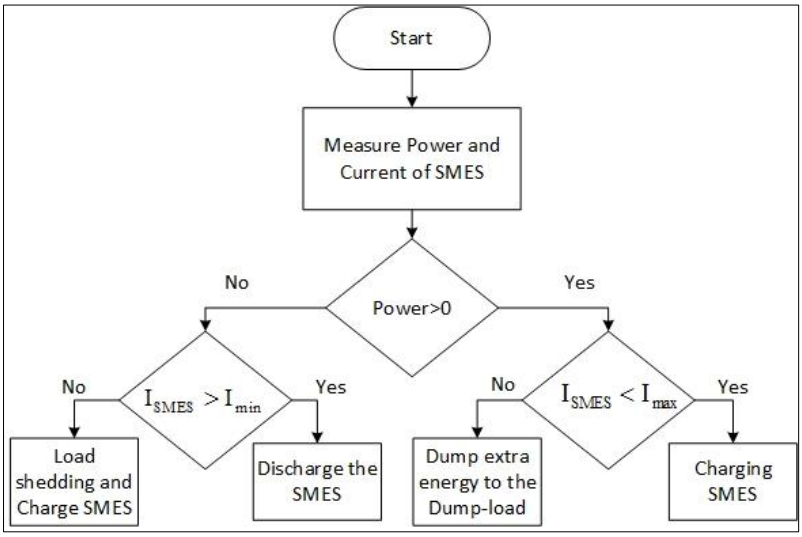

Figure 4.5 Simple Algorithm for SMES and Dump-Load

A dump-load can also be used in this method to allow better stability for the system. The power management scheme used in this method is similar as for the battery bank and dump-load system. In case of having higher input power levels, the SMES coil will absorbs the excess power until its current reaches the maximum limit. If the current reaches its maximum limit than the dump-load is activated. Correspondingly in the case of having less power from the source, the SMES coil will start to discharge up to a lower current limit. Figure 4.5 briefly explains the working of this energy management scheme.

Chapter 5 Implementation of Battery Storage Unit and Dump-Load Controller

In this section a suitable control algorithm has been selected from chapter 4, which is implemented and studied using simulations. An energy management strategy using a battery bank and a dump-load is a suitable control algorithm for the down-hole applications. So, the main focus of this section is to implement an intelligent control strategy for the system using dc-dc converters. The system response with a dedicated battery bank converter and a dedicated dump-load converter is analyzed to keep a stable power across the load. The complete system model has been simulated in Simulink and several simulations have been performed to investigate the stability and the performance of the system. The control scheme of the system is accomplished by controlling a bi-directional buck-boost converter for the battery bank connected in parallel to the filter capacitor. While the dump-load converter and its control loop has been modified for different cases. The dump-load is either connected through a switch parallel to the filter capacitor or it is connected via buck converter. Three different types of methods for the system model has been analyzed and the stability of each method has been conferred using various simulation results. For each method, the control loops for the converters have been described at the beginning, which is then used for simulating the system.

5.1. Method 1: Buck-boost Battery Converter and Dump-load Switch

The first method is studied by connecting the dump-load across a switch and the aim is to dump the excess energy by controlling the duty cycle of the switch when the battery bank reaches its maximum limit. The Simulink model constructed for this case can be displayed in Figure 5.1.

5.1.1. Battery Bank Controller

The battery bank controller is designed to control the switches of the bi-directional buck boost converter for the charging and discharging mode. The control structure for the converter is shown in Figure 5.2. This control loop consists of an outer voltage control loop and an inner current control loop which is used to regulate the dc link voltage. The outer loop takes the difference between the measured and reference voltage and generates a voltage error signal for the first PI controller. The output of the first PI controller will provide the reference value of battery current. The inner loop measures the battery current and substrates it with the reference value of battery current to give a current error signal for the second PI controller. So, the output

of the second PI controller is used to generate the PWM signals for the switches of the bi-directional converter. The status of the battery bank is monitored using the SOC of the battery bank to keep it in the allowable range of operation for the charging and discharging mode. It is important to mention that the negative current of the battery indicates that the battery bank is in charging mode and the positive current indicates the discharging mode. The PI controllers are tuned using the PID Tuner window in Simulink.

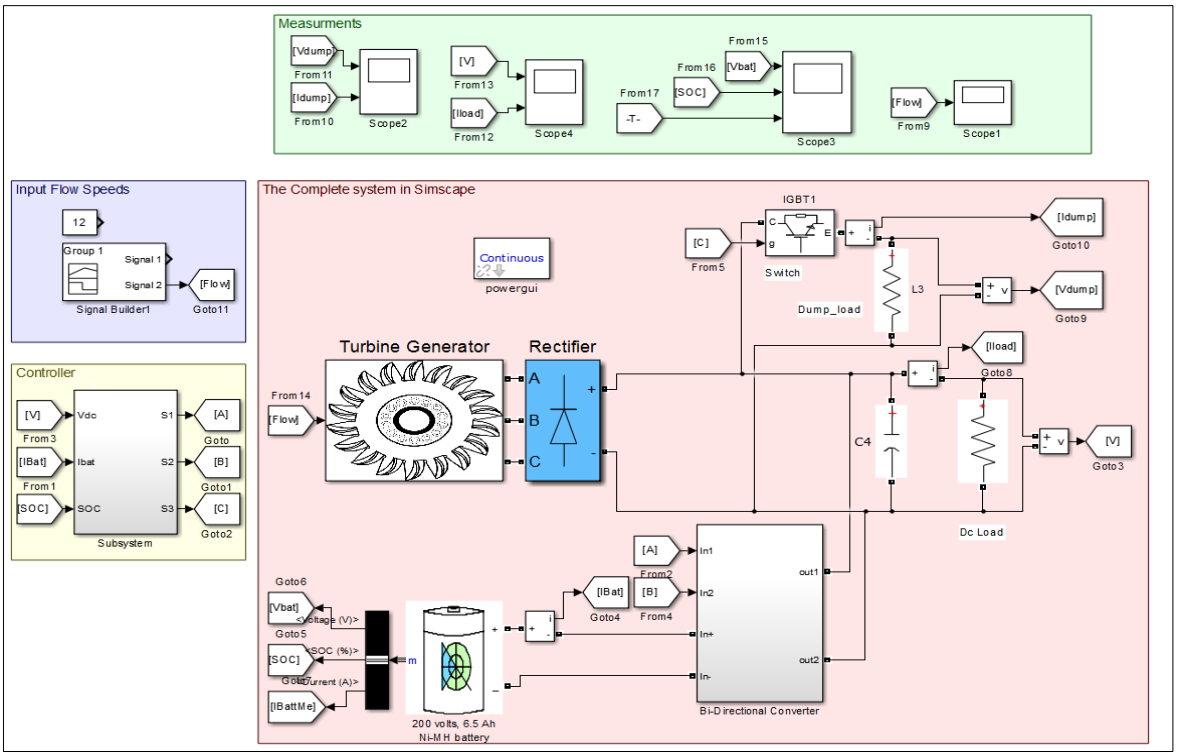

Figure 5.1 Simulink Model for the Method 1

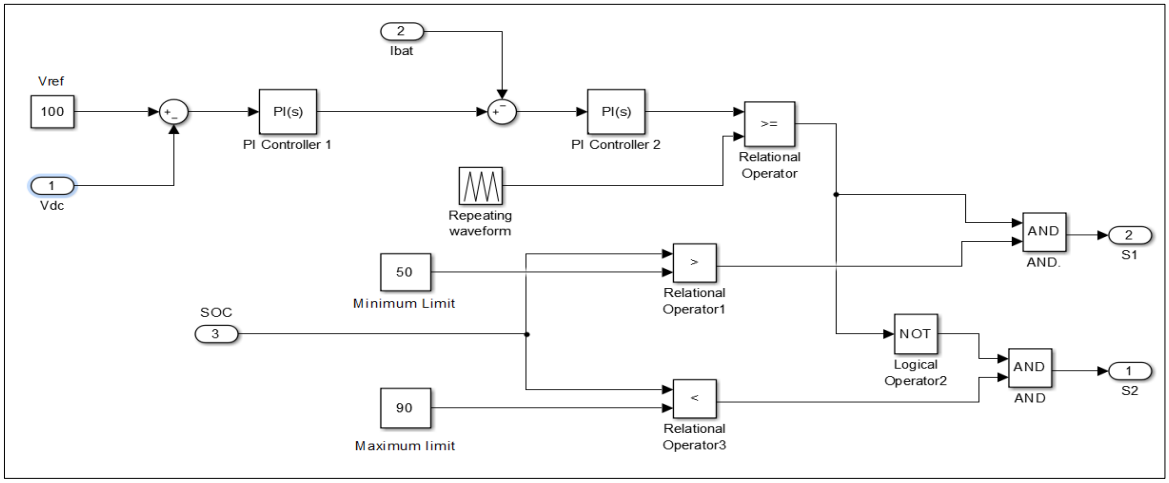

Figure 5.2 Control Loop for the Bi-Directional Dc-Dc Converter

5.1.2. Dump-load Controller

The dump-load controller is activated when the storage unit is fully charged. The dump-load is connected in series with a controllable switch which is turned on when the excess power has to be delivered to the dump-load resistor. The on-off pulses for the switch is generated by comparing the voltage error signal with a predefined waveform. The voltage error signal is generated by taking the difference between the reference voltage and the measured voltage across the dc load. The SOC of the battery bank is taken into consideration while activating this control loop, which means that the controller is switched on when the SOC of the battery bank exceeds its maximum limit. The control loop for the dump-load is shown in Figure 5.3.

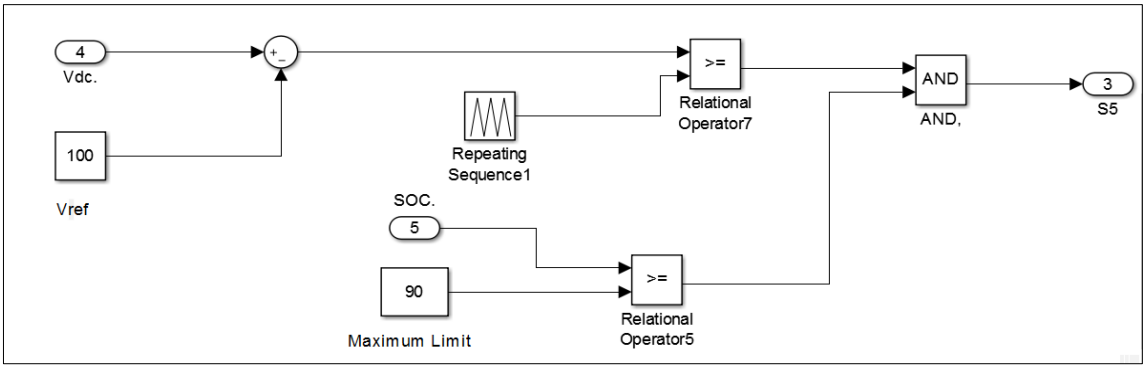

Figure 5.3 Control Loop for the Dump-Load Converter

5.1.3. Results, Simulations and Discussions

The results from simulation of the control system has been recorded for various scenarios to fulfill the objective of the system. The main aim of the simulation is to maintain a fixed voltage of 100 volts across the dc loads. The power flow in the system between the sources and the loads is determined by the flow of electric current. The simulation is carried out for two different scenarios. The first scenario is to observe the voltage stability across the dc link for variable flow rates and a constant dc load. The second scenario is to study the system for a fluctuating load demand, by keeping the flow speed constant. More over the results for the case of a dump-load activation has been obtained as well.

5.1.3.1. Variable Flow Speed Without the Activation of the Dump-load

To study the response of the system, the first scenario of a variable flow speed and constant load is considered in this section. A variable input flow rate with respect to time as shown in Figure 5.4, is applied on the input side of the turbine.

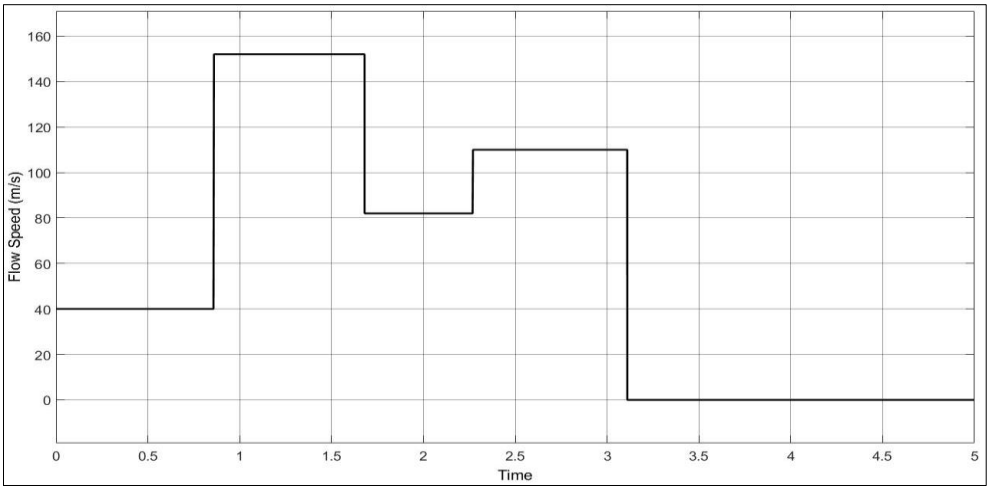

Figure 5.4 Variable Flow Speed

The dc load considered in this case is equal to 50 ohms and the dc link capacitor is equal to 15mF. A varying nature of the flow rate yields a fluctuating power at the output side of the turbine. The variable power flows towards the load side and affects the power balance of the system. In this situation, the battery bank keeps the power balance in the system by absorbing the excess or supplying the deficit power to system. So, it keeps a stable voltage across the dc load which is within the allowable range of operation. A lead acid battery is considered as a storage unit for the system shown in Figure 5.1. The parameters of the battery bank used in this simulation is shown in Table 5.1.

Table 5.1 Battery Bank Parameters

Parameters	*Values*
Nominal Voltage (V)	50
Rated Capacity (Ah)	6.5
Initial State-of-charge (%)	60
Battery response time (s)	30

In the absence of the control loops the voltage across the dc load will be uncontrolled and it can exceed from the allowable range of voltage limits. The dc link voltage without having any control strategy is displayed in Figure 5.5.

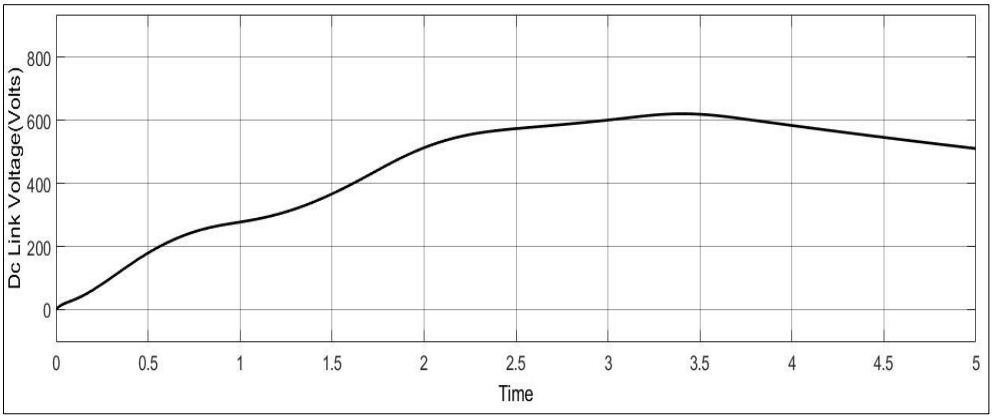

Figure 5.5 Dc Link Voltage Without Any Control Strategy

After applying the control strategy as discussed above by using a storage unit and a dump load, the dc voltage is regulated at a reference value of 100 volts. The regulated voltage and the amount of current flowing through the dc load is shown in Figure 5.6, while the parameters for the battery bank have been displayed in Figure 5.7 which represents the battery voltage, battery current and its state of charge.

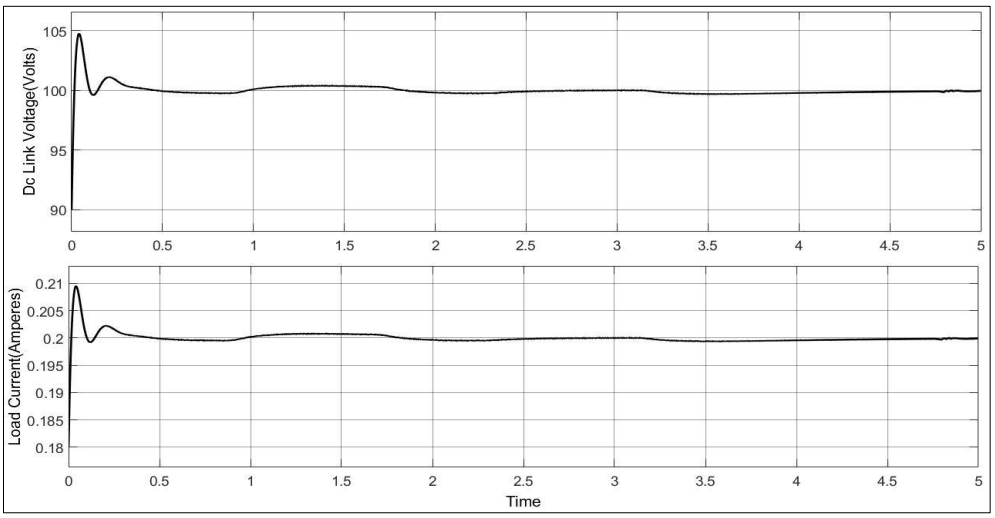

Figure 5.6 Dc Link Voltage and Current After Applying a Control Strategy

It can be observed that at t= (0.5-0.9) s, the flow rate is equal to 40m/s as shown in Figure 5.4 and the control algorithm is able to keep a regulated voltage of 100 volts across the load. The battery bank in this period is in the charging mode and the SOC of the battery increases from 60% to 60.04%. The battery current is negative in this duration which also indicates that the charging mode of the battery unit. At t= (0.91-1.6) s, the flow rate jumps to 150m/s and the dc link voltage is observed to be approximately equal to 100.4 volts which is in the tolerable

voltage range. The battery current in this period falls nearly to -18 amperes and the SOC of the battery increases to 60.08%. At t= (1.6-2.3) s, the flow speed declines to 80m/s while the dc voltage is still regulated at 100 volts. The SOC of the battery in this period reaches 60.1% and the current starts to increase. At t= (2.3-3.1) s, the input flow increases again and jumps to 110m/s by keeping the dc voltage constant. In this period the battery current has almost a steady response of -13 amperes which is due to a small change on the input side of the system. After t=3.3s the input flow drops to 0m/s which tends the battery current to starts rising from -13 amperes towards the positive values and the SOC of the battery bank gets to a steady value of 60.2%. After t=5s, if the input flow speed remained low then the battery bank will start discharging and the SOC will start to drop. The flow rate must increase from this value otherwise the SOC falls beyond the minimum limit and the system can cause failure.

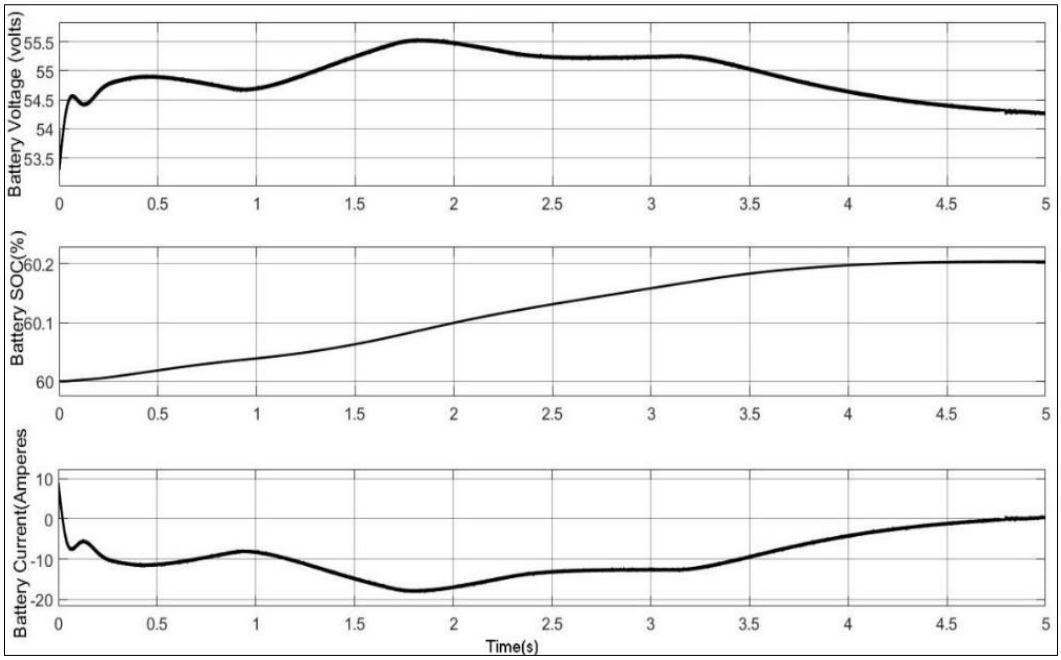

Figure 5.7 Battery Bank Parameters

5.1.3.2. Variable Flow Speed with the Activation of the Dump-load

In this experiment the maximum value of the SOC is considered equal to 60.09% for observing the situation when the dump-load is being activated. Therefore, when the SOC of the battery bank reaches the maximum defined value then the dump-load starts to absorb the excess power coming from the source. The input flow speed of the system is kept the same as used in the previous experiment. The dc link voltage and the dc load current has been displayed in Figure 5.8 while the SOC, the battery voltage and the battery current is presented in Figure 5.9.

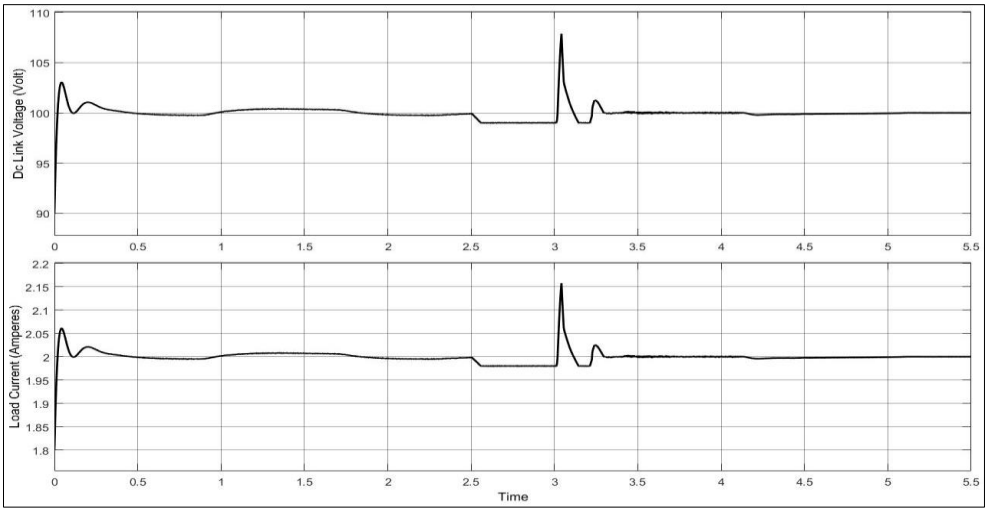

Figure 5.8 Dc Load Voltage and Load Current

At t= (0-0.9) s, the input flow speed is equal to 40m/s and the battery bank is in the charging mode. The SOC of the battery bank in this period starts to rise from its initial value of 60%. At t= (0.91-1.6) s, the flow speed jumps to 150m/s and the SOC of the battery bank continues to grow. The dump-load is activated at t=2.5s, when the SOC reaches its maximum limit.

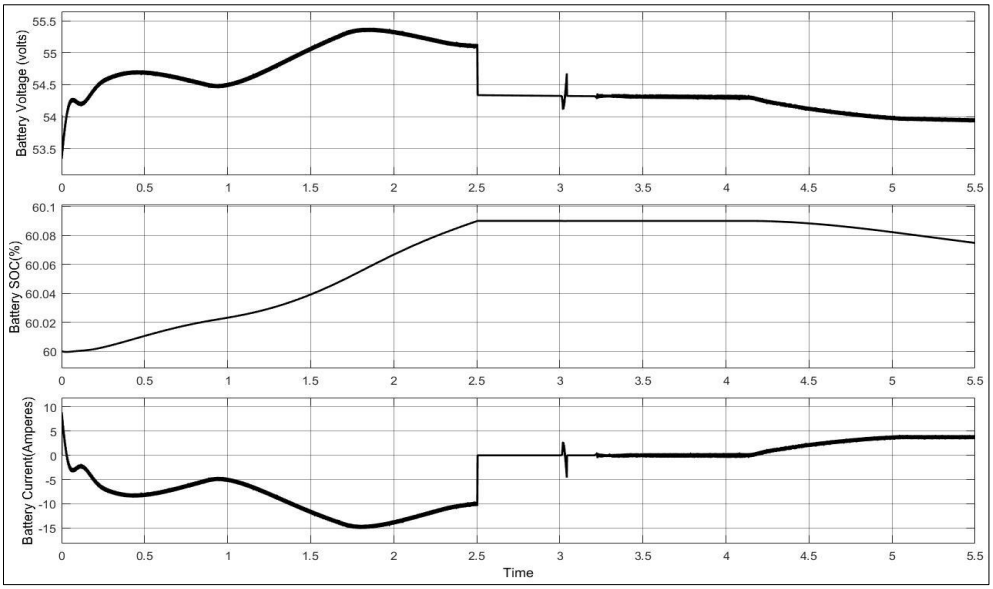

Figure 5.9 Battery Bank Parameters for the Case of Dump-Load Activation

The dc link voltage marginally falls when the dump-load is consuming the excess power but at t=3s, the voltage rises sharply and then settles down to the reference value again. This is due to the reason of the deactivation of the dump-load which transfers the dc link control back to the battery bank's controller. The deactivation of the dump-load occurs because the flow rate falls

to lower values and the SOC gets back into the desirable limits of operation. The voltage and current of the dump-load is demonstrated in Figure 5.10. It can be seen that the dump-load is consuming the excess power, when the SOC of the battery bank is greater or equal to 60.09%.

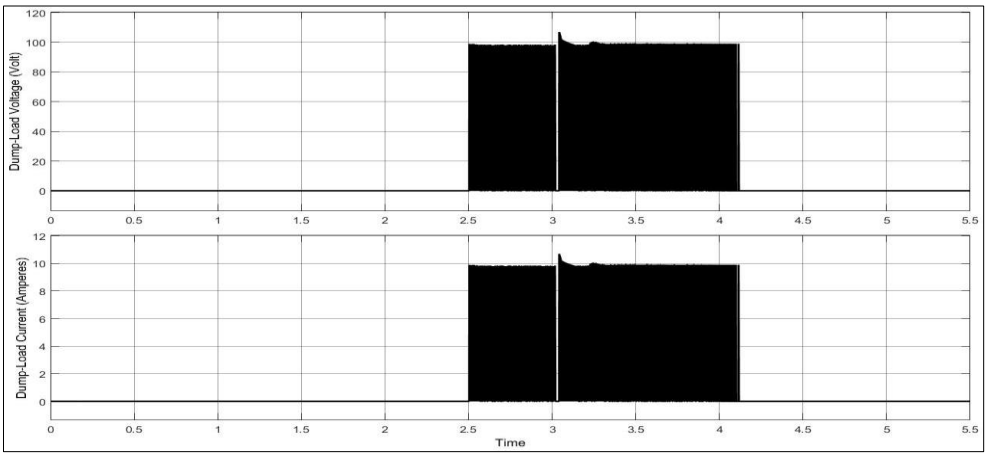

Figure 5.10 Voltage and Current of the Dump-load

5.1.3.3. Variable Load Demand

The second scenario is to study the behavior of the system for a variable load demand by having constant input flow rates. The load demand varies with respect to the time and it is varied by considering seven parallel connected resistive loads. The resistive loads are switched on/off over the whole simulation period to vary the load demand. Figure 5.11 shows the varying load demand for a complete period of simulation. A system model connected to a variable load is shown in the Simulink model of Method2 presented in section 5.2.

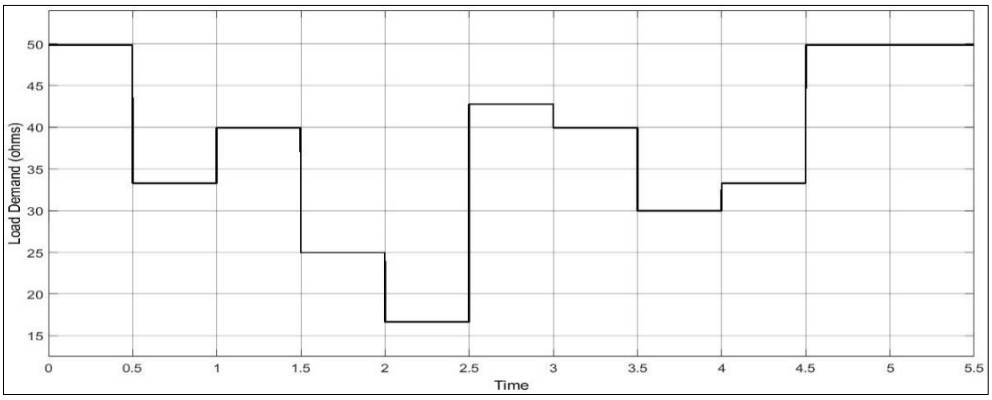

Figure 5.11 Variable Load Demand

The simulation result for the voltage and current of the variable load is displayed in Figure 5.12 and the result for the battery bank parameters can be seen in Figure 5.13.

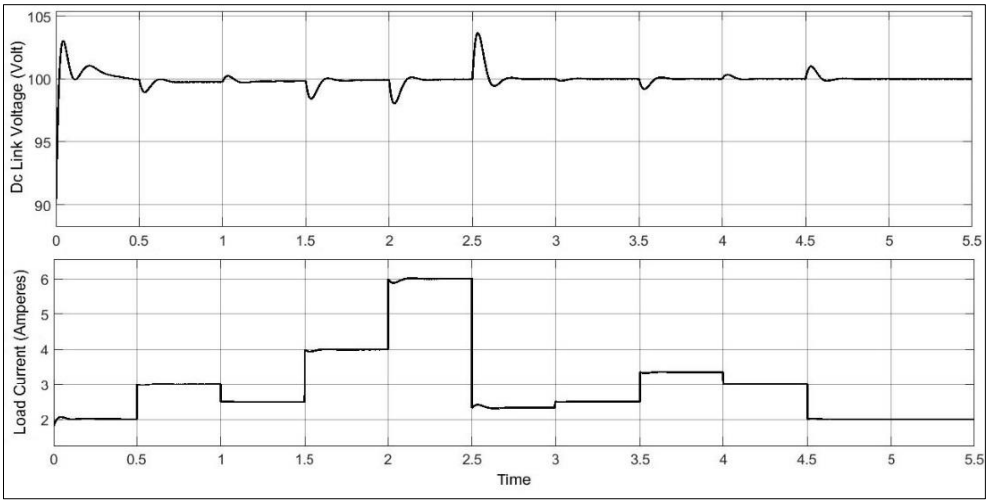

Figure 5.12 Dc Link Voltage and Current through the Variable Load

Starting from t= (0-0.5) s, the load demand is equal to 50 ohms and the current flowing through the load is approximately equal to 2 amperes. In this period the battery bank is in the charging mode as the SOC is rising and the battery current is nearly equal to -8.5 amperes. At t= (0.5-1) s, the load demand drops to 33.2 ohms due to which the current flowing through the load increase to 3 amperes. The battery current starts rising and the SOC of the battery moves towards a steady value of 60.02%.

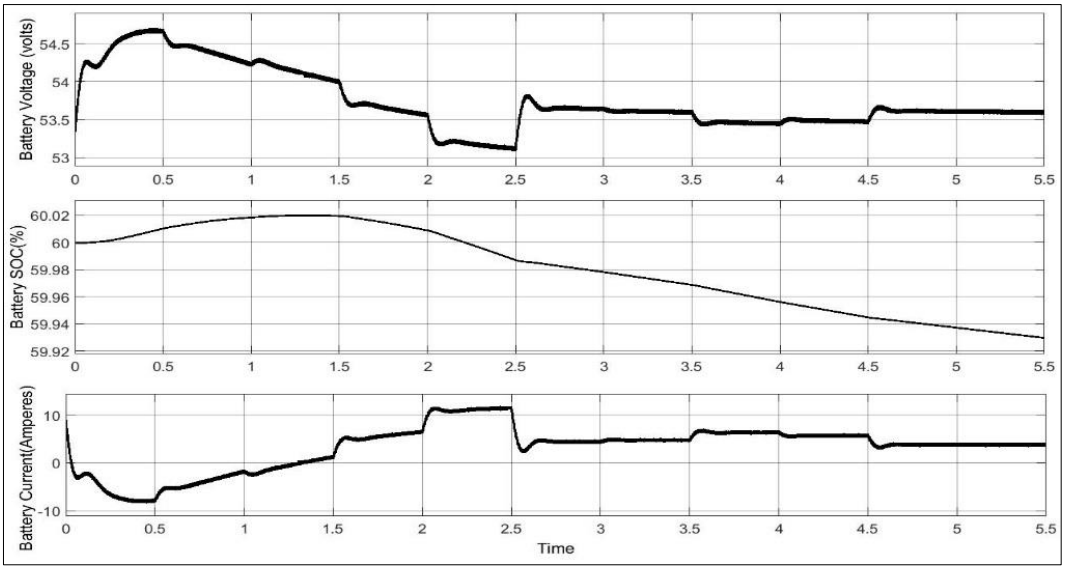

Figure 5.13 Battery Bank Parameters

At t= (1-1.5) s, there is an increase in the load demand which deceases the load current to 2.5 amperes and the SOC in this period gets a steady value of 60.02%. The load demand decreases

to 25 ohms and 16.65 ohms for t= (1.5-2) s and t= (2-2.5) s, due to which the load current increases to 4 and 6 amperes respectively. In these periods of time the battery starts discharging as SOC of the battery bank declines and the battery current goes to positive values. The dc link voltage across the load remains regulated for the complete period of simulation, with slight fluctuations.

5.2. Method 2: Battery Bank Connected via Bi-directional Buck Boost Converter and Dump-load Connected via Buck Converter

In this section the main objective is to modify the dump-load controller, by replacing the chopper with a buck converter. The duty cycle of the buck converter switch is varied in such a way that a constant voltage is maintained across the dc load, when the dump-load is activated. The control loop for the battery bank converter is kept unchanged in this method, which consists of a double loop control for a bi-directional buck-boost converter. The control loop of the buck converter connected to the dump-load can be designed either using a single loop voltage mode control, or a double loop current mode control. The benefit of using the dump-load with a buck converter is that, it will allow the system to be more stable when the state of charge of the battery reaches its maximum limit. The steady state error is also minimized, as the duty cycle of the buck converter switch is generated using a PI controller.

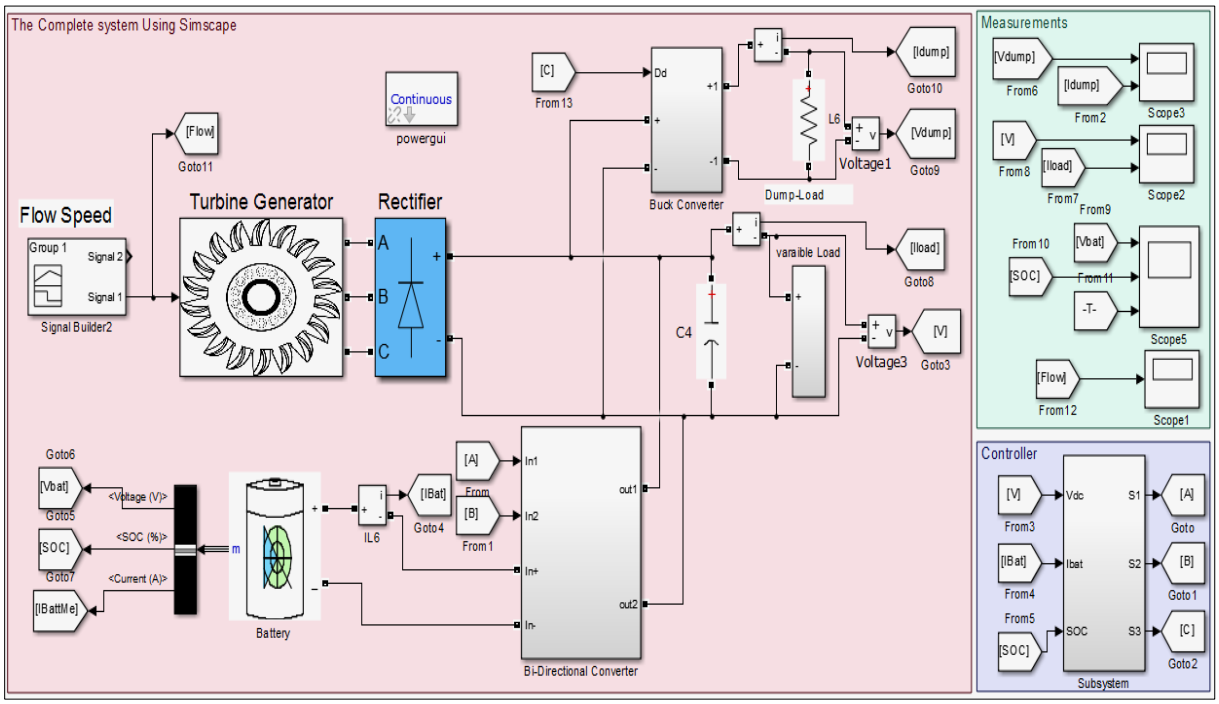

Figure 5.14 Simulink Model for Method 2

The system model for this method is displayed in Figure 5.14, where the upper section of the system shows a buck converter connected to the dump-load. The dc load in this figure is displayed as a variable load, while the rest of the system is unchanged from method 1.

5.2.1. Voltage control for the dump-load converter

As mentioned above the battery bank controller is the same as discussed in method 1, so in this section only the control loop for the dump-load converter is analyzed and discussed. Initially the control loop is designed as a single loop voltage mode control using a PI controller. The error signal for the PI controller is generated by taking the difference between the measured dc load voltage and the desired reference voltage. The duty cycle of the buck converter is varied by comparing the voltage error signal with a repetitive waveform. It means that buck converter switch is turned on when the measured voltage is greater than the desired reference to deposit the excess power to the dump-load. The value of the dump-load is very crucial and it can vary depending on the amount of available power at the input side of the turbine. If the input power increases too much, then additional dump-loads must be activated to dump out all the excess power. The dump-loads are connected in parallel across the capacitor terminal of the buck converter. The effect of activating additional dump-loads have been analyzed in Method3 presented in section 5.3. The voltage mode control loop for the buck converter is indicated using the red line boundary in Figure 5.15.

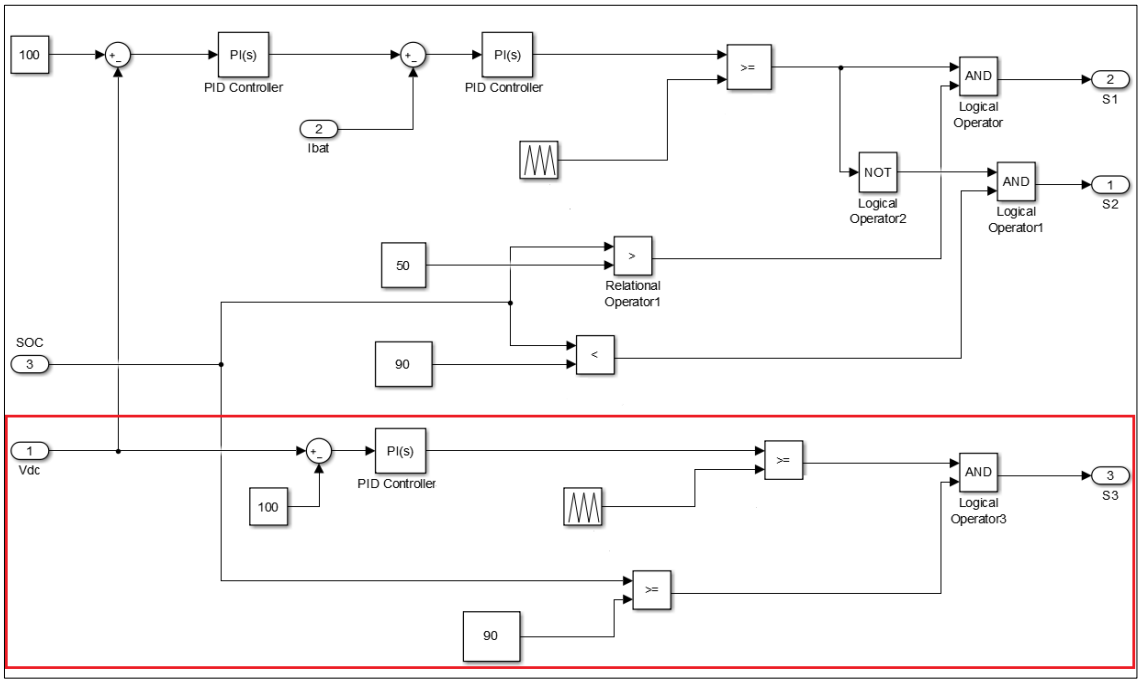

Figure 5.15 Control Loops for the Battery Bank and Dump-Load Converters

5.2.2. Current mode control for the dump-load controller

The buck converter of the dump-load can also be controlled using a double loop control loop. In this case the outer loop comprises of a voltage control loop as described above which gives the reference current on the output of the first PI controller. The inner current loop takes the difference between the generated reference current value and the measured current of the dump-load to generate an error signal for the second PI controller. In this way, the duty cycle of the buck converter is varied by keeping the status of dc load voltage and the dump-load current. This double loop current mode control is shown in Figure 5.16.

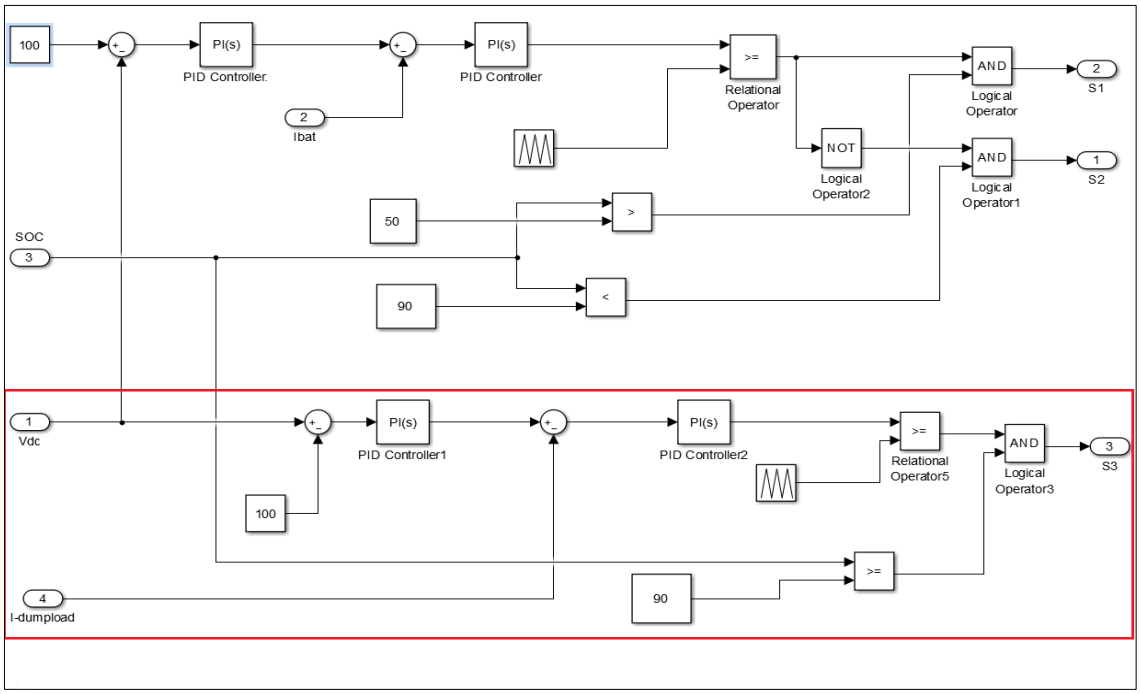

Figure 5.16 Double Loop Control Loop for Dump-Load Converter

5.2.3. Results and Discussions for Method 2

In this section the system with a dump-load connected to a buck converter is investigated using both the control methods. Several experiments have been performed to analyze the stability of the system by having variable load demands and variable input flow rates. The value of the dump-load is also altered for various experiments to observe its effect on the overall system.

5.2.3.1. Experiment 1(a): Voltage Control for Variable Flow Rates Using 5 Ohms Dump-Load.

The first experiment has been carried out by applying variable flow rate at the input side, while the load resistance is assumed to be a constant value of 50 ohms. The dump-load in this case is

equal to 5 ohms and the initial SOC of the battery bank is equal to 90%. The input flow speed for a period of 10 seconds has been displayed in Figure 5.17. This experiment illustrates that due to a variable nature of input, the dc load voltage varies which must be maintained in a certain range of operation by using the battery bank and the dump-load controller.

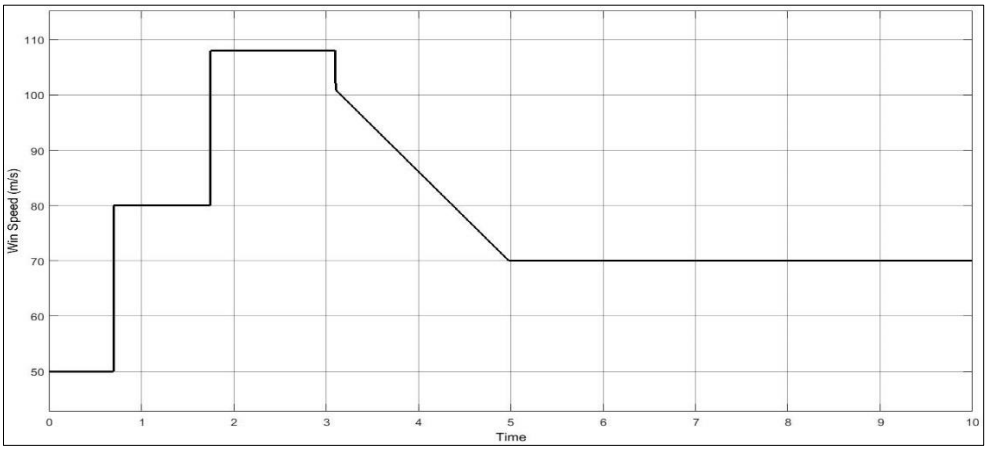

Figure 5.17 Input Flow Speed

As the flow rate rises from a low value of 50m/s to 108m/s, the battery bank starts to charge and the SOC of the battery bank starts increasing from the initial value of 90%. The maximum limit of the battery bank in this experiment is considered equal to 90.1%, to analyze the effect of dump-load activation on the system's dc voltage response.

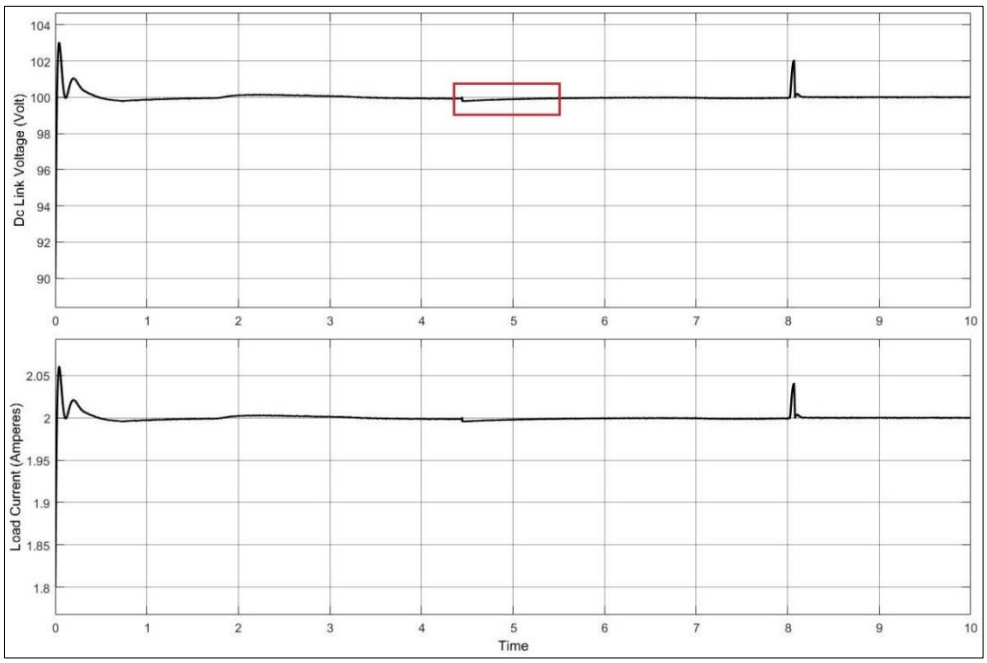

Figure 5.18 Dc Link Voltage and Load Current

Figure 5.18 and Figure 5.19 shows the dc link voltage across the load and the response of battery bank's parameters for this simulation case. Starting from t=0s, the battery bank controller regulates the dc voltage across the load by absorbing the excess power from the input side. At t=4.44s, the SOC of the battery bank reaches 90.1% and the excess power is directed towards the dump-load. The battery current at this instant of time becomes zero ampere and the excess current starts flowing into the dump-load. The voltage and current flowing through the dump-load from a buck converter is displayed in Figure 5.20.

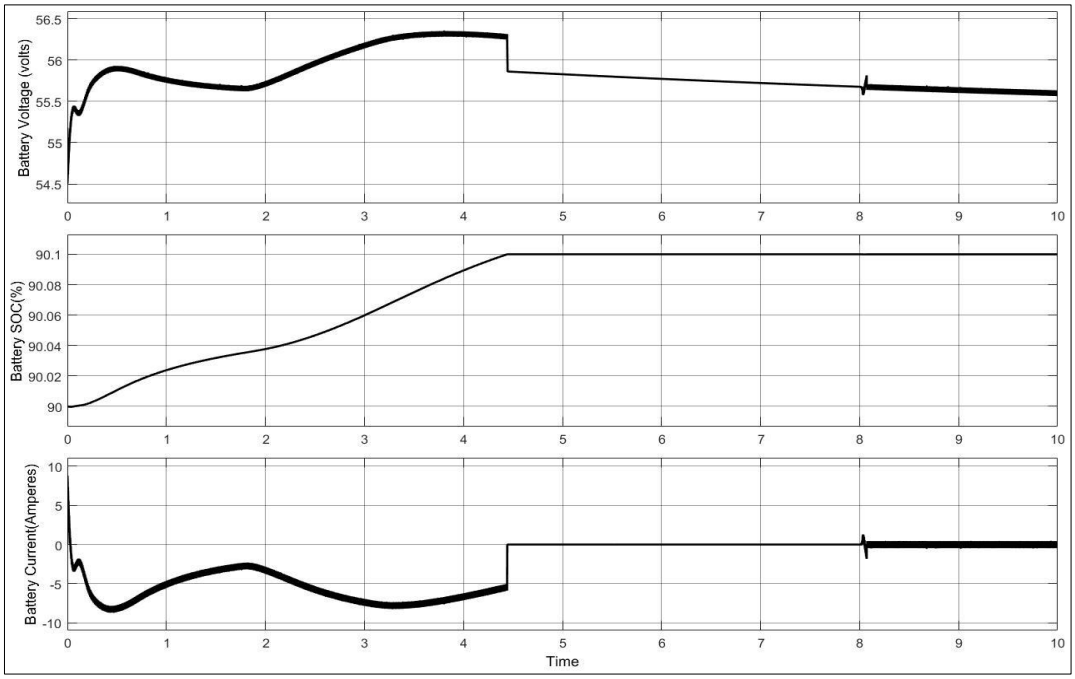

Figure 5.19 Battery Bank Response

The dc link voltage is important to observe at the instant of activation of the dump-load. Figure 5.18 shows that when the battery bank is suddenly switched off and the dump-load is activated, the dc link voltage slightly falls. This effect is indicated in the red boundary region of the figure. At this moment, the control loop of the dump-load is responsible to take the dc link voltage back to the desired reference value of 100 volts by dumping the excess power of the source. At t=5s, the flow rate drops to 70m/s and remains approximately constant over the complete period. It can be observed that at t=8s, the dump-load current suddenly drops to zero ampere (displayed in the red box region in Figure 5.20) and the dc link voltage rises to 102 volts. After t=8s, a small amount of current starts flowing through the battery bank and at the same time the dump-load is also consuming some amount of power. This effect occurs at a critical value of a flow rate which causes the SOC of the battery bank to fluctuate across the maximum limit.

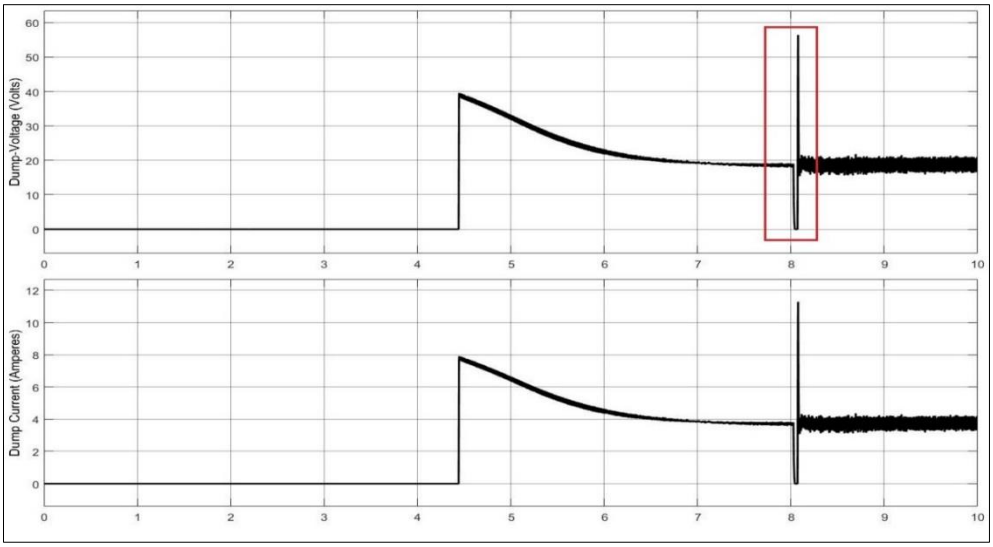

Figure 5.20 Voltage and Current of the Dump-Load

Figure 5.21 depicts the zoomed image of the battery bank parameters which displays this effect. At a critical value of input flow the available power from the source side is less than the required power of the load which tends the dump-load current to fall suddenly to zero ampere (dc link voltage drops from 100 volts in absence of the battery bank controller, this effect is shown in the next section). As the SOC starts to decrease from its maximum limit, the dump-load for a small instant turns off and the battery bank takes the control again. It rises the dc link voltage to 102 volts, which increases the SOC again. In this way, the SOC starts fluctuating across the maximum limit until the flow rate decreases or increases from this critical level.

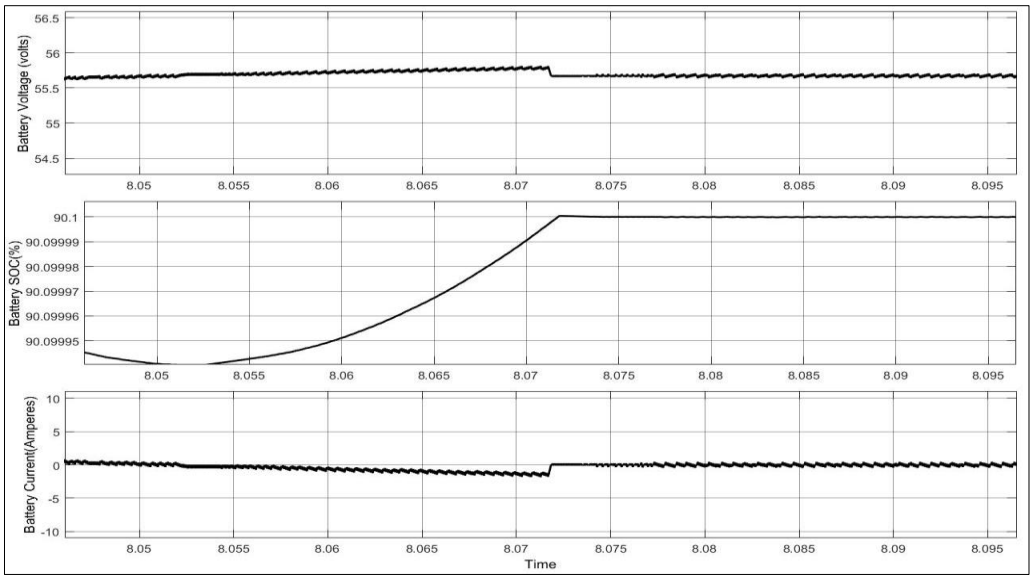

Figure 5.21 Battery Bank Response (Zoomed)

5.2.3.2. Experiment 1(b): Voltage Control for Modified Variable Flow Rates.

In this experiment the input flow speed has been modified, which decreases from the critical level of 70m/s to 60m/s as shown in Figure 5.22.

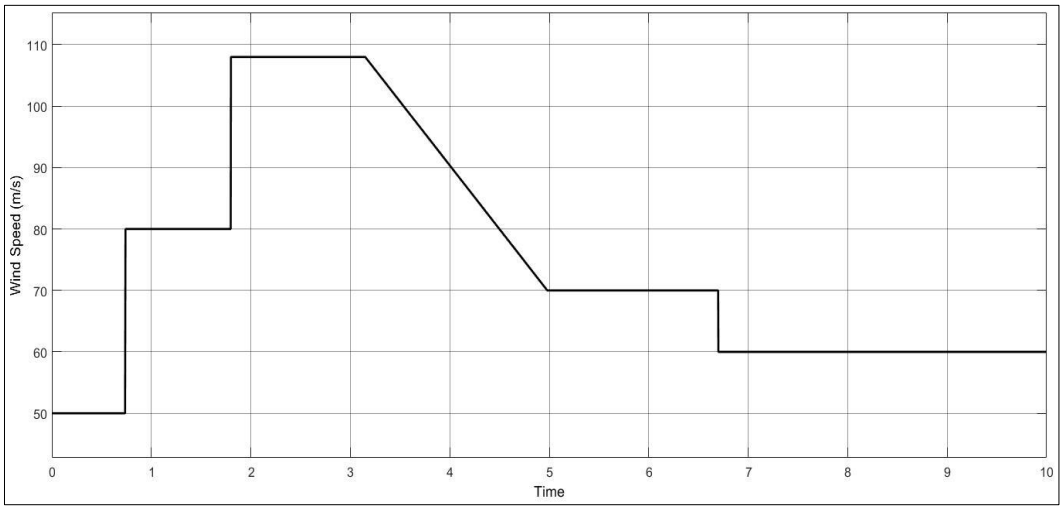

Figure 5.22 Input Flow Speed (Modified)

The main objective in this experiment is to observe the behavior of the SOC of the battery bank and the dc voltage across the load as shown in Figure 5.23 and Figure 5.24, when the source power drops from a higher level to a lower value.

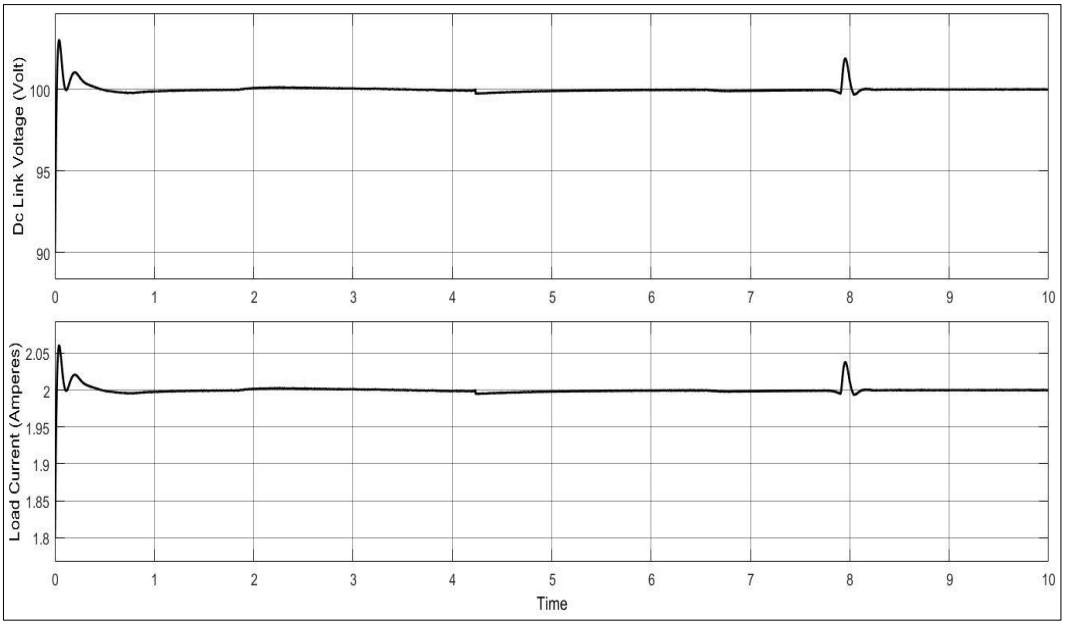

Figure 5.23 Dc Link Voltage and Load Current

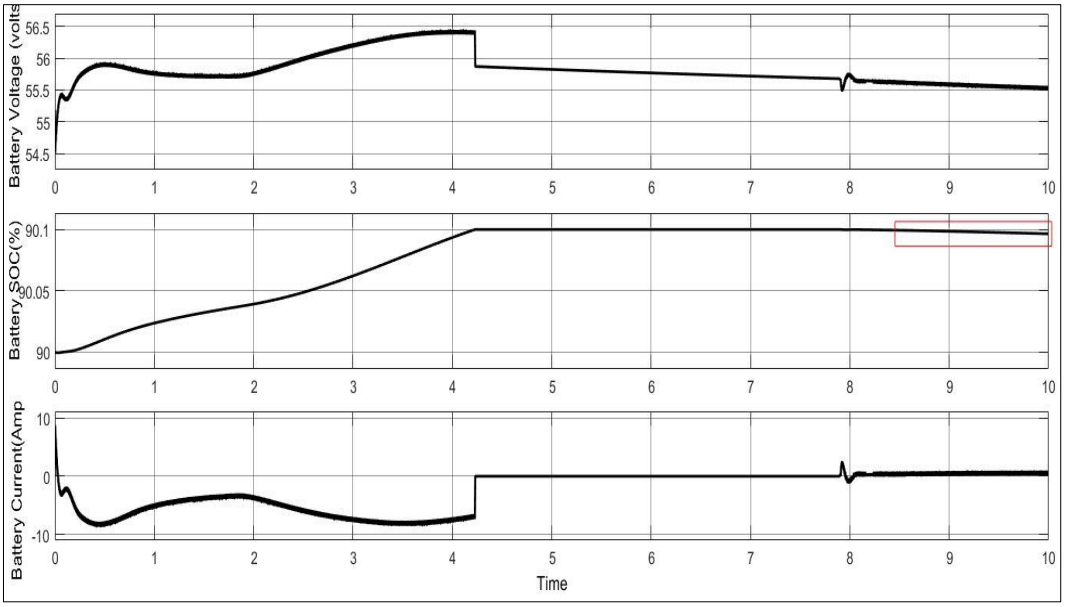

Figure 5.24 Batter Bank's Parameters

At t=6.5s, the flow speed drops to 60m/s and the dump-load is deactivated at t=8s as displayed by the red box in Figure 5.24. The time difference is due to the slow nature of the state of charge of the battery bank. At t=8s, the dc voltage falls and then rises again to approximately 103 volts, before settling down to the desired reference value. The reason behind such a response is that, at a low value of flow speed the steady state generated power from the source is much lower than the required power of the load. So, at this instant of time the battery bank is switched on again and starts discharging due to which the dc link voltage overshoots for a small interval of time. Finally, the voltage and current response of the dump-load is displayed in Figure 5.25.

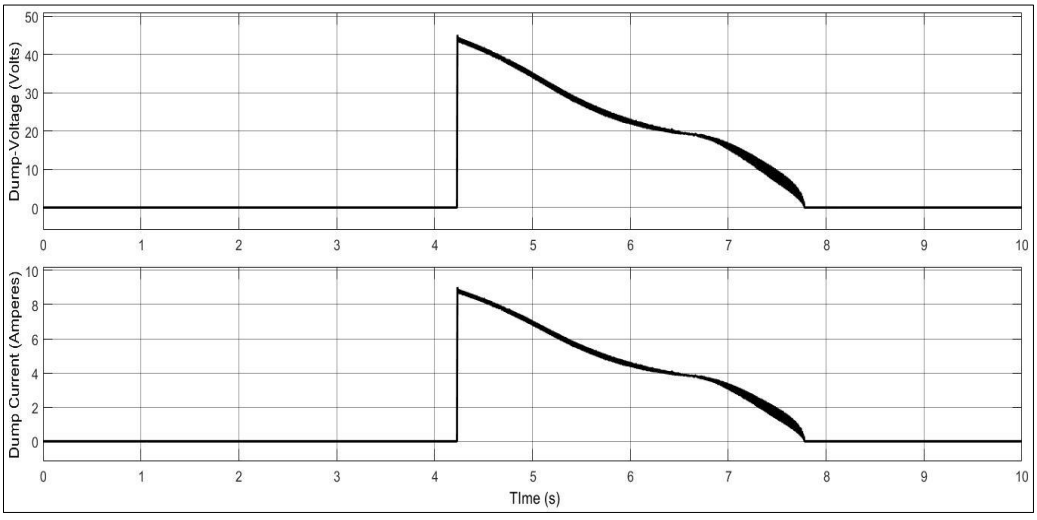

Figure 5.25 Voltage and Current of the Dump-Load

5.2.3.3. Experiment 2: Voltage Control for variable Load demand using 5 ohms of Dump-load

The second experiment is carried out by considering a constant flow speed of 75m/s and the dc load is varied with respect to the time as shown in Figure 5.26. The dump-load resistance is considered the same as in the previous experiment.

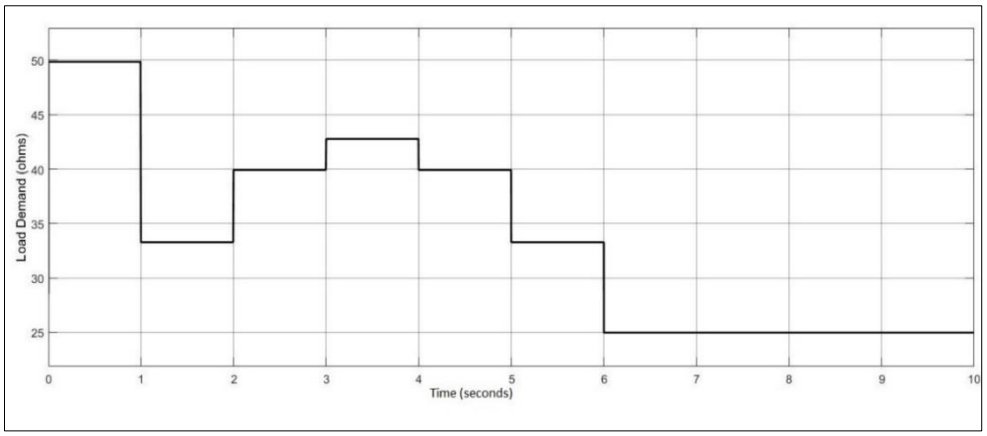

Figure 5.26 Variable Dc Load Demand

The overall current through the dc load varies with respect to time due to the variable nature of load whereas, the voltage across the load needs to be constant.

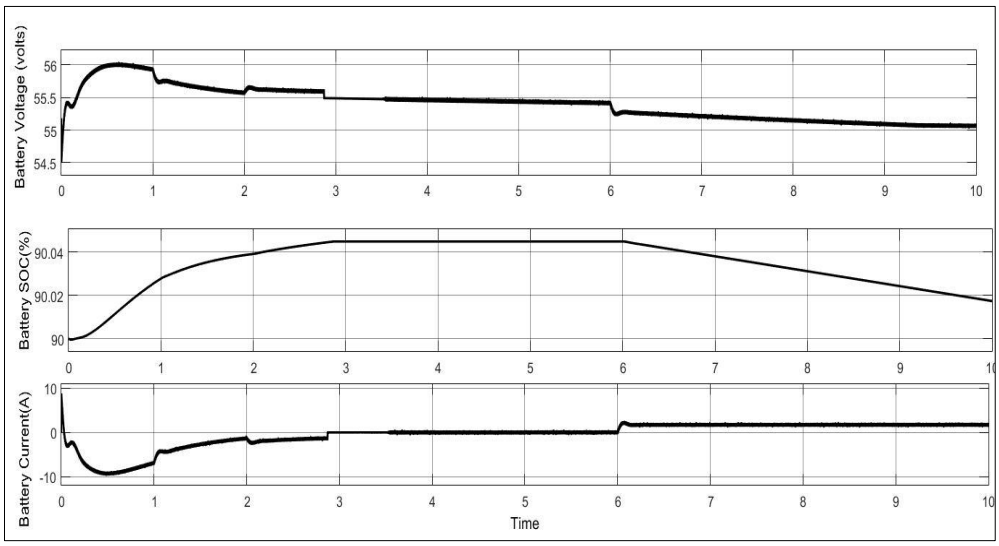

Figure 5.27 Battery Bank's Response

The initial value of SOC of the battery bank is again considered equal to 90%. To observe the effect of activation and deactivation of the dump-load, the maximum limit of the SOC of the battery bank is considered equal to 90.045% for this experiment. The battery bank's SOC,

current and voltage has been displayed in Figure 5.27. The dc voltage and the total current through the variable load is shown in Figure 5.28. It can be observed that with a fluctuating load demand, the current through the load changes but the dc load voltage is kept constant.

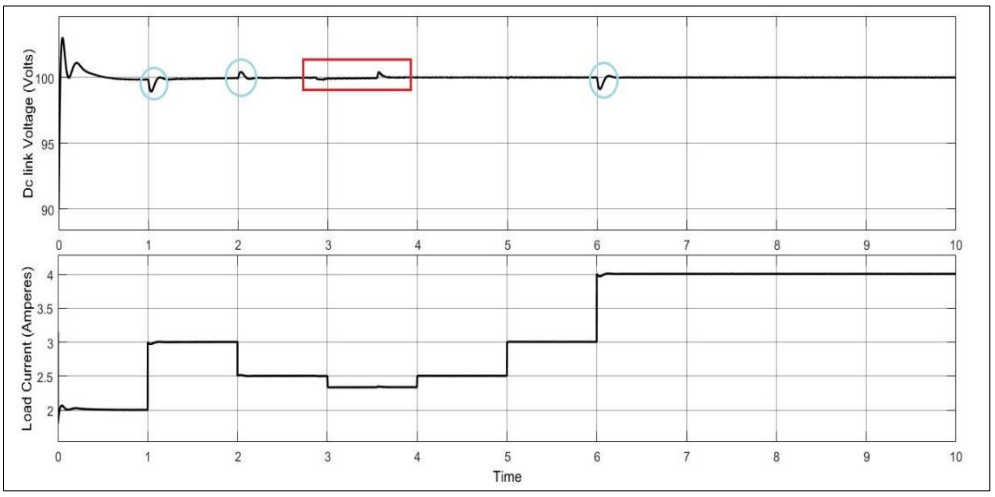

Figure 5.28 Voltage and Current of the Variable Load

From the figure, it can be seen that at t=1s as the load demand changes from 50 ohms to 33 ohms it increases the current from 2 amperes to 3 amperes. The dc voltage at this instant is indicated by a blue circle in the figure, which slightly falls and then gets back to the desired reference of 100 volts. At t=2.9s, the SOC of the battery bank reaches its maximum limit and the dump-load is activated. The dc link voltage slightly falls when the dump-load is activated but the dump-load controller regulates the voltage by consuming the excess power. This effect is displayed using the red boundary region in the figure.

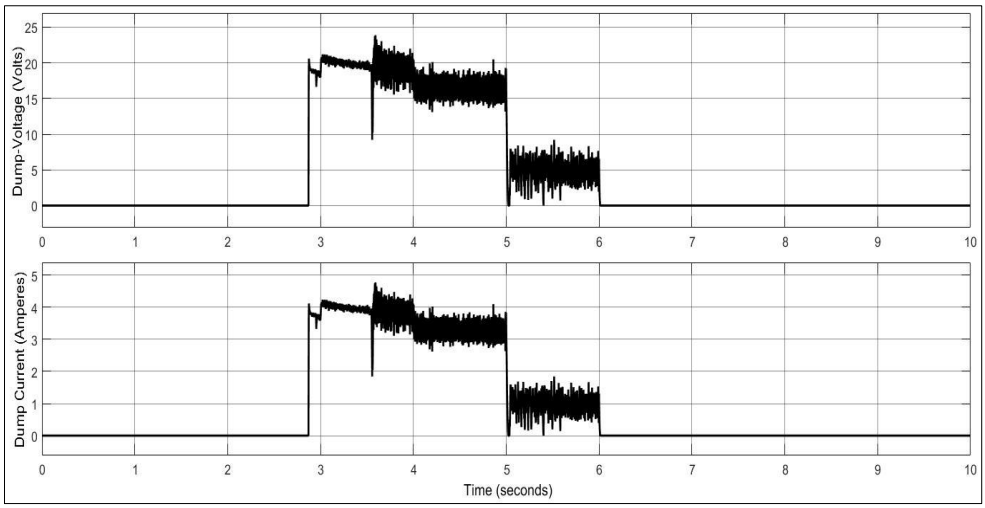

Figure 5.29 Voltage and Current of the Dump-Load

At t=6s, the load demand declines to 25 ohms and the dump-load is deactivated because the SOC drops from its maximum limit. The current and voltage across the dump-load for this experiment is shown in Figure 5.29.

5.2.3.4. Experiment 3: Current Control for Variable flow rates using 5 ohms' Dump-load.

In this experiment the effect of a double loop control of the dump-load controller is analyzed. In this control method, the current through the dump-load is sensed and used as a feedback for the second loop. The objective is to verify, whether a double loop control can provide a better stability to the system then using a single loop control. To examine the response of the dc link voltage, the dump-load is set to 5 ohms and the dc load is considered equal to 50 ohms. Variable nature of flow is applied on the input side of the system as shown in Figure 5.22 . The SOC of the battery bank and its maximum value is considered to be the same as in the previous experiment. The dc link voltage for this experiment is presented in Figure 5.30.

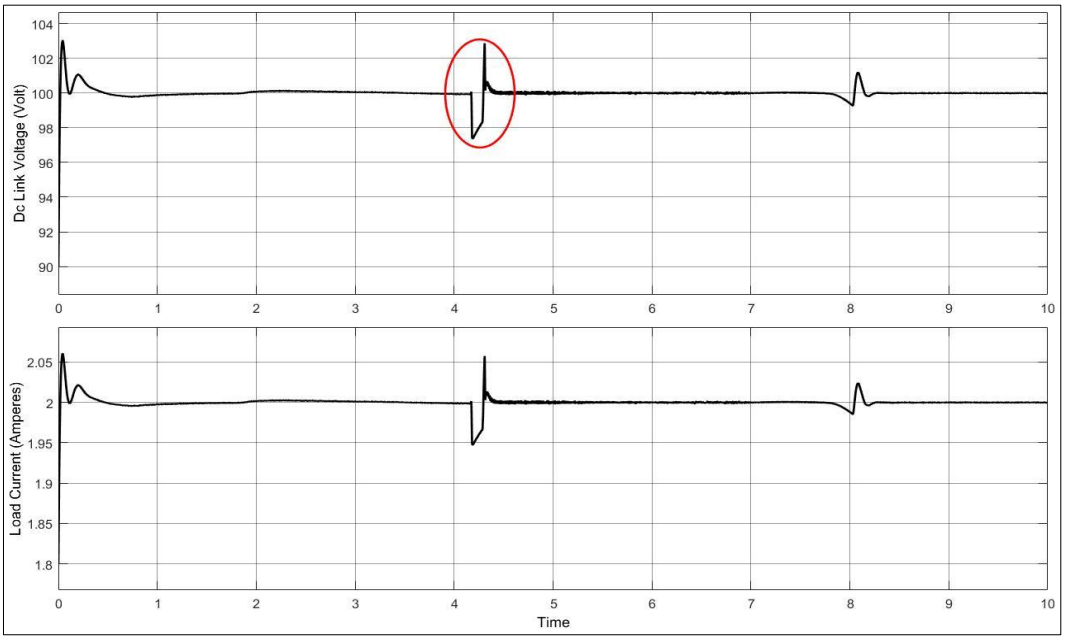

Figure 5.30 Dc Load Voltage and Current

The input flow rate increase to approximately 110m/s at the starting stage of the simulation period and the dc link voltage is kept constant by directing the excess power to the storage unit. The response of the battery bank's is shown in Figure 5.31 which shows that the battery bank is in a charging mode and its state of charge is rising towards the maximum limit. At t=4.15s, the SOC reaches its maximum limit and the dumped load is activated.

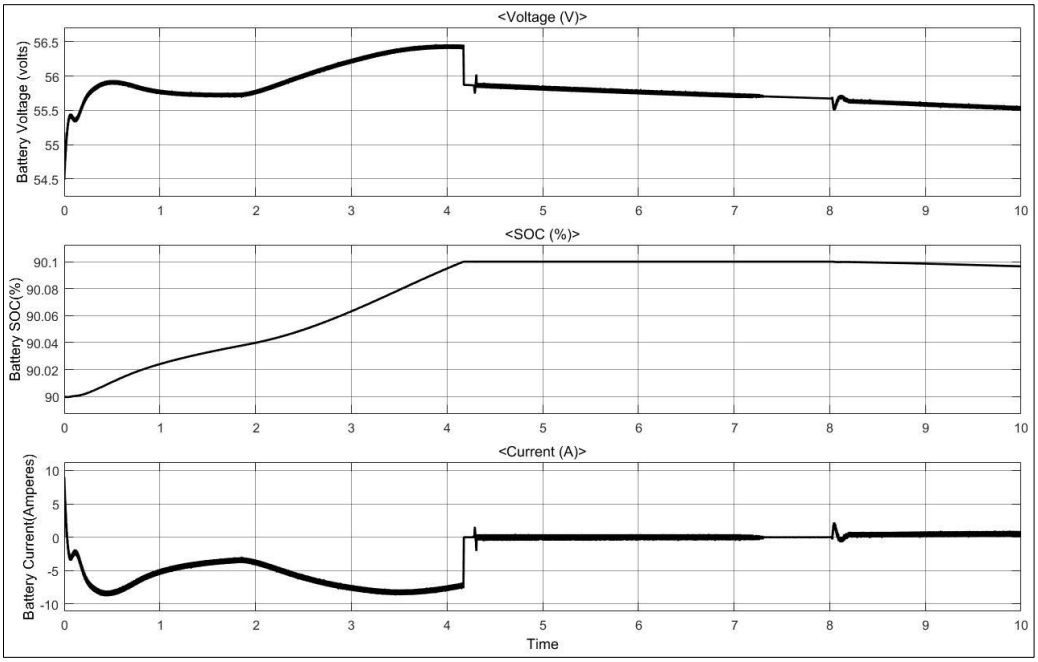

Figure 5.31 Battery Bank Response

It is noticed that the dc link voltage has a lumbering nature at the time of the activation and deactivation of the dump-load. This effect is due to the variation of the dump-load current which cannot have a predictable response because it is the excess unwanted power from the source. So, depending on the variable flow the current through the dump-load is always variable.

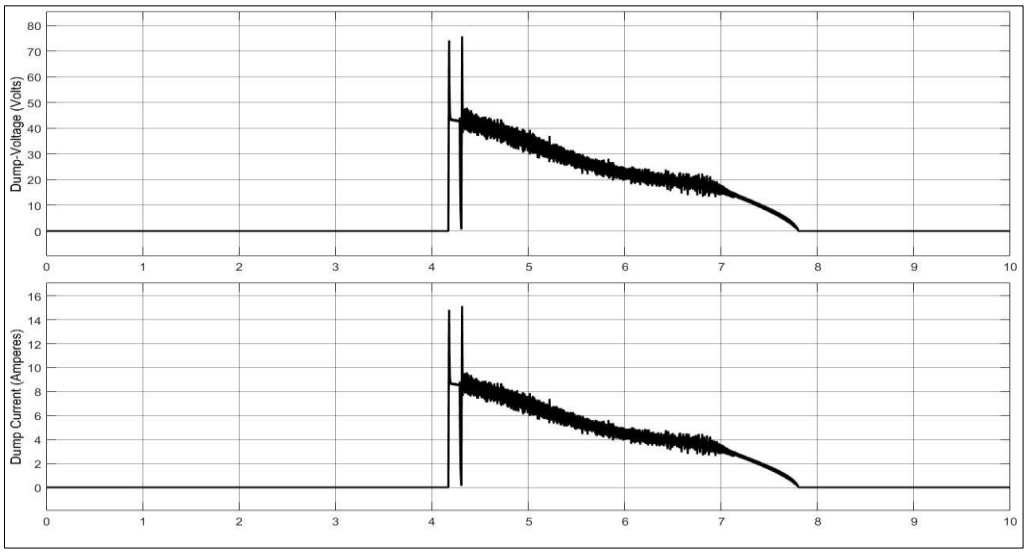

Figure 5.32 Dump-Load's Voltage and Current

When the SOC reaches 90.1%, the dc load voltage drops to 97 volts because at this instant the dump-load is activated. After the activation of the dump-load converter the dc load voltage

starts rising towards the reference value and overshoots to 103 volts. This overshoot occurs because, for a very small instant of time the dump-load current goes to zero and then rises again as shown in Figure 5.32. After this overshoot the SOC of the battery bank starts fluctuating across the maximum limit, which will fall from its maximum limit when the flow rate decreases. This experiment shows that the double loop control for the dump-load converter results in hefty voltage fluctuations. Several other simulations were performed by changing the dc load, the flow rate and the dump-load and it has been witnessed that voltage fluctuation rises and exceeds the allowable range of operation. So, it can be said that a single loop control of the buck converter provides more stability to the dc load voltage. Hence, a single loop control technique is used in the next section to analyze the effect of the dc voltage by having a battery less system.

5.3. Method 3: System with a Dump-load Converter & without any Storage Unit

In this section the system has been analyzed without having any storage unit. The battery bank connected via buck-boost converter has been removed in this case and the system is being operated using a source, a dc load and a dump-load converter as shown in Figure 5.33.

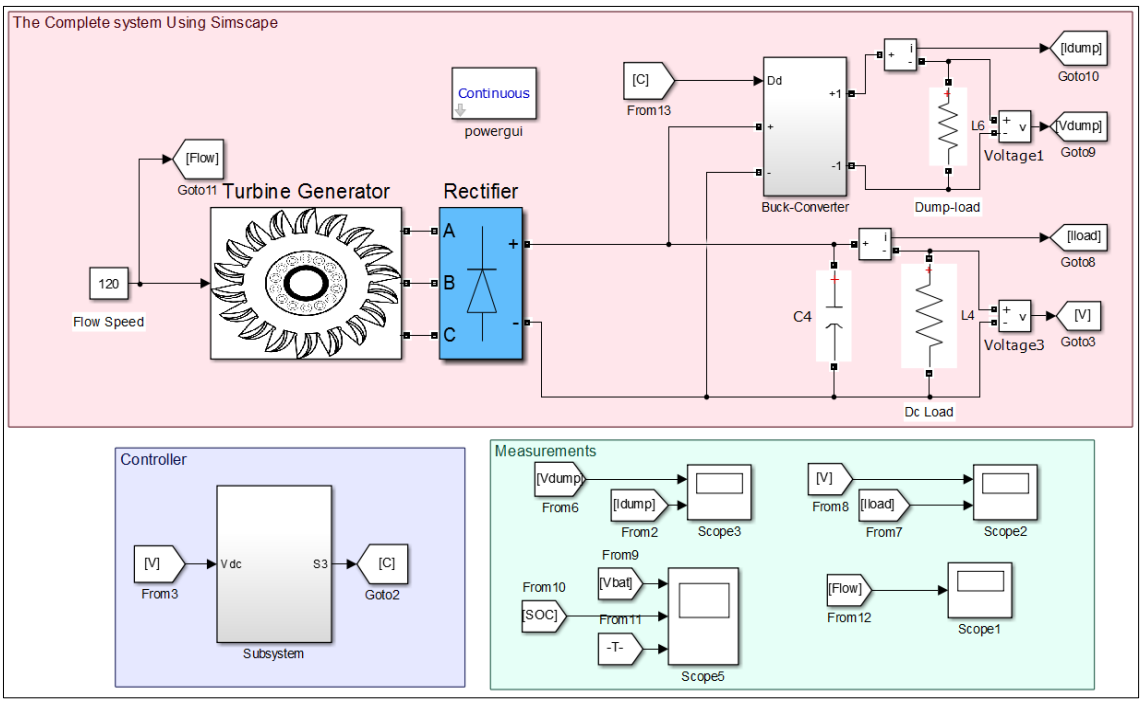

Figure 5.33 Simulink Model for Method 3

The purpose of eliminating the battery bank from the system is to visualize the effect of operating the system with a dump-load converter only. It is necessary to analyze this method because rechargeable batteries aren't available in the market for very harsh down-hole

environments where the temperature and pressure is very high. Only non-rechargeable batteries have been discovered in the market for up-to 100's of degrees Celsius. By removing the battery bank, the challenges for operating the system in desirable range of operation increases because the dump-load converter can only consume the excess amount of power from the source. In the absence of a storage unit the excess power cannot be stored and the possibility of supplying the deficit power to the dc load vanishes in this method. Therefore, the system becomes unstable when the flow drops to a very low value which goes beyond the allowable limits as the system is having only one source of energy for the dc load. In this case load shedding has to be introduced, which means that the dc loads have to be shut down based on their assigned priorities. The second possibility in this case is to disconnect the complete load from the system. The effect of load shedding and load disconnection is not discussed in this report. The system can also behave abnormally when the flow rates goes too high. For this case, additional dump-loads are turned on, to consume the extra amount of power which cannot be dissipated using a fixed value of a dump-load. A more detailed explanation can be found in the results of this section, which has been taken for different values of flow rates and dump-loads.

5.3.1. Experiment 1(a): System with 1 ohm Dump-load and 60m/s Flow speed.

To observe the response of the system at a low value of input flow, a constant flow speed of 60m/s is applied at the source side to supply power to a dc load of 50 ohms. The dump-load is considered equal to 1 ohms in this case which is connected via buck converter and it is being controlled using a single loop control algorithm.

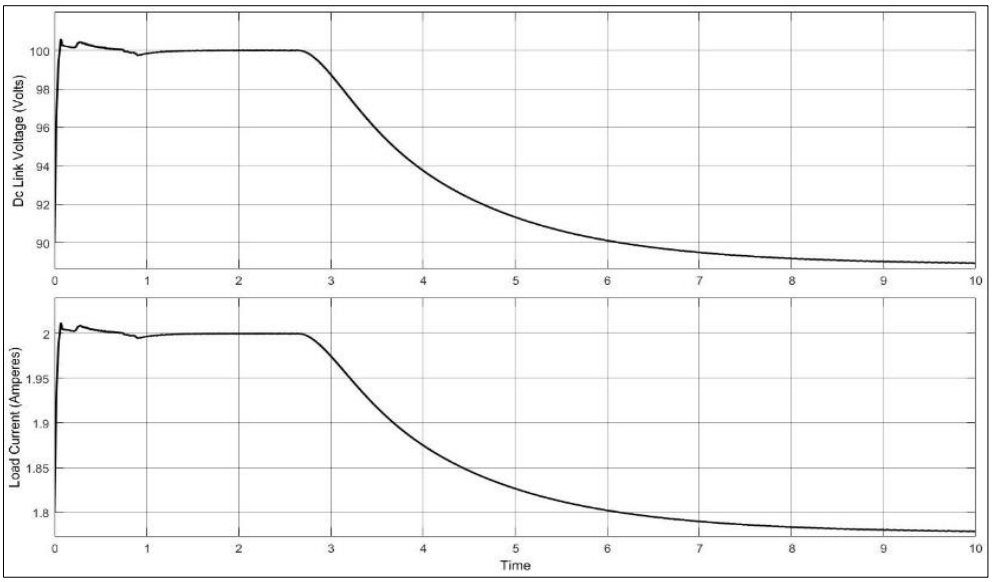

Figure 5.34 Dc Link Voltage and Load Current

Figure 5.34 shows the dc link voltage across the dc load in this case. It can be inspected that initially the dc link voltage is regulated at 100 volts. At t=2.7s, the voltage across the load drops beyond the desirable range. The reason behind this voltage drop is that the excess current across the dump-load in steady state situation falls to zero. In other words, it can be summarized that the energy from the source side is not enough to supply the load demand in steady state conditions. The voltage and current response for the dump-load is presented in Figure 5.35.

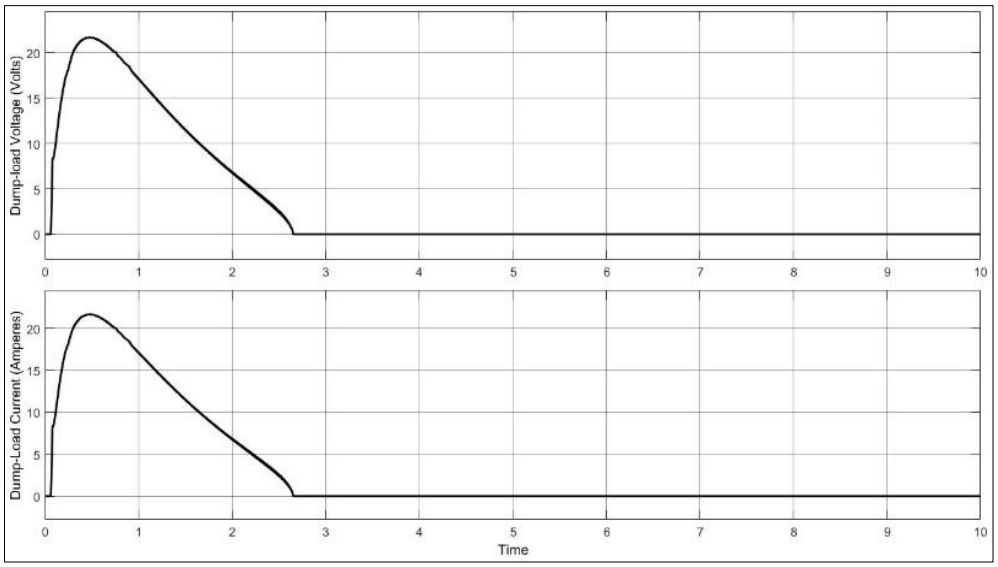

Figure 5.35 Voltage and Current of the Dump-Load

The dump-load response shows that the system is initially in the transient phase and the excess energy is being dumped out. When the system reaches the steady state condition, the dump-load power goes to zero. For this condition, it can be concluded that the system cannot be stable for an input flow of 60m/s and the dc link voltage cannot be regulated around 100 volts. By performing several simulations, it has been investigated that the flow rate at the input side of the turbine must be greater or equal to 70 m/s for the system to be stable. Moreover, the dc load must be greater or equal to 50 ohms by choosing a dump-load in a range of 1-10 ohms.

5.3.2. Experiment 1(b): System with 1 ohm Dump-Load and 200m/s Flow speed.

In this experiment the input flow speed from the source side has been kept constant at 200m/s at it is providing power to a dc load of 50 ohms. Similar to the previous experiment, a single dump-load of 1 ohm has been used to consume the excess amount of power from the source side. The dc link voltage for this experiment is presented in Figure 5.36, which shows a constant dc load voltage for the complete period of time.

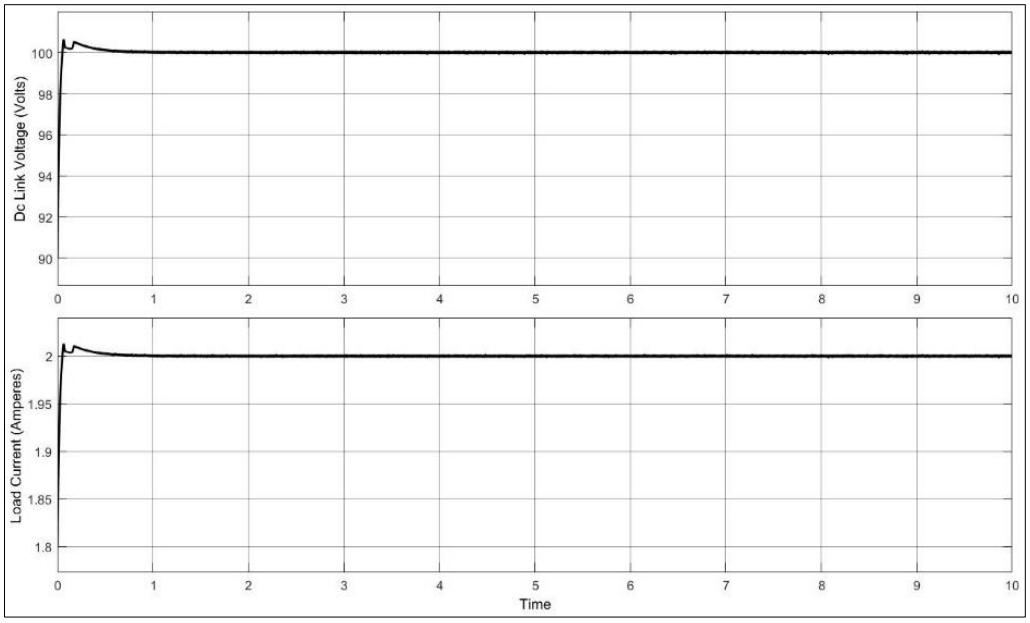

Figure 5.36 Dc link Voltage and Current Response

It can be seen that, a current of 2 amperes is flowing through a dc load of 50 ohms which keeps the dc voltage regulated across 100 volts. In this way, the load is consuming around 200 watts of power while the excess power is being deposited to the dump-load as shown in Figure 5.37.

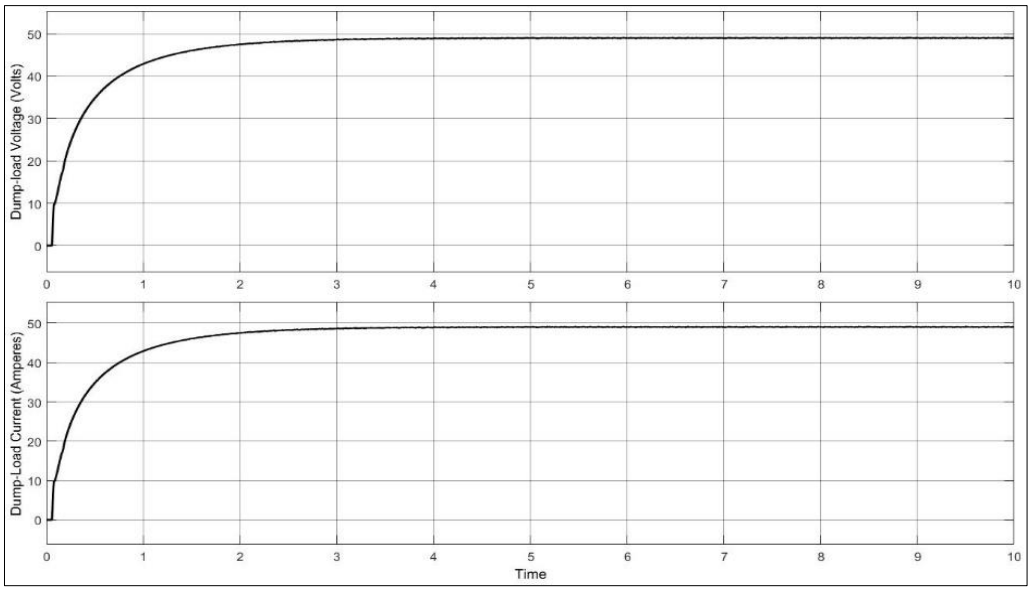

Figure 5.37 Excess Power (Voltage and Current) to the Dump-Load

By carrying out several simulations, it has been recognized that the system and the control loop is capable of regulating the dc link voltage across the desired reference value by keeping the flow speed greater than the specified level.

By considering a single dump-load of 5 ohms, it has been investigated that the input flow rate must be less or equal to 180m/s. If the input flow rises beyond this value, then the dc link voltage becomes unstable. Therefore, additional loads will be required for the stable operation of the system for dumping all the excess power to the dump-loads. Appendix A shows several simulations which are carried out to validate that the input flow rate must be less than 180m/s.

5.3.3. Experiment 1(c): System Having Input Flow Rate of 270m/s.

In this case the stability of the system has been analyzed by increasing the input flow rate to higher values. At a very high level of flow rate the input power from the source side increases too much. In this condition the dc load and the dump-load cannot consume all the available power from the source by keeping a constant dc link voltage across the load. So, in this situation the dc link voltage suddenly rises from a constant value and cannot be kept around 100 volts because the dump-load is incapable of consuming all the excess power coming from the source. In this situation, additional dump-loads are connected in parallel to the first dump-load to make the system stable for higher values of flow by consuming all the extra power from the source. The simulation has been performed by applying an input flow rate of 270m/s, supplying power to a load of 50 ohms. To examine the influence of additional dump-load, initially a single dump-load of 1 ohms has been considered for this experiment and the system response has been inspected. Moreover, additional dump-loads have been activated to consume the excess power by keeping a constant dc link voltage across the dc load. The response of the dc link voltage using a single connected dump-load is displayed in Figure 5.38.

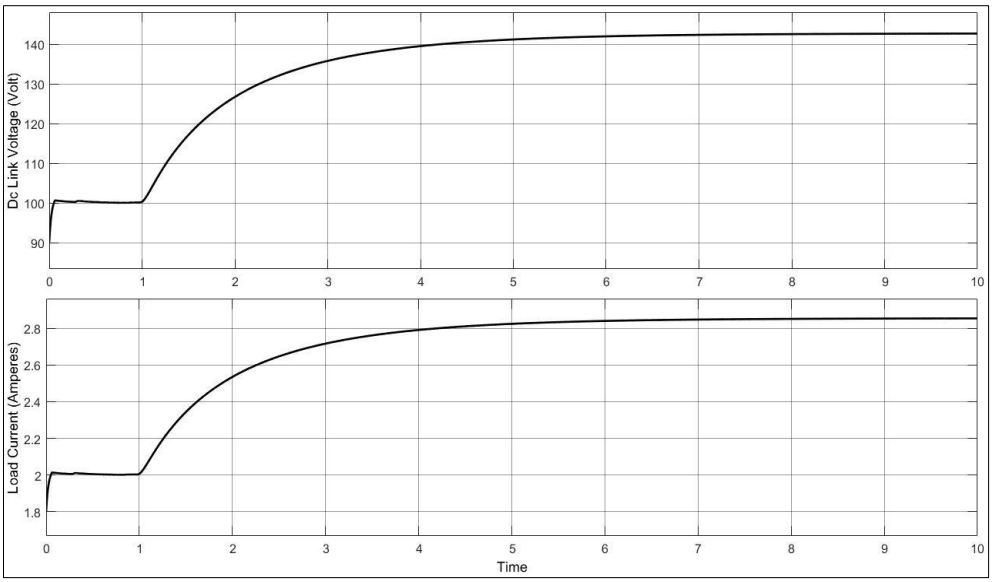

Figure 5.38 Dc Load Voltage and Current for Single Connected Dump-Load

At t=1.2s, the voltage rises to 140 volts from a regulated value of 100 volts, which makes the system unstable because at this stage the dump-load is not enough to consume all the excess power from the source. After analyzing this effect, additional dump-loads in parallel to the first one has been activated and the response of the dc link voltage and load current for this condition has been presented in Figure 5.39. It can be observed that by activating additional dump-loads, the system became stable and the dc load voltage regulates to the reference value.

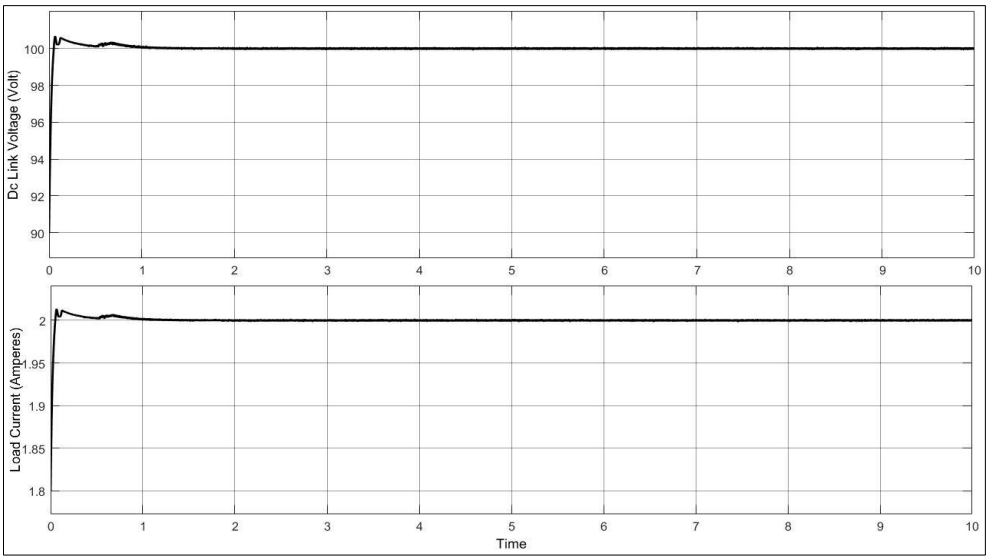

Figure 5.39 Dc Load Voltage and Current for Multiple Connected Dump-Loads

The voltage across the multiple connected dump-loads and total amount of current flowing through them is presented in Figure 5.40.

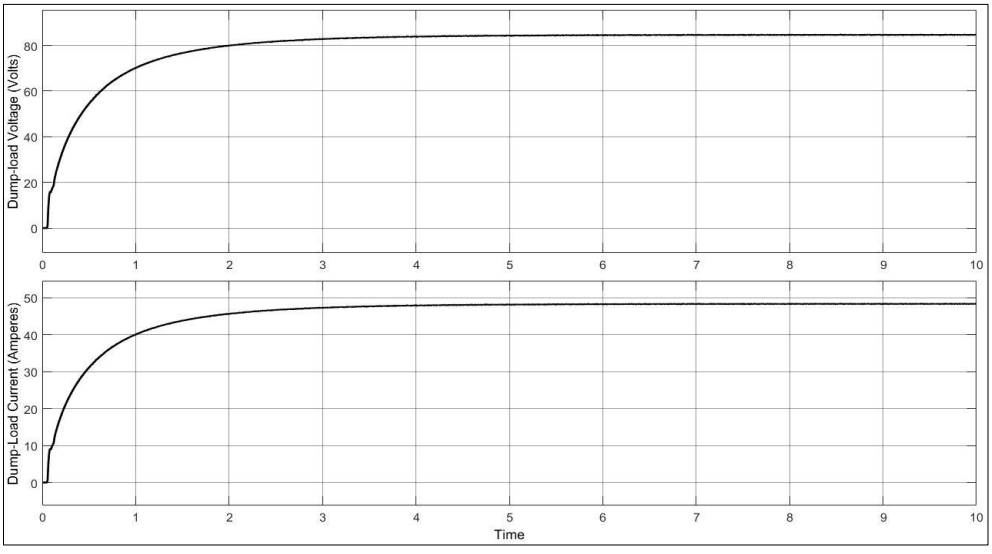

Figure 5.40 Current Flowing and Voltage across the Parallel Connected Dump-Loads

5.3.4. Experiment 1(d): System with Variable Input Flow rates

The final experiment has been carried out by applying a varying nature of input flow rate to analyze the effect of consuming extra power by the dump-load for keeping a constant dc link voltage. Figure 5.41 depicts the variable flow speed which is applied at the input side.

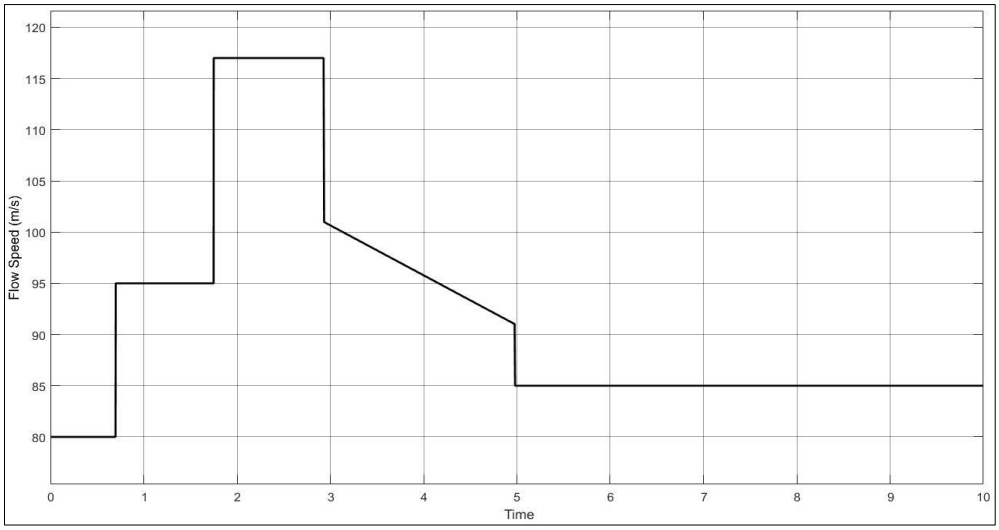

Figure 5.41 Variable Input Flow Rate

As the flow speed varies, the current flowing through the dump-load fluctuates to keep the power balance of the system. The current of the dump-load changes with the variation of the input flow rate because it consumes the unwanted power of the dc load. The voltage and current flowing through the dump-load has been presented in Figure 5.42.

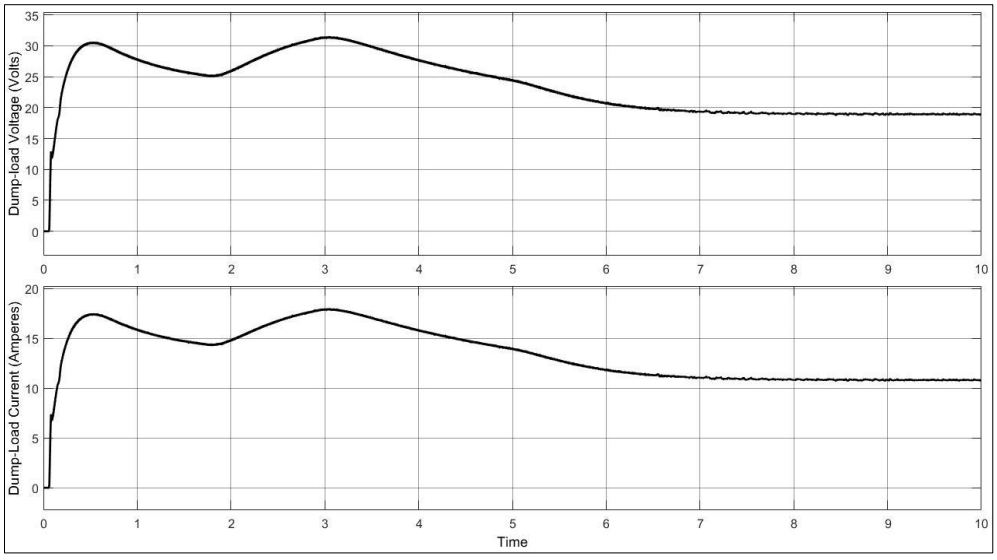

Figure 5.42 Dump-Load's Voltage and Current Response

So, the control loop of the buck converter regulates the dc link voltage across the load by keeping the power balance of the system between the source, the dump-load and the dc load. The voltage and current of the dc load for this simulation has been presented in Figure 5.43.

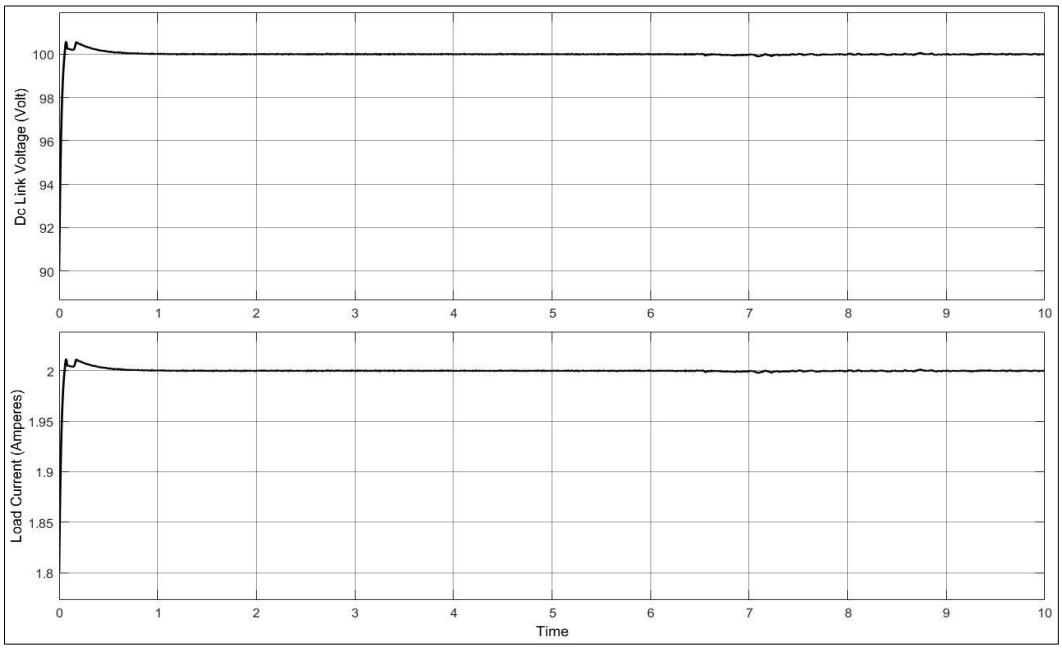

Figure 5.43 Dc Link Voltage and Load Current

5.4. Dc Load Disconnection from the System

The results presented for the system prior to this subsection had measurable amount of flow speed at the input side and the SOC of the battery bank was always above its minimum limit. In this subsection, a case of having zero value of flow rate at the input side of the system is deliberated. Lower values of input flow rates for longer periods of time is a major concern for this system because in this condition the input power will be unable to fulfill the power demanded by the dc loads and the storage units. A system failure may occur when the state of charge of the battery bank falls beyond the minimum limit and the input flow speed doesn't increase up to a desirable value. There is no such method to control the input power of the source because the fluid flow is uncontrollable. The only choice which can be adopted in this situation is to disconnect the entire load from the system. This will protect the system and the load from further damages. Another situation which can occur is, when there is an availability of a small amount of power on the input side and the SOC of the battery bank is below the minimum limit. In this situation, a method of load shedding can be utilized which disconnects some of the dc loads from the system based on their assigned priorities. The dc loads can be

prioritized and can be disconnected by keeping the status of the overall consumed and generated power of the system.

5.5. Conclusion for Implementation of Storage Unit and Dump-Load Controller

In this chapter the implementation of the system having a battery bank and dump-load has been completed using MATLAB/Simulink. The system has been investigated and simulated for three different methods. In the first and second method, the system has been studied by having a storage unit and a dump-load while in the last method the storage unit has been disconnected from the system. All three systems have been designed by using efficient control algorithms for the storage unit and the dump-load. The main objective of making the control algorithms for each method was to have a constant dc link voltage across the filter capacitor. So, the control algorithm designed for the battery bank and the dump-load converters balances the power flow of the system for the variable nature of flow and fluctuating load demands. The results verify that the control strategy is feasible as the system is stable for extreme conditions by keeping the dc link voltage constant. The controller prevents the storage unit from overcharging by using a dump-load in method 1 and method 2. In method 3, the dump-load converter is responsible for controlling the dc link voltage by keeping the input flow rates above a predefined level. The stability of the system in method 3 is also analyzed by using additional dump-loads for higher values of flow rates. Therefore, the results provide a foundation for implementing the control loops in a real target device (Microcontroller), which can be further used for the complete implementation of a real-time system.

Chapter 6 Practical Implementation of the Controllers

Texas instrument (TI) microcontrollers based on digital signal processing (DSP) has been studied in this thesis for the real-time implementation of the controllers. The system model consists of power electronic converters, which mostly requires the PWM and the ADC features of the DSP chip. Texas Instrument microcontrollers can provide high performance ADC and PWM for the implementation of the control loops for the system model considered in this report.

6.1. Microcontrollers

Texas Instrument microcontrollers have special DSP based architecture which is more useful than the microprocessors for real time controlling and high speed processing. They are normally 16 or 32-bit microcontroller used for designing advanced closed loop control algorithms and can also be utilized for various other applications. C2000 microcontroller products consists of several microcontroller families such as; C2000 Delfino, C2000 Piccolo, instaSPIN and fixed point microcontrollers. They are used for high performance closed loop applications, broad closed loop applications, advanced motor control technology on chip and dependable industrial closed loop control respectively [45].

A TMS320F28069 microcontroller can be chosen from the Piccolo family for the implementation of the control loops, which is based on C28x central processing unit (CPU). This chip is used for several control applications such as; switch mode power supplies, solar converters, ac/dc converters and power factor corrections. The control challenges are resolved using the analog to digital converter (ADC), analog comparators and the pulse width modulators (PWM). TMS320F28069 has a high efficient 32-bit fixed point Harvard bus architecture and has a fast interrupt response. This chip is an efficient C/C++ engine which can be used to design the control software in high level languages and also allows the users to develop math algorithms in C/C++. Another feature of this chip is having an on-chip flash memory unit for the code execution which can minimize the cost of having additional memory units. Furthermore, the chip contains 8 enhanced PWM (ePWM), 3 input enhanced capture (eCAP), 4 high resolution capture (HRCAP), 2 enhanced quadrature encoder pulse (eQEP), 12-bit analog to digital converter (ADC), 54 general purpose input/output pins (GPIO) and serial port peripherals. More details regarding the chip along with the functional block diagram and system device diagram can be found in the data sheet which is available on Texas Instruments webpage [46]. The ADC module contains a 12-bit core with two built-in sample and hold

circuits. The ADC can be either used in a sequential sampling mode or in a simultaneous sampling mode. It also includes up to 16 channel multiplexed inputs and 16 results register for storing the values after conversion. For starting of the conversion sequence the ADC can be triggered by multiple sources e.g. the S/W-software immediate start, GPIO XINT2 etc.

The PWM of the DSP chip is used to generate on/off pulses for the designated dc-dc converters of the system model. The ePWM module consists of two PWM output named as ePWMxA and ePWMxB which makes one complete PWM channel. A clock synchronization scheme is used to integrate all the ePWM modules which allows them to work as a unique system when required. The modules supports 16-bit time base counter with frequency and period, two PWM outputs which can be used in several type of configuration, dead-band generation with independent rising and falling edge delay control and various other feature described in [47].

6.2. Data Types and Fixed Point Representations

Digital processors are divided into floating-point processor and fixed-point processor. The internal hardware of the floating-point processor supports a floating-point operation, while a fixed-point operation is supported by a fixed-point processor. The examples of floating-point architectures are the Intel's Pentium series and TI C6000. Consequently, all the other embedded systems are operated using fixed-point operations such as, Motorola HC68x, Infineon C166 and TI C2000 and TI C5000. The embedded system applications are usually designed with high level description tools such as MATLAB/Simulink and the performance of the application is evaluated with floating-point simulations. So, if the digital signal processing algorithms are designed using floating-point data representation, then finally they are implemented using the fixed-point representation. Fixed point architecture is much faster and cheaper than the floating-point architectures. Furthermore, they are also simpler to use then the floating-point architecture which includes an exponent term and a mantissa [48].

6.2.1. Integer and Binary Numbers

All the number used in daily life for counting and solving arithmetic problems are the natural numbers which can be in the form of whole numbers or unsigned integers. In contrast the computer world can only understand binary numbers for performing all the arithmetic operation which are in the form of zeros and ones. Consequently, all the signed and unsigned integers can be converted and represented in binary form to solve various problems using digital processing. The unsigned integers are in a range of $(0\_(2^n-1))$ while the range of signed integer are $(-(2^{n-1}-1)\ \_\ (2^{n-1}-1))$. Where n represents the number of binary bits for example, if 7 is stored in 8-bit

memory using unsigned integer then its binary form can be represented as 00000111. In case of signed integer representation, if the first binary bit is '1' then the number is negative and if the first bit is '0', then the number is positive.

6.2.2. Floating Point Numbers

A stream of binary numbers may also include a binary point which is similar to a point in natural numbers. In floating point representation, the binary point can float and is not fixed at one specific position. A floating-point number has three components, the sign (+, -), the exponent and the significand ($\pm 2^e s$). Floating point binary representation can be of a single precision (32-bits) or of a double precision (64-bits). A 32-bit packet is divided into three sections; the first section consists of 1-bit only, the second section has eight bits and the third section has 23 bits. The first section indicates the sign and it can be either 0 or 1. The second section is used for indicating the exponent which ranges from 0 to 255 while to cover the negative exponent, the exponent is added to 127 to get the real exponent. The third section represents the mantissa or the significand which represents the remaining bits on the left side of the exponent term [49].

6.2.3. Fixed Point Representation

A fixed-point data type consists of a sign bit, an integer part and a fractional part. A binary point is used to separate the integral part and the fractional part while the first bit always displays the sign of the number. The fixed-point representation has fixed number of digits after the decimal point which is very useful for representing the fractional values. Signed fixed-point numbers can be represented in three ways such as; sign/magnitude, one's complement and two's complement. The position of the binary point in a fixed-point number representation determines the scaling of the number. The hardware uses the same logic circuits for solving the arithmetic problems because the logic circuits have no idea about the position of the binary point. A general representation of a fixed-point number in a binary form can be seen in Figure 6.1, where 'wl' is the word length and the binary point is placed between b_3 and b_4. [50].

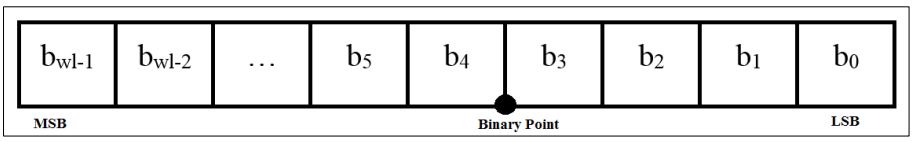

Figure 6.1 Representation of Fixed-Point Number

In this report the data type conversions has been carried out in Simulink environment while the arithmetic operations of the fixed-point numbers in Simulink can be done using IQmath library

which is discussed in the next subsection. In the IQmath library the fixed-point numbers can be represented as "*Qm.n"*, where Q shows that the number is in Q format notation, m represents the total number of bits used in the integral part and n is number of bits for the fractional part (which are the bits on the right side of the decimal point). The first bit (MSB) is always used for sign and a signed fixed point number in Q format requires m+n+1 number of bits.

6.2.4. IQmath Library and Other Libraries

The control algorithm of the system can be implemented on Simulink using the Texas instruments libraries for the specific families of the microcontrollers. The C2000 embedded target libraries has been installed through MATLAB and every chip has its own library. The specific library contains all the features of the chip in the form of blocks such as; ADC, ePWM, watchdog, SCI transmit, SCI receive, eQEP, eCAN and various other blocks. The blocks can be used in Simulink environment for making control models and then a C/C++ code can be generated using the designed Simulink model which can be stored in the chip's memory for real time operations. The libraries have a common optimization library which consists of IQmath and DMC library and they can be utilized for all the chips. The IQmath library is used to perform arithmetic operations using fixed point data types while designing a model in Simulink.

Table 6.1 Function of IQmath library Blocks

Block	*Description*
Absolute IQN	Calculate absolute value
Arctangent IQN	Calculate four-quadrant arc tangent
Division IQN	Divide two IQ numbers
Float to IQN	Convert floating-point to an IQ number
Integer part IQN	Return the integer part of the IQ number
Magnitude IQN	Calculates magnitude of two IQ numbers
Square Root IQN	Calculates square root and inverse square root of IQ number
Trig Fcn IQN	Calculates the sine, cosine or tangent of the IQ number

In Table 6.1 some of the block from IQmath library with block name and their function has been displayed, while all the blocks included in the library is shown in Figure 6.2.

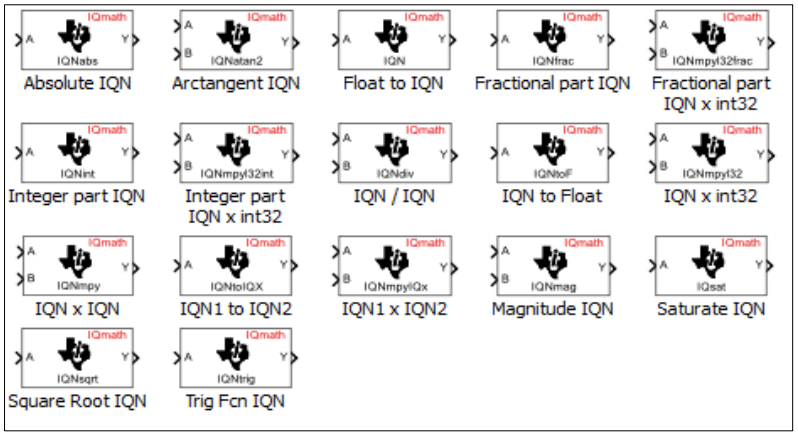

Figure 6.2 IQmath Library Blocks

The DMC library is used for designing of the control algorithms for specific type of application and the blocks included in this library works on the same fixed point data representation. It means that the input and the output of the blocks must be of a fixed-point data type. This library includes blocks named as, Clarke transformation, PID controller, park transformation, inverse park transformation, Ramp generator, Ramp control, Space vector generator and speed measurement. Figure 6.3 shows the blocks included in this library.

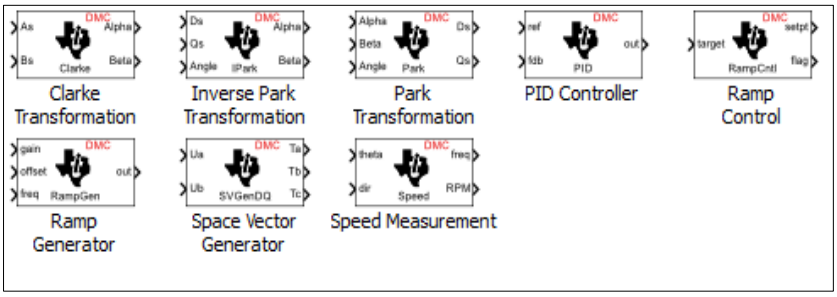

Figure 6.3 DMC Library

6.3. Implementation of the Control Algorithm Using TMS320F28069 on Simulink (Fixed-point Model)

The control algorithm of the system can be constructed in Simulink environment using proper blocks from C2000 embedded coder target library. The created Simulink model for the control algorithm can be programmed in the selected target device which can be used for real time systems. The Simulink model of the control algorithm can also be simulated by integrating it

with the Simscape model of the whole system built in Simulink. The digital controller has been designed using the embedded coder target library for two different methods. The first method is to modify the control loops of the system having a bi-directional buck-boost converter and a buck converter which are used for controlling the battery bank unit and the dump-load respectively. The second method is to make the control loop of the system having a buck converter only, which is used to control the dc load voltage using the dump-load. Initially, the control algorithms for both the methods have be verified by simulating them with the help of C2000 embedded target library and the Simscape library.

6.3.1. Method 1

The first method is investigated by modifying the control loops of the battery bank and the dump-load converter for the system model presented in Figure 5.14 Figure 5.14 discussed in chapter 5.

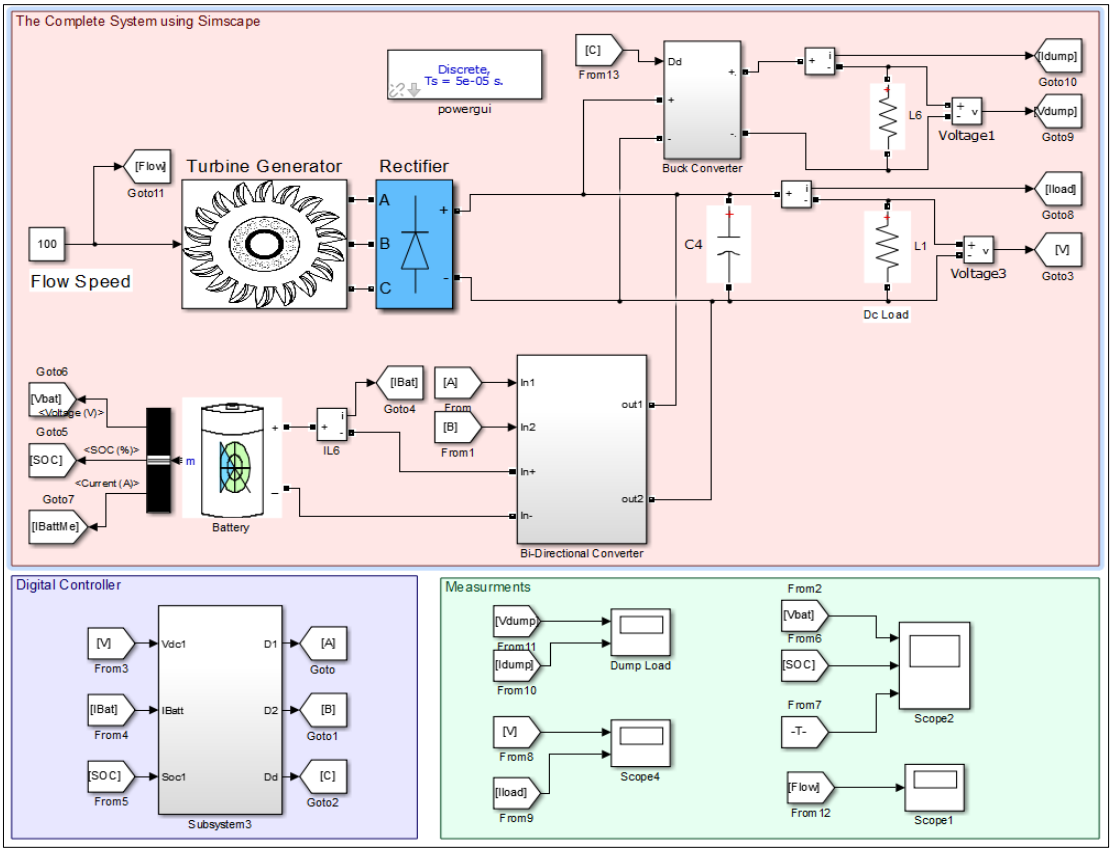

Figure 6.4 Modified System with Digital Controller

The modified system model is shown in Figure 6.4 and digital converter which is the main modification of the system model is displayed in Figure 6.5. As it can be recognized from the figure that the control loops have been constructed using the Simulink library and the C2000

embedded code target library which represents the peripherals and algorithms of the target device specific to that family.

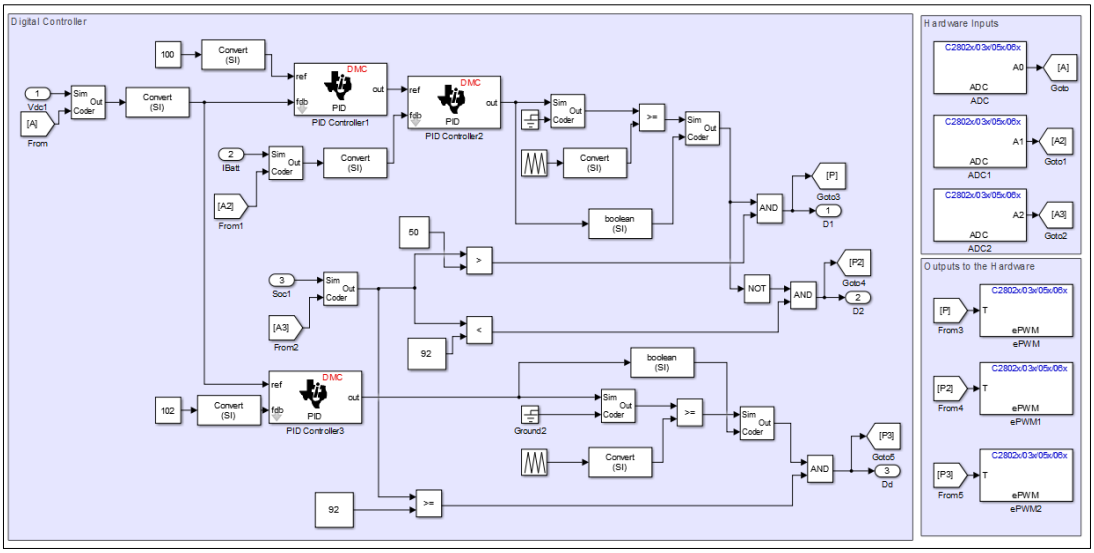

Figure 6.5 Digital Controller Using Embedded Target Libraries

The control algorithm has been implemented using the fixed-point data type. It can be seen that the inputs of the PI controllers have been converted into fixed-point data type using the conversion block from the Simulink library. The PI controllers used in the model is taken from the C2000 embedded target library and the PI controller block only accepts data type of a fixed-point representation. Another block which has been used from the Simulink library is the environment control block, which has one input named as ‘sim’ and the other input termed as ‘coder’. It will output the simulation input when the model is utilized for simulation purpose. If the model is used to generate codes for the target chip, then this block will output its coder input. The model will take the inputs (dc voltage across the load, battery current and SOC) from the analog to digital converters (ADC) when it is used for generating code for the target chip. It will take the inputs from the Simscape model when it is used for the simulations. Similarly, the model will output the control signals to the ePWM when it is used to generate codes, while the control signals are directed to the Simscape model when the system is in simulation mode. Another important thing which has to be noticed in the control loop of the buck converter is that, the reference value is set equal to 102 volts. It means that when the dump-load is activated then the dc load voltage regulates at 102 volts. The difference of 2 volts is kept to have a stable response for the system, when the battery controller is switched off and the dump-load controller is activated. The complete model of the system is being simulated by using a fixed step size of 5e-5.

6.3.1.1. Without the Activation of the Dump-Load

The first simulation is carried out by setting the maximum value of SOC equal to 92%. In this case the effect of the activation of the dump-load controller cannot be observed because within the simulation period the SOC of the battery bank will not exceed its maximum limit. An input flow rate of 100m/s has been applied at the input side of the turbine which supplies power to a dc load of 75 ohms.

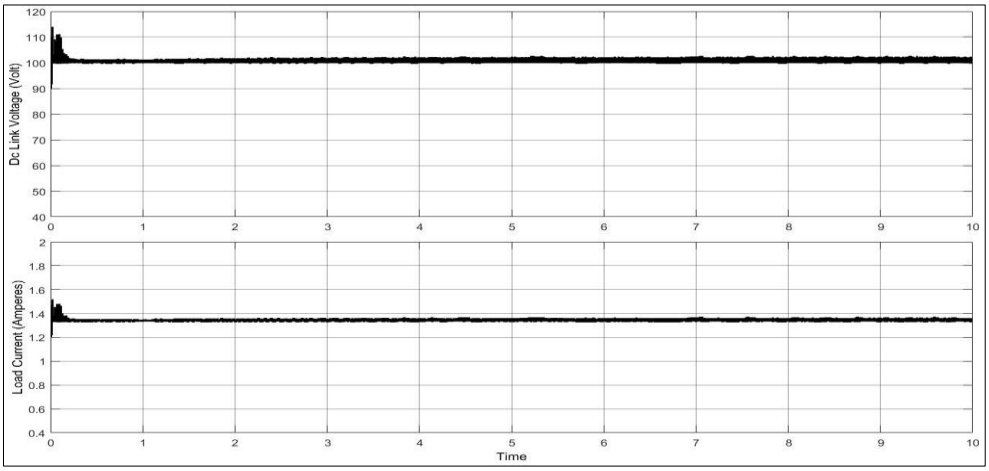

Figure 6.6 Dc Link Voltage and Load Current

The simulated dc voltage across the load has been shown in Figure 6.6, which shows that the control loops made by using the embedded target library is able to regulate the dc voltage across the reference value. The battery current, voltage and its SOC has been shown is Figure 6.7.

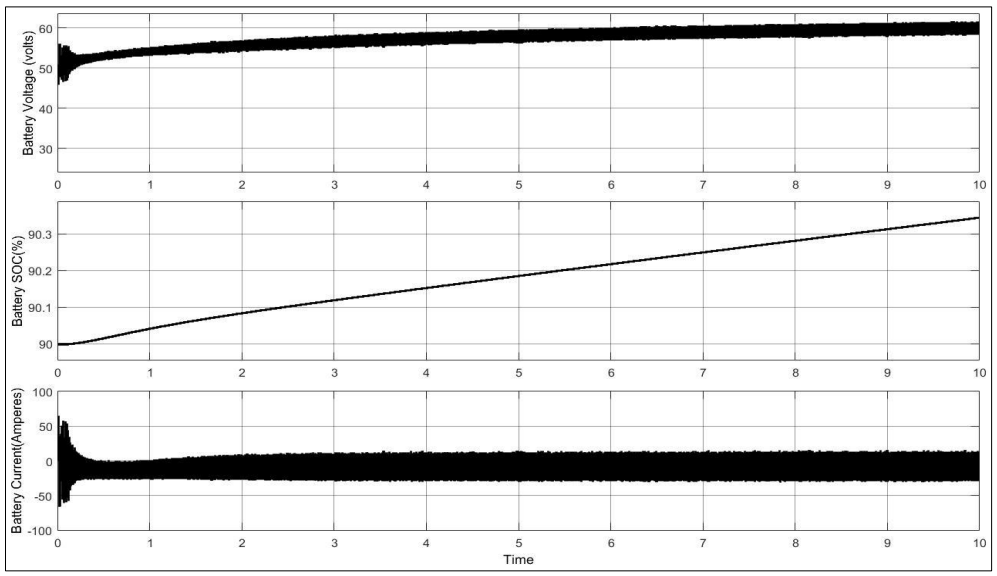

Figure 6.7 Battery Bank's Parameters

It can be seen from the figure that the SOC of the battery is kept on increasing from its initial value of 90% as the input speed is a constant value of 100m/s for the complete period of simulation.

6.3.1.2. System response with the activation of dump-load

The second simulation is carried out to observe the response of the system, when the excess energy needs to be dumped out using the dump-load. The controller is designed in such a way that voltage across the dc link is regulated on two different levels, for the activation and deactivation of the dump-load. Therefore, it can be examined that the dc voltage regulates at 100 volts when the dump-load controller is not into operation. The dc link voltage jumps to 102 volts, when the dump-load controller is activated and the dc link voltage regulates at this level as long as the battery bank is operating above its maximum limit. To observe this effect, the maximum value of the SOC is set to 90.15% and the input flow speed is kept the same as in the previous simulation. The dc link voltage and the load current for this experiment has been displayed in Figure 6.8, while the battery banks parameters have been shown in Figure 6.9

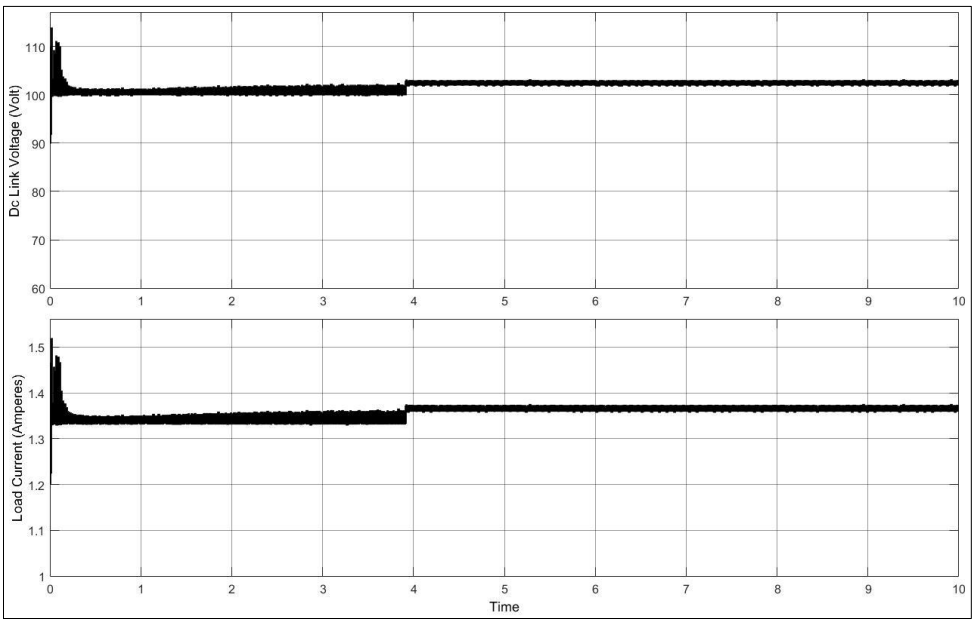

Figure 6.8 Dc Link Voltage and Load Current

It can be seen that as the SOC of the battery bank reaches 90.15% the voltage jumps to 102 volts and then keeps on to the new level as long as the SOC is above the maximum defined limit. The battery current in this period will remain zero. The effect of deactivation of the dump-load cannot be observed in this experiment, but the dc link voltage falls back to 100 volts when the dump-load is deactivated.

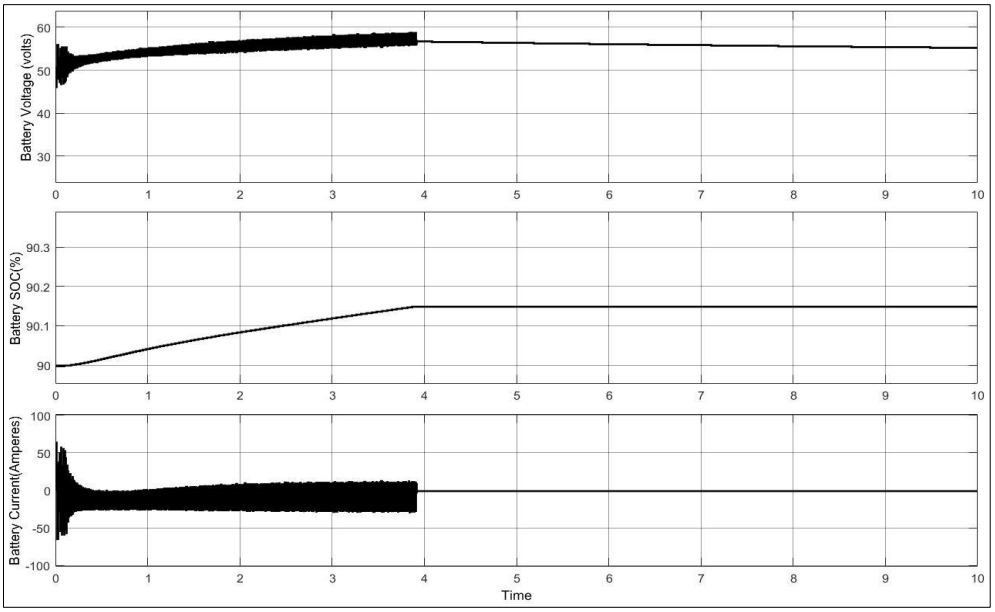

Figure 6.9 Battery Bank's Parameters

6.3.2. Method 2

In the second method, the system without having any storage unit as discussed in chapter 5 is being considered. The control loop of the system as shown in Figure 5.33 is modified in this section, while the rest of the system remains unchanged. The remodeled control loop using the embedded coder target library and the Simulink library is shown in Figure 6.10.

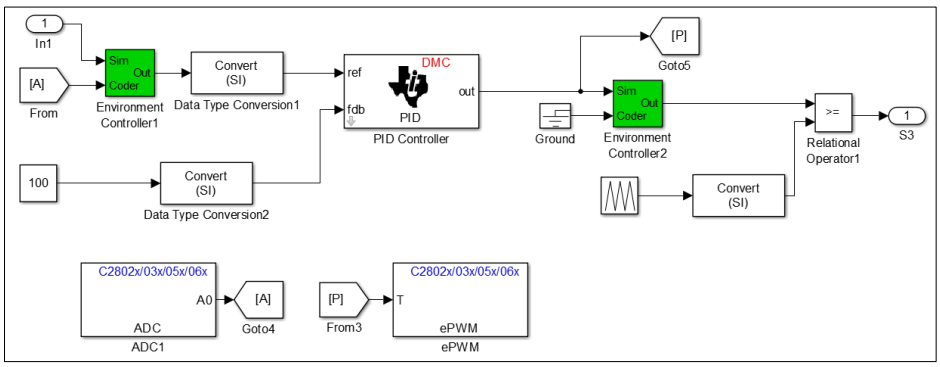

Figure 6.10 Digital Controller for Method 2

It can be realized that the controller is designed using the fixed-point data type with the help of the conversion block from the Simulink library. Same as in the previous method the environment controller block is used to execute the model either in simulation environment or in code generation for a target chip. Initially the model is simulated using the Simscape model of the plant and the simulation is carried out by having a fixed step size of 5e-5. An input flow

speed of 90m/s is considered at the input side of the turbine which is supplying power to a load of 50 ohms. A dump-load of 1 ohm is connected via a buck converter for dumping the excess energy of the source by keeping a constant power across the fixed load. The load current and the voltage across the dc load is presented in Figure 6.11, which shows a constant dc load voltage of 100 volts and a constant dc current of 2 amperes through a dc load of 50 ohms.

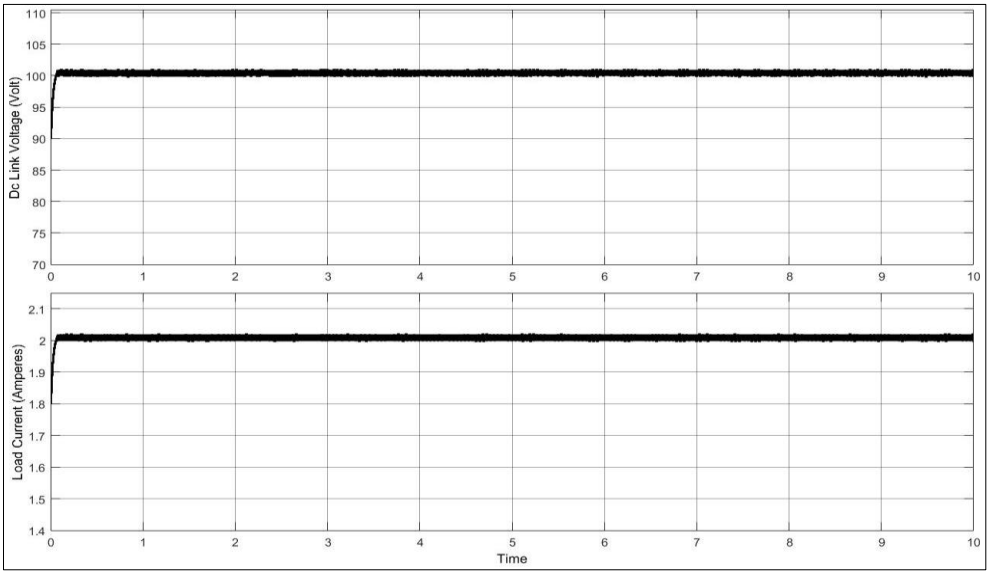

Figure 6.11 Dc Link Voltage and Load Current

The excess amount of power which is wasted by using the dump-load is presented in Figure 6.12. It can be noticed that a single dump-load is enough to dump the excess amount of power generated by a flow rate of 90m/s from the source.

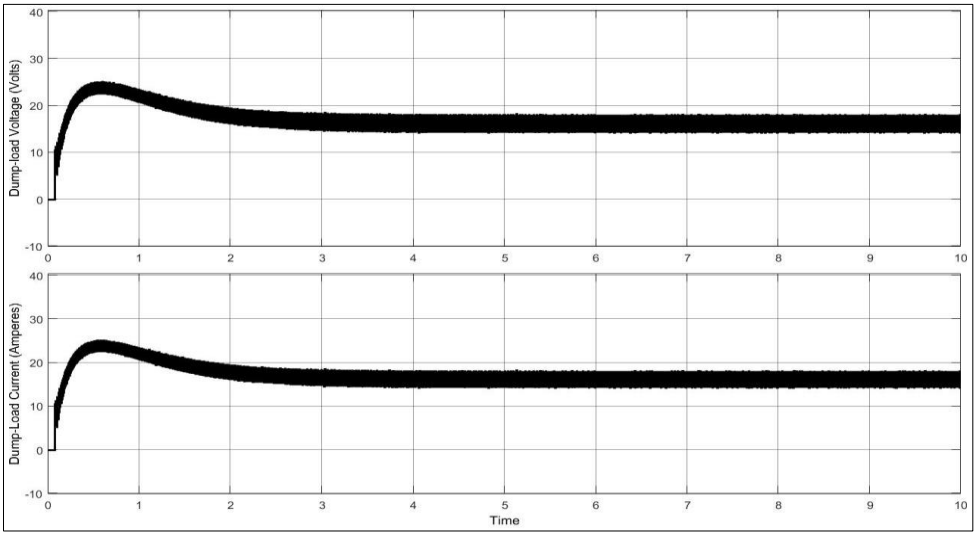

Figure 6.12 Excess Power (Voltage and Current) to the Dump-Load

6.4. Code generation

To understand the process of the code generation the primary step is to recognize the difference between MIL, SIL, PIL and HIL. When a system has to be designed, the initial stage is to model the plant and the controller in Simulink. So, in the first step the stability of the system is analyzed using model in loop (MIL) simulation to check whether the controller is implementable or not. The Simulink models used for several experiments in chapter 5 can be included in the category of MIL, where the system has been being analyzed in the Simulink environment. The second stage of designing a system includes the software in loop (SIL) simulation which can be implemented after the model is verified in MIL. In this type of loop the user is still working in the Simulink environment, where the control algorithms are implemented using software codes depending on the specific type of processor used in the system. The simulation carried out in section 6.2 can be included in the category of SIL, where the controller is redesigned using the C2000 embedded target library. The control algorithm can be verified using SIL simulation by connecting it with the Simscape (Simulink) model of the plant. If any unwanted result occurs from the SIL model of the controller, then the user should go back to the MIL model of the plant and make modifications for the controller.

After the controller is constructed using the C2000 embedded target library and tested in SIL mode, then the next phase is to implement the control algorithm on a real target device using code generation. This is process can be carried out by using process in loop (PIL) simulation, where the generated C/C++ code is loaded into a selected target chip and the simulation of the plant is carried out by having real-time data exchange between the Simulink plant model (host) and the target device. After verifying the controller model using the PIL, the plant model is assembled by having real hardware in laboratory. The target chip including the generated code is interfaced with a real hardware to test the whole system in real time and this phase can be termed as hardware in loop (HIL). The domain of the scope of this project is to explore the method of C/C++ code generation for the target chip, which must be capable of operating in a PIL environment. The real-time data exchange is carried out by using the RTDX instrumentation library from the C2000 target libraries, which consists of two blocks named as ‘From RTDX’ and ‘To RTDX’. RTDX enable the user to receive and transmit data between a target device and a host without interrupting the application. The baseline of the real-time data exchange is provided by the emulation logic included on the C2000 microcontrollers. Therefore, the data is transferred using the JTAG debug connection used for all other debug and control operations. So, RTDX is supported on C2000 target devices without assuming any

input/output peripherals. The RTDX blocks which can be used for the communication between the host and the target device can be displayed in Figure 6.13.

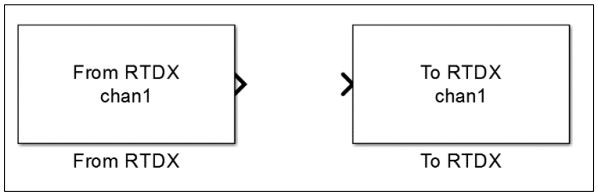

Figure 6.13 RTDX Blocks

6.4.1. Converting the controller block into PIL

As discussed above, in a PIL simulation the generated code runs on the C2000 embedded processor. For this purpose, the initial step is to configure the controller model block for a PIL simulation. The configuration is carried out by converting the controller block into referenced model in Simulink environment. The window used for converting the model into referenced model is presented in Figure 6.14.

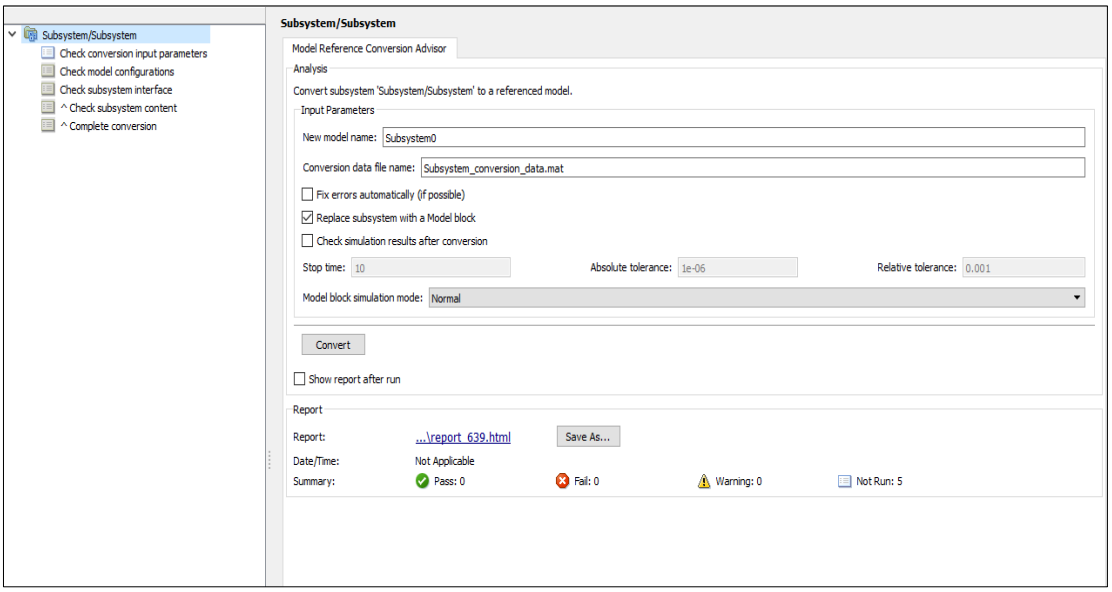

Figure 6.14 Conversion into Referenced Model

The simulation environment is transformed into PIL simulation, after the block is converted into referenced model. The transformation can be done by selecting PIL from the 'simulation mode' drop-down list in 'Block Parameters (ModelReference)'. For specifying the code to be tested, model reference option has to be chosen from the code interface drop-down list. The Block Parameters menu for selecting the PIL or SIL option is shown in Figure 6.15.

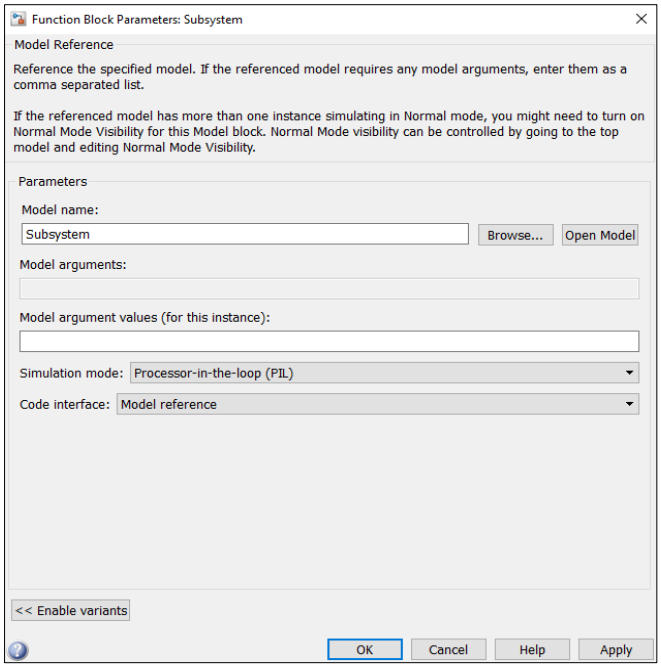

Figure 6.15 Block Parameters Menu

The appearance of the controller block is altered after its conversion for using in PIL simulation as shown in Figure 6.16. When the system is running the Simscape plant model will be sending and receiving data from the PIL block, which is actually running onto a real target device.

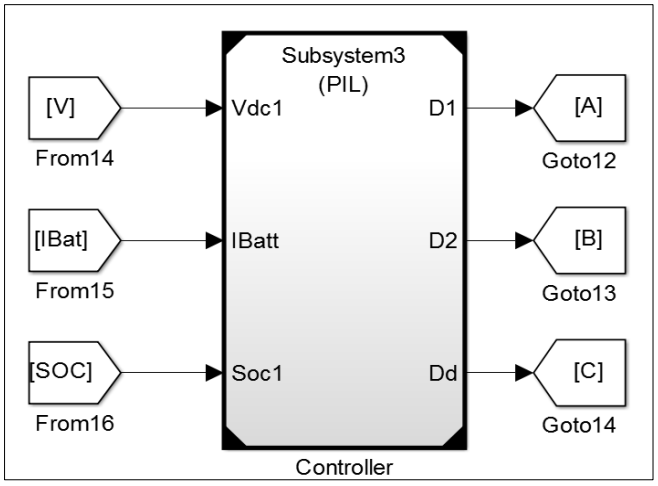

Figure 6.16 Digital Controller in PIL

As the PIL block runs on a real hardware so, it requires a code which can be generated from Simulink. The code generation process for the target hardware is carried out by setting up the model to generate C/C++ code for the selected chip. To set up the code generation process, the user should type “targetupdater” in MATLAB command window. This will allow the user to

select the support package and the code composer studio toolchain for installing the third-party software for the embedded processor. To start the code generation, the user must open the model configuration window and apply some changes to the Simulink model. The first step is to select a fixed-step type solver by keeping the step-size equal to 5e-5s as shown in Figure 6.17.

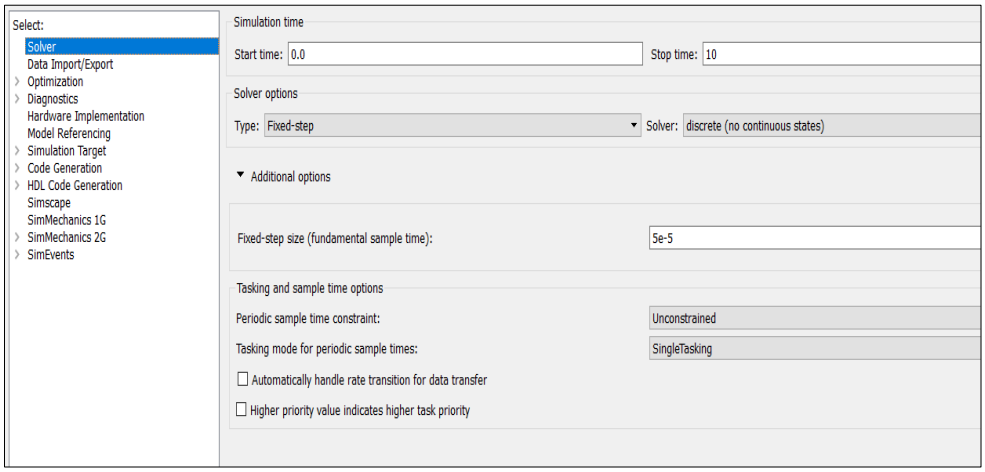

Figure 6.17 Model Configuration Window

Then, the family of the target device must be selected from the Hardware Implementation pan of the configuration window as shown in Figure 6.18. The user can configure all the resources of the target hardware by selecting and modifying each option one by one.

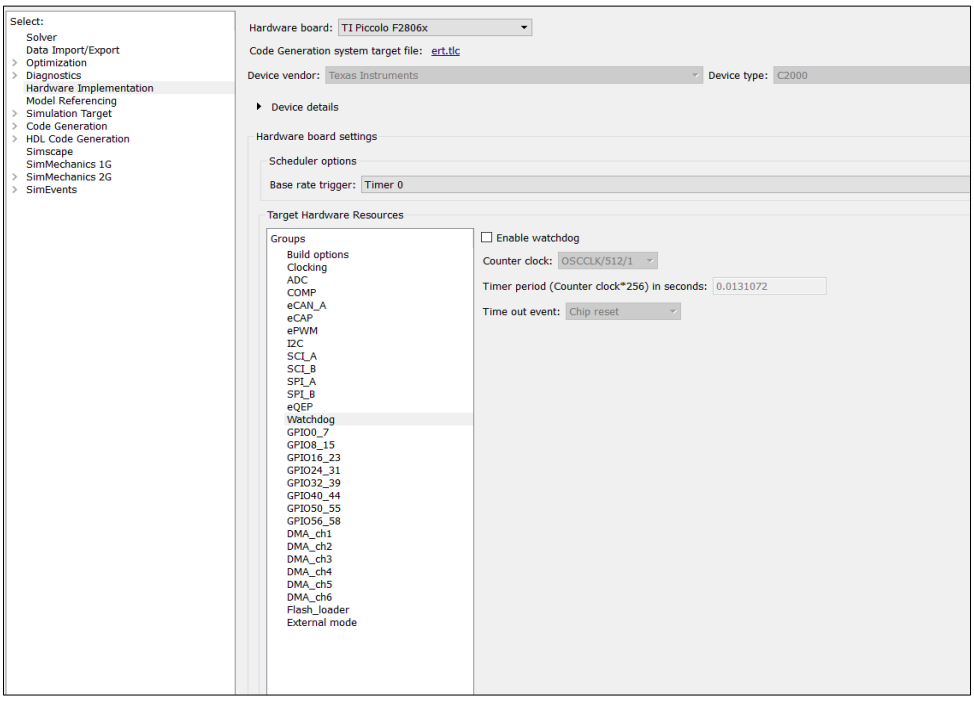

Figure 6.18 Hardware Implementation Pan of the Configuration Window

In the code generation pan as shown in Figure 6.19 the user should select the system target file as ‘ert.tlc’, which is supported by the CCS version 6 and in the toolchain option ‘Texas Instrument Code Composer Studio v6 (C2000)’ must be selected. In the ‘Report’ subsection of the code generation pan, the user can check the ‘create code generation report’ to display the code and all its detailed information after the code generation process is finished. Finally, the C/C++ code for the target hardware can be generated by clicking on the ‘Build Model’ button in the Simulink environment, which will automatically generate the code and displays the code report.

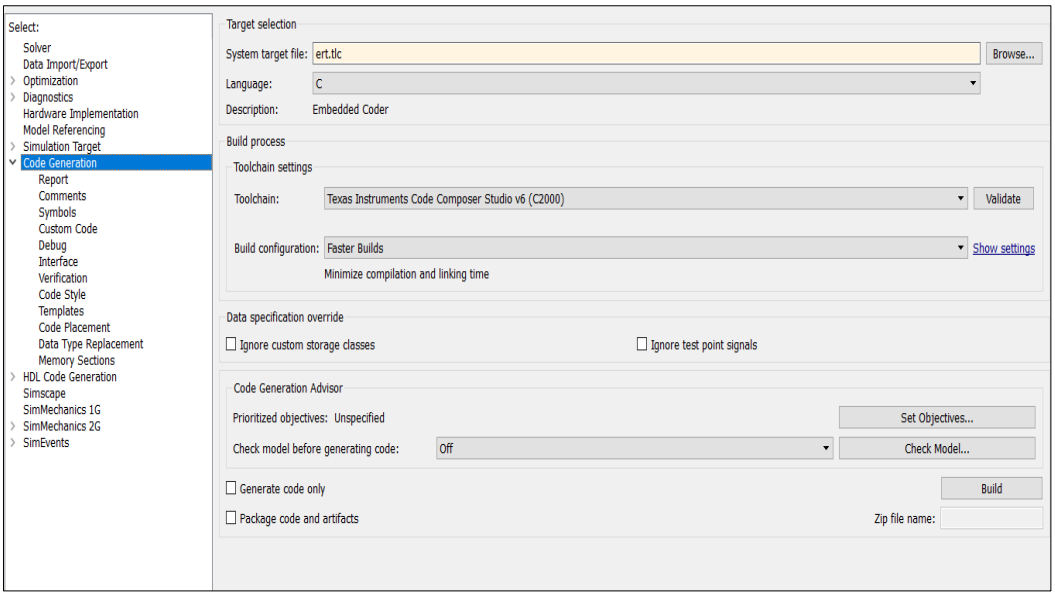

Figure 6.19 Code Generation Pan of the Configuration Window

In the PIL simulation the Simulink model of the plant will be communicating with the target device using serial communication and the support packages for TI C2000 supports serial communication interface for PIL over SCI-A. The serial connection will be used to exchange data between the Simulink plant and the target hardware for serial communication. The serial connection can be established by the ‘COM’ port of the computer using RS-232 or it can also be established by using the USB cable between the target and the host. The ‘COM’ port associated with the target must be found after a serial connection is established. It can be done by expanding the section ‘Ports (COM&LPT)’ after opening the ‘Device manager’ on the host computer. In this section the ‘COM’ port number of the ‘USB serial port’ has to be noted down. Several commands can be used to enable the settings for running the PIL simulation with serial communication. In the command shown in C1, the ‘COM1’ is replaced with the ‘COM’ port number noted down from the ‘Device manager’.

setpref('MathWorks_Embedded_IDE_Link_PIL_Preferences','COMPort','COM1'); (C1)

The command used for setting the baud rate for PIL communication can be shown in C2 and the command shown in C3 is used to enable the PIL over serial connection.

setpref('MathWorks_Embedded_IDE_Link_PIL_Preferences','BaudRate','115200'); (C2)

setpref('MathWorks_Embedded_IDE_Link_PIL_Preferences','enableserial','true'); (C3)

The above discussion explains the complete code generation process for the real target hardware device and also indicates the settings for building the communication between the host computer and the target hardware. At this stage of the project the code isn't loaded in the target hardware because using a physical hardware was outside the scope of this thesis work. So, the complete hardware implementation of the PIL simulation for the controller model and the plant model will be done in future research work. After the verification of the PIL simulation of the controller, the complete implementation of the system can also be carried out by using a physical turbine coupled to a permanent magnet synchronous generator and connected to a rectifier, a storage unit, a dump-load and dedicated dc-dc converters for these units.

Chapter 7 Conclusion and Future Work

7.1. Conclusion

A switched mode power supply model designed for feeding power to the down-hole electronic devices has been presented in this thesis. The power supply model is investigated using two different types of system models along with their power management control algorithms. The objective of regulating the dc link voltage across the filter capacitor and maintaining the power balance of the system is achieved for both the system models, irrespective of the input disturbances and varying load demands. The first type of system model includes a storage unit and a dump-load for its stable operation and the second type of system model is analyzed by having a dump-load only. The system model without having any battery bank has some certain operating limits. The inputs for this type of system configuration must be within a predefined limits of flow rates. Therefore, to supply minimum demanded power to the load the input flow speed for this configuration must be always higher than its minimum specified limit. Secondly the input flow rate must not exceed the maximum limit, which saturates the flow of excess power through the dump-load. The dc load is completely disconnected from the system when the SOC of the battery bank is less than minimum limit and the input flow rate is negligible. The method for hardware implementation of the system's control loops for the storage unit and the dump-load has also been presented in this thesis. The control algorithms have been implemented using the embedded coder target libraries and the objective of having constant dc voltage across the load has been achieved. The control loops have been designed using fixed-point numbers, which can be implemented in a real target device using PIL simulation.

The conclusions for the work carried out in each chapter are presented as:

In chapter 1, a general background and motivation of the work presented in the thesis is discussed. The requirement of electrical power for feeding the down-hole devices has been highlighted which are used to fulfill the demand of high productivity of oil and gas fields. In addition, the planning and scope of the research work is presented which gives a general overview for modelling of the system.

In chapter 2, an overview of all the available energy sources in down-hole application has been discussed. Consequently, a literature review on the methods used for the utilization of these energy sources has been presented. The chapter also focuses on the general method of using a turbine for capturing the available source of kinetic energy. The discussion about the various

types of storage unit have presented and a secondary type of battery bank is chosen for the system. The equation for calculating the dump-load resistor considering a no-load situation is also shown towards the end of this chapter.

The basic structure of the system is deliberated and modelled in chapter 3 using MATLAB/Simulink. The system presented in the work has been designed using the Simscape blocks of the turbine and the PMSG, which are based on the same type of modelling for these components as it has been shown in this chapter. The working of a buck-boost converter in a bi-directional way for the charging and discharging of the storage unit has been investigated as well. The flow of power in the buck and boost mode shows the flow of current from the storage unit and to the storage unit. At last a buck converter is shown which is used for controlling the dump-load for dumping the excess amount of input power from the source.

In chapter 4, the control strategy of the system having a turbine and PMSG is investigated using several types of energy management schemes for various types of storage units. The possibility of making an energy management system similar to a standalone power system or a dc micro grid is reviewed. So, in this chapter a control algorithm for a battery bank used as a storage unit and a dump-load is adopted for the implementation of the system in the later sections. The chapter also includes flow charts for the various type of energy management algorithms studied in the literature.

In chapter 5, the implementation of the control strategy of the system using dedicated dc-dc converters for the battery bank and the dump-load is proposed. The aim of the chapter was to design an intelligent control algorithm for keeping a constant dc voltage across the load, irrespective of input disturbances and varying load demands. The results verify that the control strategy is feasible as the system is stable for these conditions. The control strategy prevents the battery bank from overcharging by wasting the excess energy of the source to the dump-load. The performance of the system without having a storage unit is also examined in this chapter. So, the stability of the dc load voltage for the battery less system has been studied as well and the results shows that the system is stable by keeping the input flow rates within a certain limit.

In chapter 6, the power management control strategy for the battery bank and the dump-load is implemented using embedded coder target libraries. The model of the controller is implemented using fixed-point data representation. The results verify that the controller model can be programmed in a real-time target hardware using the MATLAB/Simulink code generation

process. The implemented code for the target device can also be verified by using PIL simulation of the target device and the Simscape model of the plant.

7.2. Future work

- The complete system implementation using real hardware devices can be carried out in the future. The complete system hardware can be implemented step by step using PIL and HIL simulations.
- Hybrid storage unit can be investigated more in details and can be verified for the betterment of the system.
- The capability of the system to work at high temperature must be investigated and the converters used for the system model shall be designed using high temperature electronics. So, a deep analysis of wide band gap devices for the designing of the converters must be done in the future.
- A deep analysis of the methods used for the complete disconnection of the dc loads from the system can be the part of future work as well.
- The method of load shedding based on the defined priorities of the dc loads can also be included in the future research work.
- A practical research regarding the methods for installation of the mechanical system (turbine coupled to a PMSG) inside the well without interrupting the fluid flow can also be done in the future.

References

[1] S. A. Holditch and R. R. Chianelli, "Factors that will influence oil and gas supply and demand in the 21st century," *MRS bulletin*, vol. 33, pp. 317-323, 2008.

[2] R. Zhao, S. A. Morris, and A. Kwasinski, "A dual-input forward converter for downhole drilling applications," in *2014 IEEE 57th International Midwest Symposium on Circuits and Systems (MWSCAS)*, 2014, pp. 459-462.

[3] M. L. Dock and B. G. Stephenson, "Downhole generator for horizontal directional drilling," ed: Google Patents, 2004.

[4] P. Tubel, M. W. Holcombe, J. L. Baugh, A. M. I. I. Albert, and R. C. Ross, "Downhole apparatus for generating electrical power in a well," ed: Google Patents, 1998.

[5] C. T. Webb, "Counterbalance enabled power generator for horizontal directional drilling systems," ed: Google Patents, 2010.

[6] R. L. Schultz, P. D. Ringgenberg, C. E. Robison, R. K. Michael, and R. I. Bayh, "Vibration based downhole power generator," ed: Google Patents, 2001.

[7] M. L. Fripp and R. K. Michael, "Vibration based power generator," ed: Google Patents, 2007.

[8] C. J. Zabcik, "Downhole apparatus for absorbing vibratory energy to generate electrical power," ed: Google Patents, 1985.

[9] R. Wetzel, S. Hiron, A. Veneruso, D. Patel, T. MacDougall, and J. Walter, "Harvesting Vibration for Downhole Power Generation," ed: Google Patents, 2006.

[10] M. A. Schnatzmeyer and C. E. Robison, "Method and apparatus for generating electric power downhole," ed: Google Patents, 2000.

[11] L. P. TOSI, H. M. Cornette, and D. R. Underdown, "Flow-induced electrostatic power generator for downhole use in oil and gas wells," ed: Google Patents, 2013.

[12] C. F. VanBerg, "Apparatus and method for providing electrical power in a well," ed: Google Patents, 1993.

[13] M. Dimanchev and M. P. Mintchev, "Energy Harvesting in Horizontal Drilling Processes for the Purpose of Information and Navigation Monitoring," *INFORMATION THEORIES & APPLICATIONS*, p. 180, 1993.

[14] A. H. Fathima and K. Palanisamy, "Energy Storage Systems for Energy Management of Renewables in Distributed Generation Systems," in *Energy Management of Distributed Generation Systems*, L. Mihet-Popa, Ed., ed Rijeka: InTech, 2016, p. Ch. 07.

[15] N. Achaibou, M. Haddadi, and A. Malek, "Lead acid batteries simulation including experimental validation," *Journal of Power Sources*, vol. 185, pp. 1484-1491, 12/1/ 2008.

[16] M. Dürr, A. Cruden, S. Gair, and J. R. McDonald, "Dynamic model of a lead acid battery for use in a domestic fuel cell system," *Journal of Power Sources*, vol. 161, pp. 1400-1411, 10/27/ 2006.

[17] O. Gergaud, G. Robin, B. Multon, and H. Ben Ahmed, "Energy Modeling of a Lead-Acid Battery within Hybrid Wind/Photovoltaic Systems," in *European Power Electronic Conference 2003*, TOULOUSE, France, 2003, p. 8pp.

[18] MathWorks. *Implement generic battery model*. Available: https://se.mathworks.com/help/physmod/sps/powersys/ref/battery.html;jsessionid=919d82cda77bacb2d6e2e7a539e3

[19] Q. Zhang, W. Deng, S. Zhang, and J. Wu, "A Rule Based Energy Management System of Experimental Battery/Supercapacitor Hybrid Energy Storage System for Electric Vehicles," *Journal of Control Science and Engineering*, vol. 2016, p. 17, 2016.

[20] A. S. Sengupta, A. K. Chakraborty, and B. K. Bhattacharyya, "Modeling super capacitor discharge profile," in *2016 IEEE 1st International Conference on Power Electronics, Intelligent Control and Energy Systems (ICPEICES)*, 2016, pp. 1-4.

[21] M. Uzunoglu, O. C. Onar, and M. S. Alam, "Modeling, control and simulation of a PV/FC/UC based hybrid power generation system for stand-alone applications," *Renewable Energy*, vol. 34, pp. 509-520, 3// 2009.

[22] P. Thounthong, S. Raël, and B. Davat, "Energy management of fuel cell/battery/supercapacitor hybrid power source for vehicle applications," *Journal of Power Sources*, vol. 193, pp. 376-385, 8/1/ 2009.

[23] M. Y. El-Sharkh, A. Rahman, M. S. Alam, P. C. Byrne, A. A. Sakla, and T. Thomas, "A dynamic model for a stand-alone PEM fuel cell power plant for residential applications," *Journal of Power Sources*, vol. 138, pp. 199-204, 11/15/ 2004.

[24] M. Uzunoglu and M. S. Alam, "Dynamic modeling, design, and simulation of a combined PEM fuel cell and ultracapacitor system for stand-alone residential applications," *IEEE Transactions on Energy Conversion*, vol. 21, pp. 767-775, 2006.

[25] A. Anzalchi and A. Sarwat, "Analysis of carbon tax as an incentive toward building sustainable grid with renewable energy utilization," in *Green Technologies Conference (GreenTech), 2015 Seventh Annual IEEE*, 2015, pp. 103-109.

[26] A. Moghadasi, A. Sundararajan, and A. Sarwat, "Power Management and Control Strategy in Standalone DC Microgrid alongwith SMES Solenoid Coil," *Power*, vol. 3, 2014.

[27] (2013). Available: http://solarhomestead.com/dump-load-diversion-load/

[28] M. Rezkallah, A. Chandra, D. R. Rousse, H. Ibrahim, A. Ilinca, and D. Ramdenee, "Control of small-scale wind/diesel/battery hybrid standalone power generation system based on fixed speed generators for remote areas," in *IECON 2016 - 42nd Annual Conference of the IEEE Industrial Electronics Society*, 2016, pp. 4060-4065.

[29] C. N. Bhende, "Stand-alone wind energy supply system," in *2009 International Conference on Power Systems*, 2009, pp. 1-6.

[30] A. M. O. Haruni, A. Gargoom, M. E. Haque, and M. Negnevitsky, "Dynamic operation and control of a hybrid wind-diesel stand alone power systems," in *2010 Twenty-Fifth Annual IEEE Applied Power Electronics Conference and Exposition (APEC)*, 2010, pp. 162-169.

[31] C. Jie, C. Jiawei, G. Chunying, and D. Xiang, "Energy management and power control for a stand-alone wind energy conversion system," in *IECON 2012 - 38th Annual Conference on IEEE Industrial Electronics Society*, 2012, pp. 989-994.

[32] J. L. Márquez, M. G. Molina, and J. M. Pacas, "Dynamic modeling, simulation and control design of an advanced micro-hydro power plant for distributed generation applications," *International Journal of Hydrogen Energy*, vol. 35, pp. 5772-5777, 6// 2010.

[33] A. Acakpovi, E. B. Hagan, and F. X. Fifatin, "Review of hydropower plant models," *International Journal of Computer Applications,* vol. 108, 2014.

[34] N. Mohan, *Advanced Electric Drives: Analysis, Control, and Modeling Using MATLAB/Simulink*, 1 Aug 2014.

[35] P. R. Nilsen. (2016). *Electric Drives (4 ed.)*.

[36] S. M. Allam, M. F. Elmorshedy, and E. M. Rashad, "Load power and state-of-charge management strategy with MPPT of wind-driven isolated PMSG," in *2016 XXII International Conference on Electrical Machines (ICEM)*, 2016, pp. 1098-1104.

[37] D. Chen, L. Xu, and L. Yao, "DC Voltage Variation Based Autonomous Control of DC Microgrids," *IEEE Transactions on Power Delivery,* vol. 28, pp. 637-648, 2013.

[38] L. Xu and D. Chen, "Control and Operation of a DC Microgrid With Variable Generation and Energy Storage," *IEEE Transactions on Power Delivery,* vol. 26, pp. 2513-2522, 2011.

[39] N. Mendis, K. M. Muttaqi, S. Perera, and M. N. Uddin, "Remote Area Power Supply System: An Integrated Control Approach Based on Active Power Balance," *IEEE Industry Applications Magazine,* vol. 21, pp. 63-76, 2015.

[40] N. H. Samrat, N. Ahmad, I. A. Choudhury, and Z. Taha, "Technical Study of a Standalone Photovoltaic–Wind Energy Based Hybrid Power Supply Systems for Island Electrification in Malaysia," *PLoS One,* vol. 10, 2015.

[41] N. Mendis, K. M. Muttaqi, and S. Perera, "Management of Battery-Supercapacitor Hybrid Energy Storage and Synchronous Condenser for Isolated Operation of PMSG Based Variable-Speed Wind Turbine Generating Systems," *IEEE Transactions on Smart Grid,* vol. 5, pp. 944-953, 2014.

[42] E. Jamshidpour, S. Saadate, and P. Poure, "Energy management and control of a stand-alone photovoltaic/ultra capacitor/battery microgrid," in *2015 IEEE Jordan Conference on Applied Electrical Engineering and Computing Technologies (AEECT)*, 2015, pp. 1-6.

[43] D. Ipsakis, S. Voutetakis, P. Seferlis, F. Stergiopoulos, and C. Elmasides, "Power management strategies for a stand-alone power system using renewable energy sources and hydrogen storage," *International Journal of Hydrogen Energy,* vol. 34, pp. 7081-7095, 8// 2009.

[44] A. I. Sarwat and A. Moghadasi, "A Downsizing Strategy for Combinatorial PMSG Based Wind Turbine and Micro-SMES System Applied in Standalone DC Microgrid," *International Journal of Energy Science,* vol. 4, p. 50, 2014.

[45] TexasInstruments. *C2000 32-bit microcontrollers*. Available: http://www.ti.com/lsds/ti/microcontrollers-16-bit-32-bit/c2000-performance/real-time-control/overview.page?DCMP=dsp_C2000&HQS=c2000

[46] TexasInstruments. *Technical Documents for Piccolo F2906x*. Available: http://www.ti.com/lsds/ti/microcontrollers-16-bit-32-bit/c2000-performance/real-time-control/f2802x-f2803x-f2806x/technical-documents.page

[47] T. Instruments, "TMS320x2806x Piccolo Technical Reference Manual," *Preliminary, Texas Instrument,* 2011.

[48] D. Menard, D. Chillet, and O. Sentieys, "Floating-to-fixed-point conversion for digital signal processors," *EURASIP journal on applied signal processing,* vol. 2006, pp. 77-77, 2006.

[49] N. Representation, "Computer Arithmetic, Article to appear in Encyclopedia of Information Systems," ed: Academic Press, 2001.

[50] (08.05). *Fixed-Point Numbers*. Available: https://se.mathworks.com/help/simulink/ug/fixed-point-numbers.html

Appendix A: Method3-System with 5ohms Dump-Load

The First simulation shows a stable dc link voltage with an input flow Speed of 170m/s.

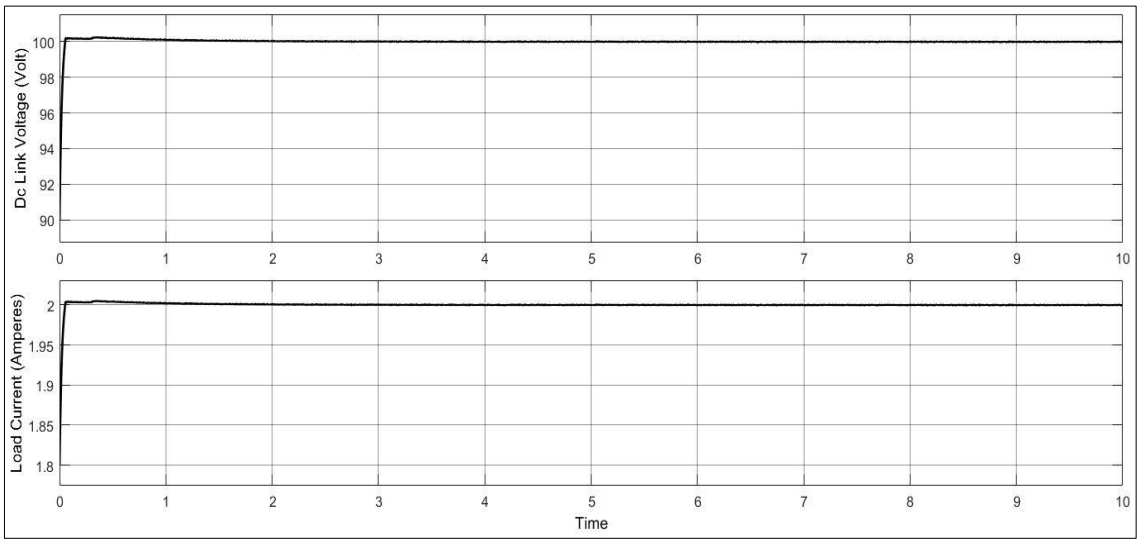

Figure A. 1 Voltage and Current of Dc Load for Input Flow of 170m/s

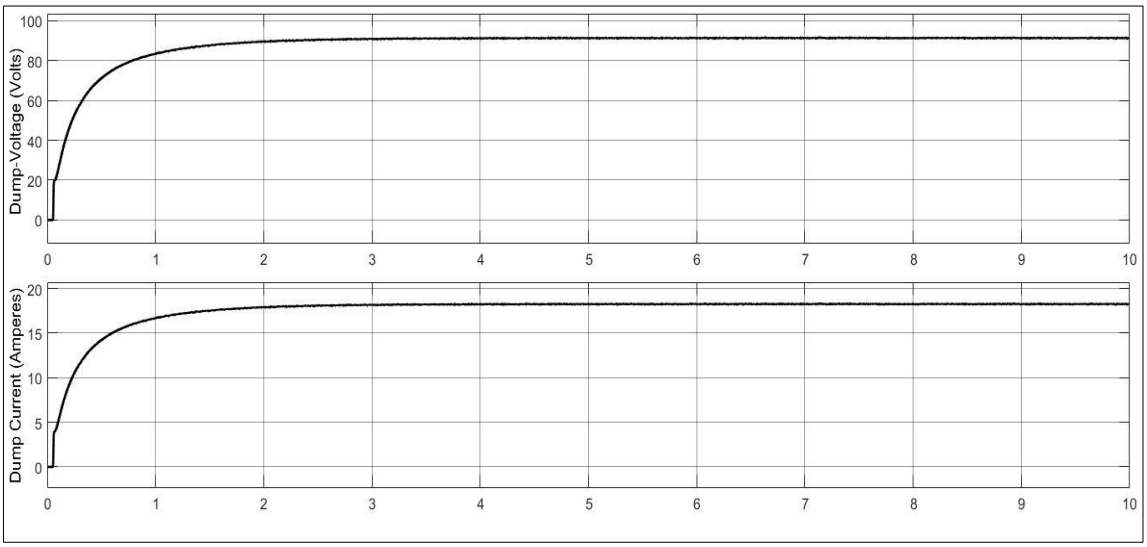

Figure A. 2 Voltage and Current of Dump-Load for Input Flow of 170m/s

The Second Simulation is carried out for the input flow rate of 180m/s, and the system is stable.

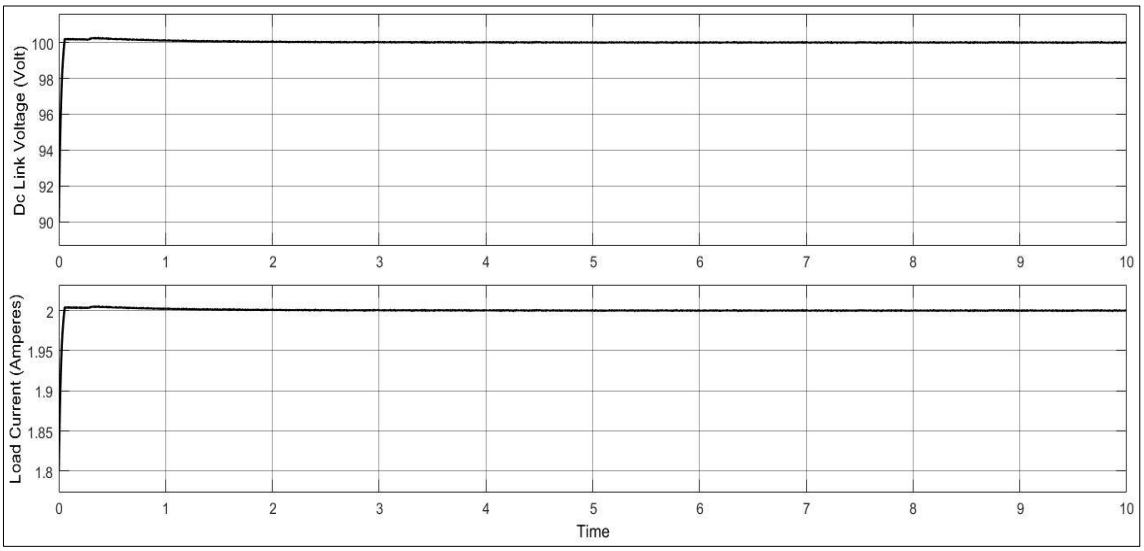

Figure A. 3 Voltage and Current of Dc Load for Input Flow of 180m/s

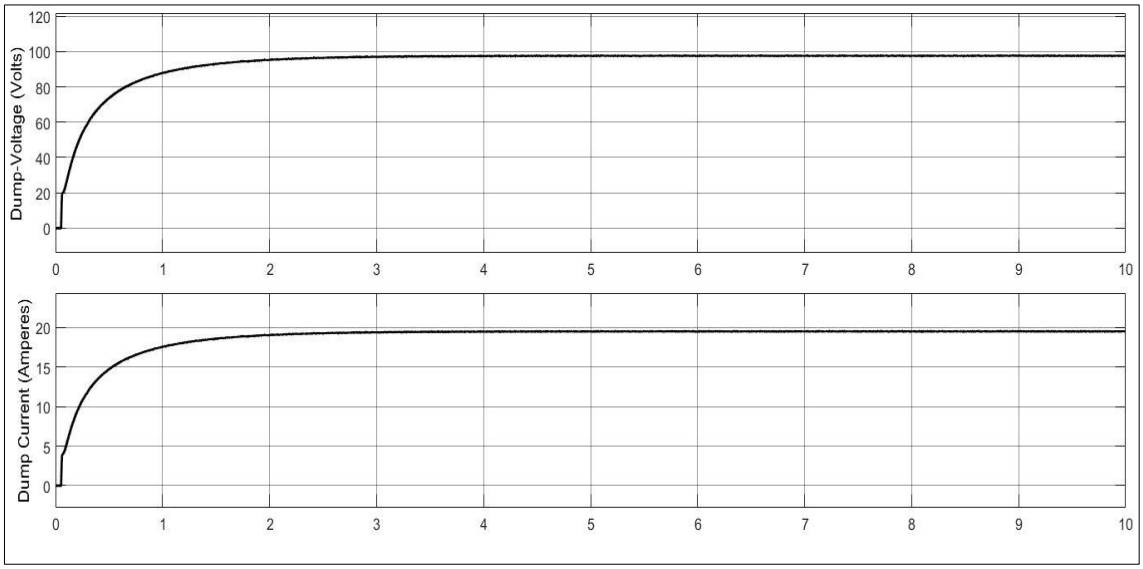

Figure A. 4 Voltage and Current of Dump-Load for Input Flow of 180m/s

The simulation shows that the system is unstable for an input flow speed of 190m/s and there is a requirement of additional dump-load.

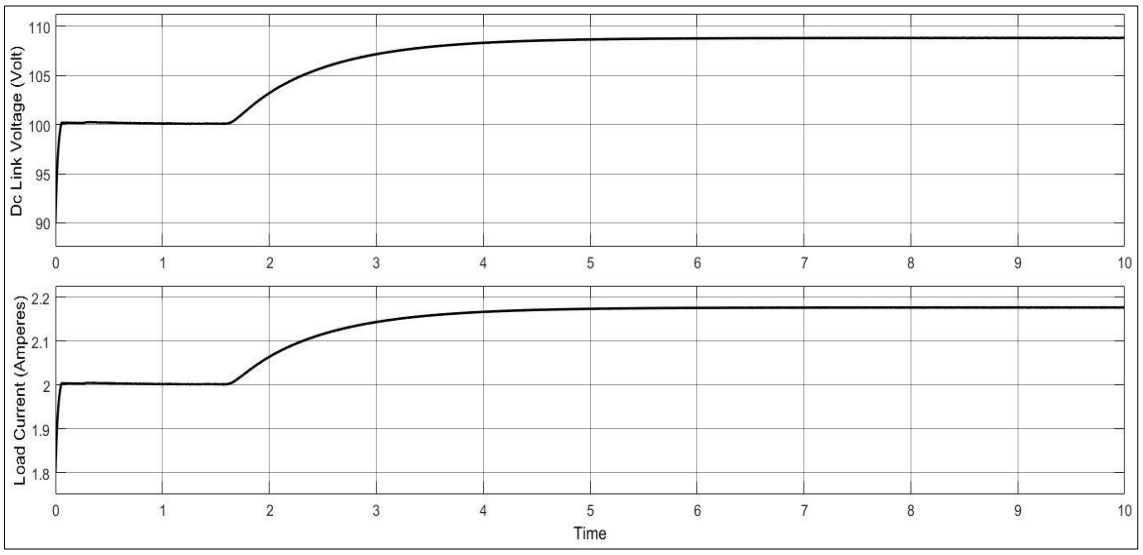

Figure A. 5 Voltage and Current of Dc Load for Input Flow of 190m/s

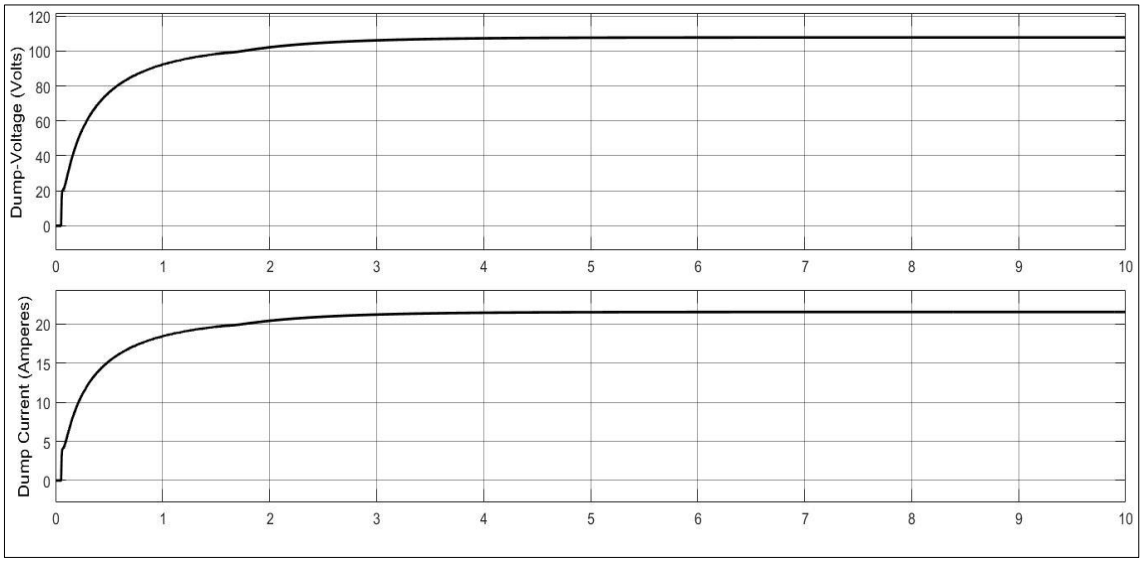

Figure A. 6 Voltage and Current of Dump-Load for Input Flow of 190m/s